

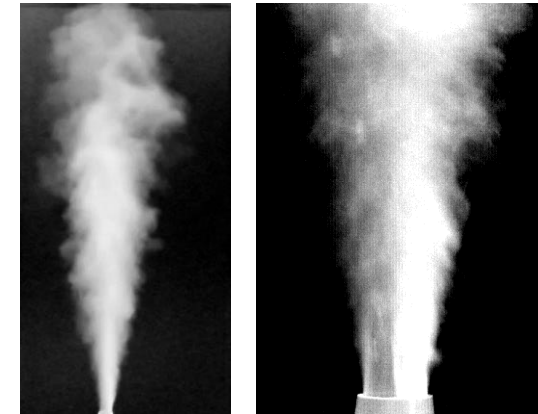
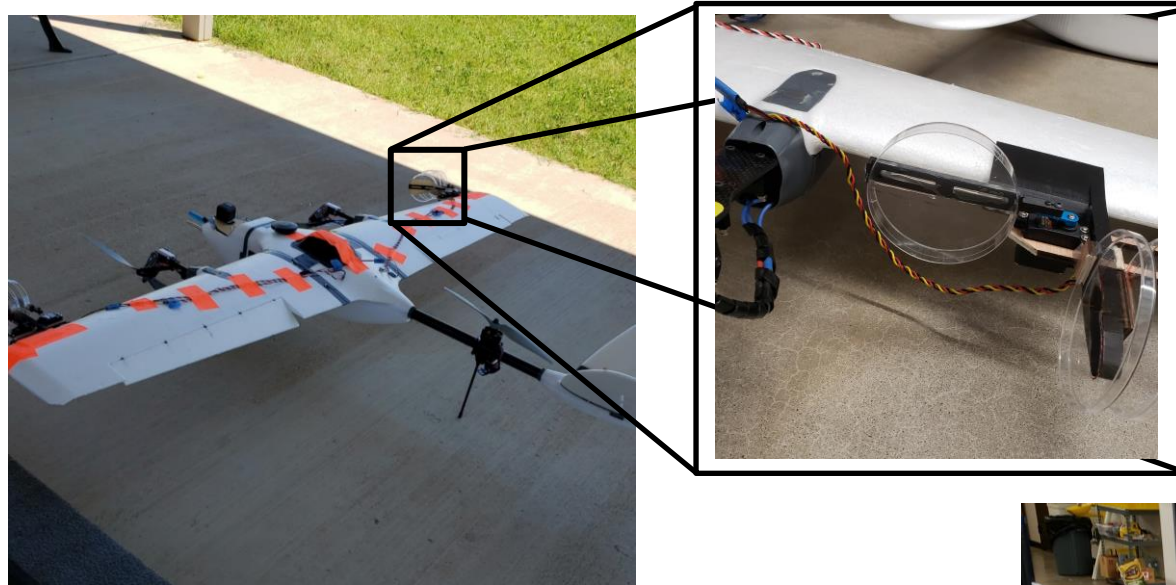
40th ASME/AIAA Online Regional Symposium
Blitz Presentations



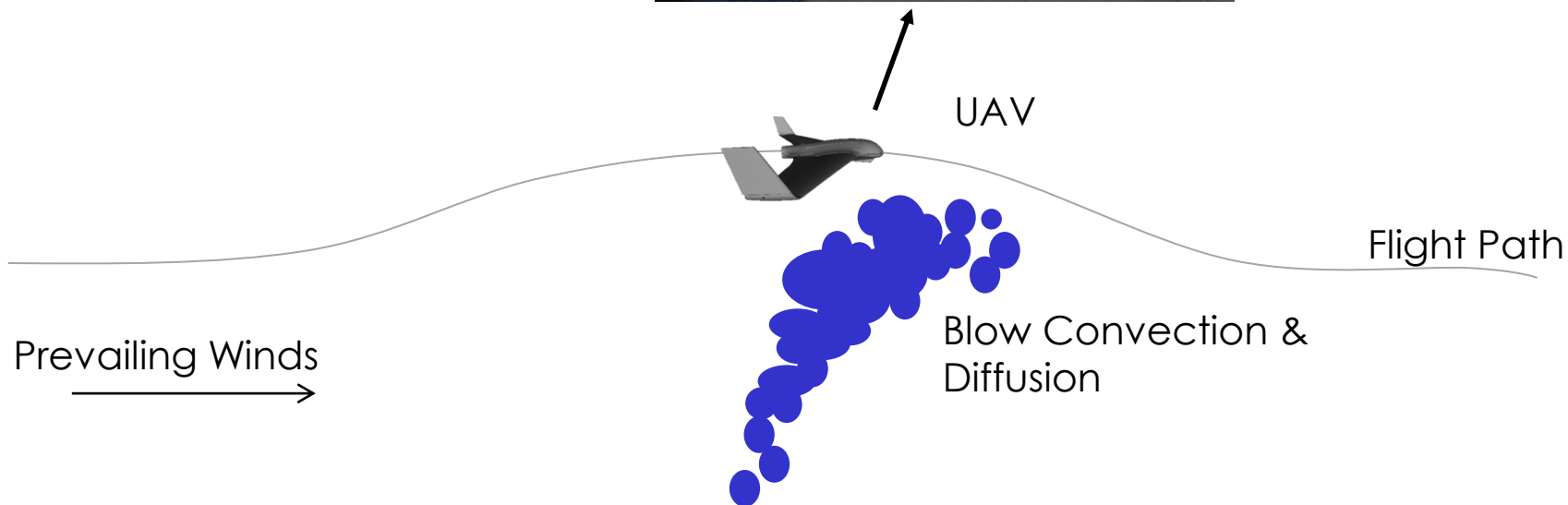
Collection Device for Dolphin Hormone Sampling in Blowhole Jet Flow Field

Eric Abele (OSU), Kerrick Ray, and Jamey Jacob

- Biologists are looking for a new non-invasive method to collect cortisol samples from wild dolphins without causing them stress
- Cortisol levels can be sampled from mucous in dolphin blowhole breaths
- Fixed wing UAV with collection mechanism is being designed to meet this need

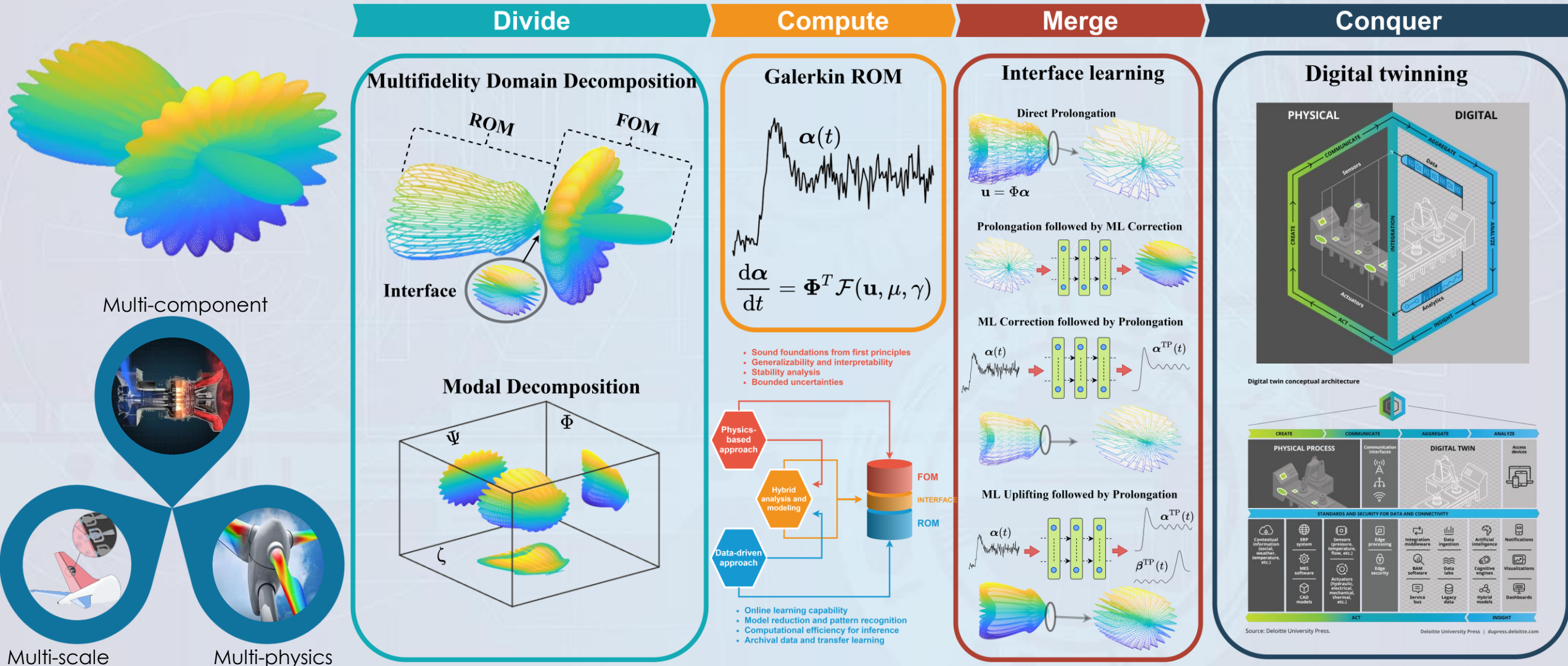


Turbulent jet expelled from Chuffsim



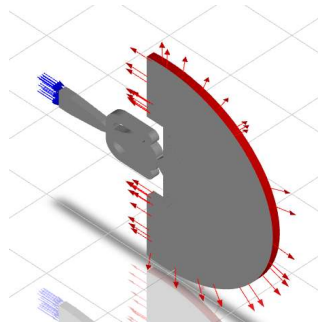
Interface learning for coupling full and reduced order models in multifidelity simulations

Shady Ahmed (OSU), Omer San (OSU), Kursat Kara (OSU), Rami Younis (TU), and Adil Rasheed (NTNU)



Sweeping Jet Actuator(SWJA) in Water

Mobashera Alam, Dr.Kursat Kara

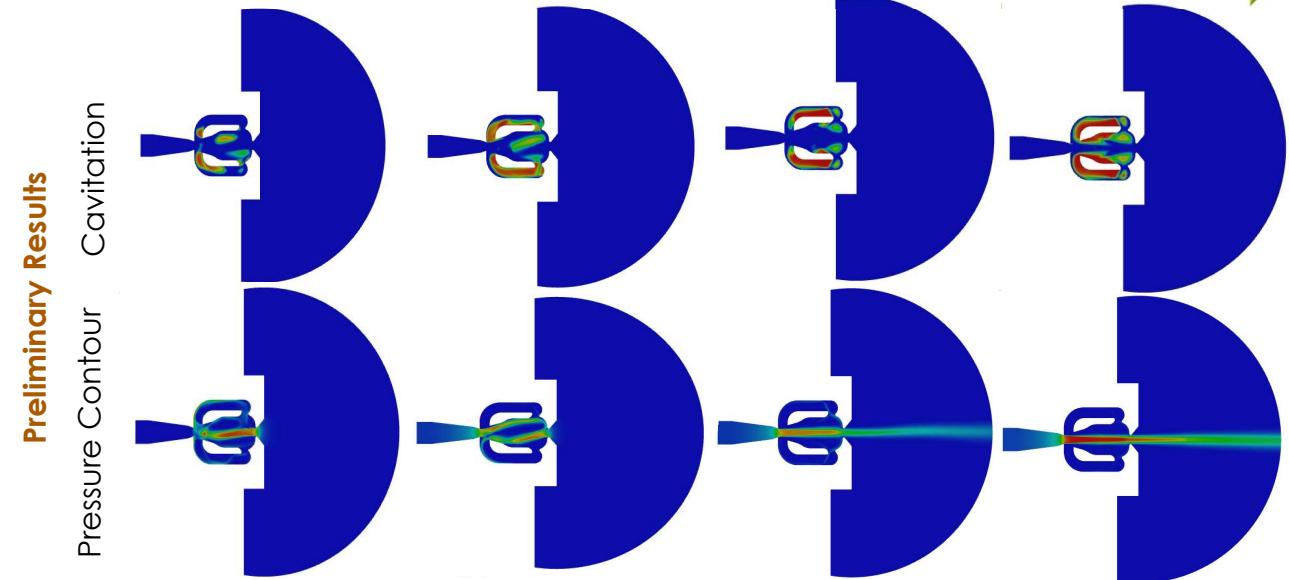


Sweeping Jet Actuator

Numerical Model

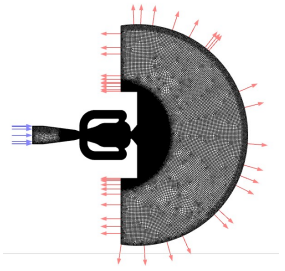
- Multiphase- mixture(3D)
- No of Elements:1292520
- Continuity
- Steady RANS
- Energy

kara2018	Flow separation control	→	Aerodynamics
koklu2016	Coanda Extension effect	→	Geometric Modification
Lin2019	Testing on Vertical Tail	→	Fuel consumption
Schmidt2017	Separation control in bluff body	→	Hydrodynamics

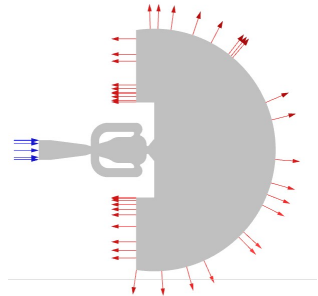


Preliminary Results

Cavitation
Pressure Contour



Inlet Velocity



Outlet Pressure

Summary:

- no effect of cavitation
- $\uparrow \dot{m}$ $\uparrow P$ \uparrow momentum

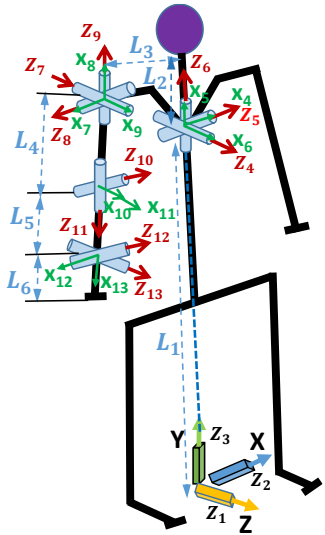
Future Work:

- Transient simulation
- oscillatory frequency, bluff body flow optimization

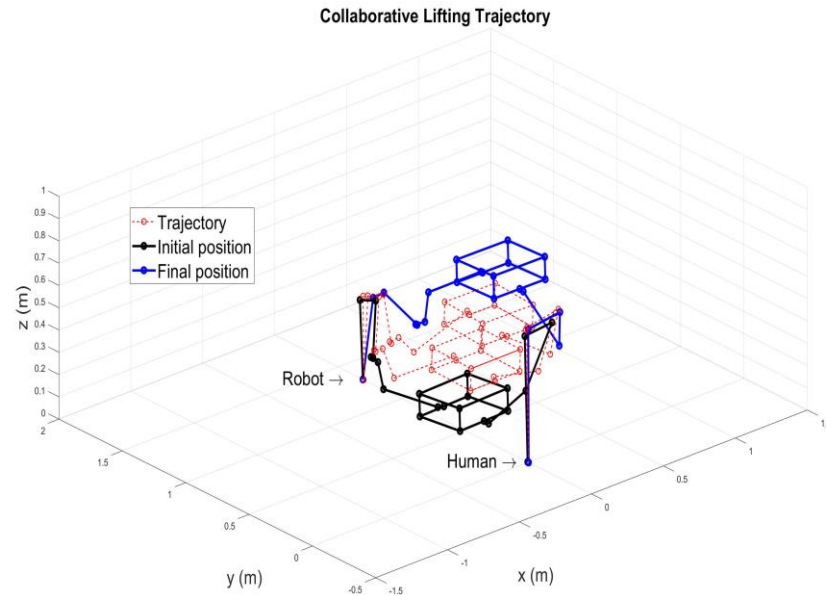
Human-robot Asymmetric Lifting Prediction

Asif Arefeen (OSU), and Yujiang Xiang

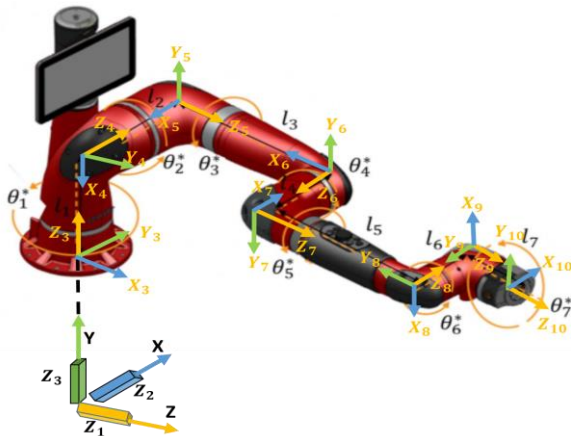
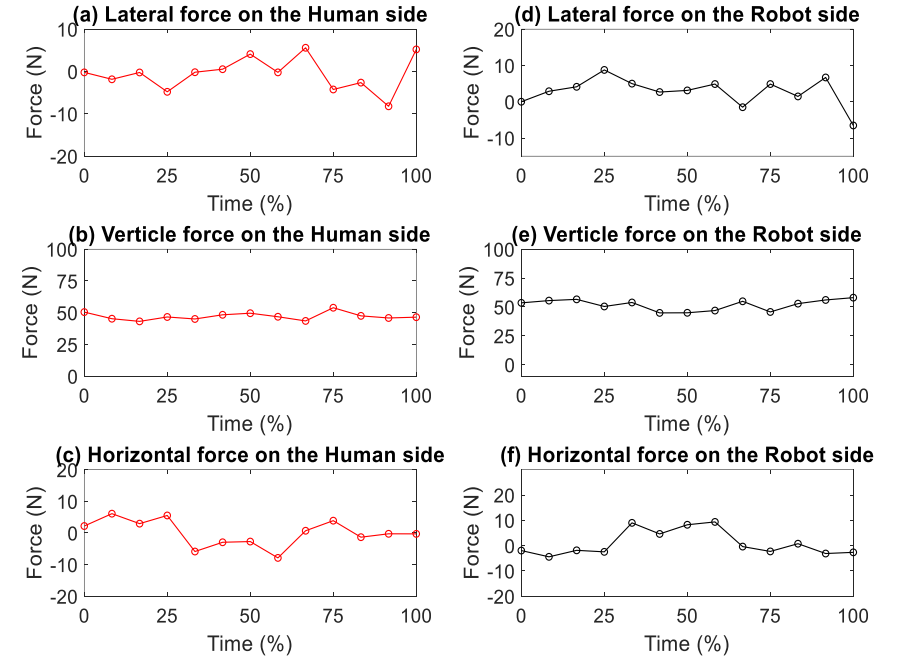
Human-robot model



Simulated lifting motion



Load sharing



Optimal solution and the lifting techniques can be adopted for preventing the human injuries.

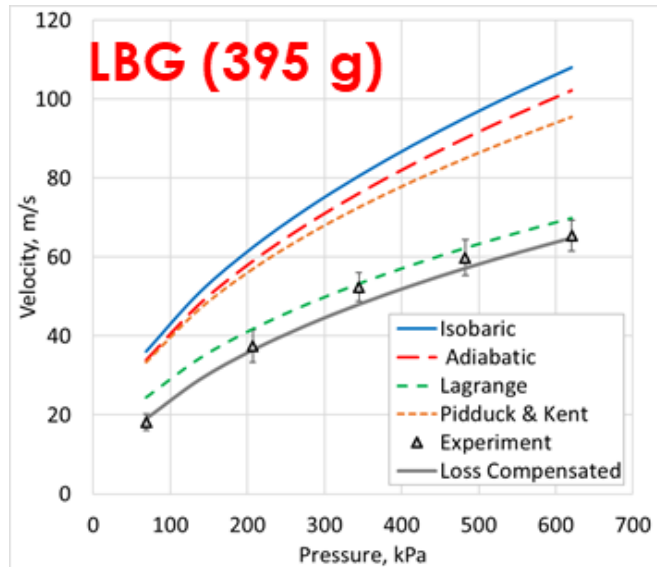
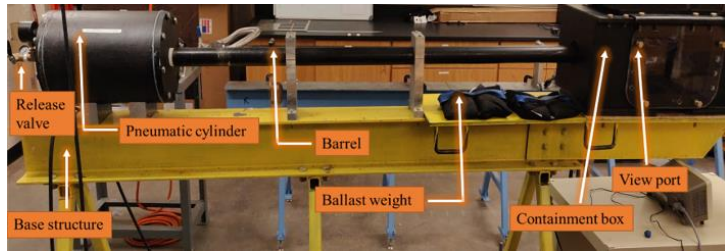


Ballistic Performance Evaluation of Carbon Graphite Foam and Nanoparticle-Kevlar Composites using Compressed-Air Guns

Muhammad Ali Bablu(OSU), James M. Manimala

Loss Compensated Model (LCM)

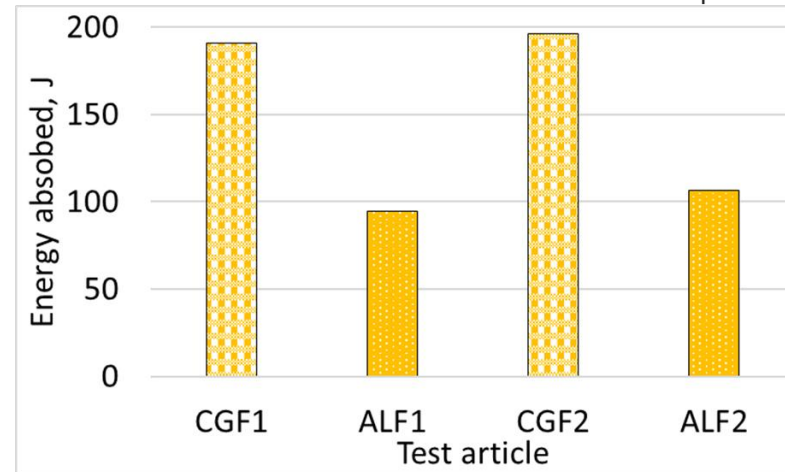
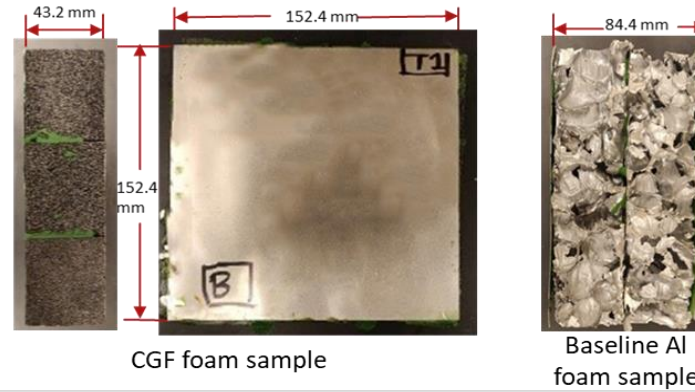
Builds upon Lagrange's model by including surface friction, air-drag and gas leakage losses



LCM yields better agreement with measured projectile velocities than classical models.

Carbon Graphite Foam (CGF)

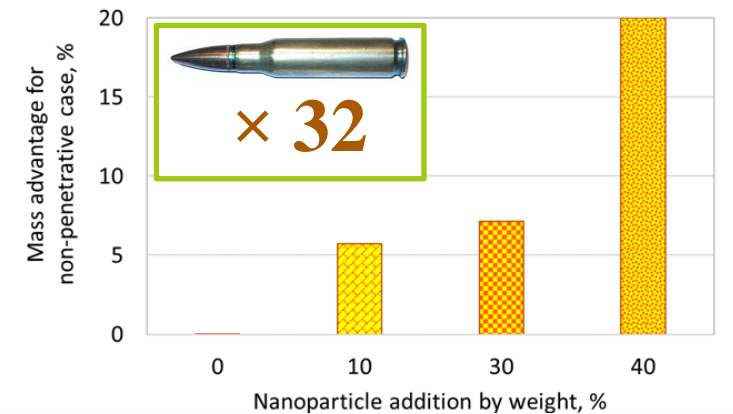
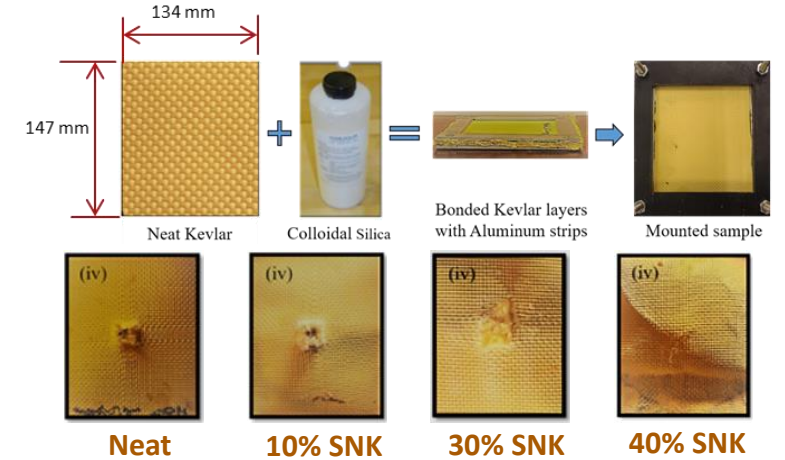
CGF has excellent thermal, mechanical and acoustic properties – How good is it for ballistic protection?



Energy absorbed by CGF is nearly double that of the mass-equivalent baseline Aluminum foam sample

Silica Nanoparticle-Impregnated Kevlar (SNK)

Can SNK deliver better specific ballistic performance than neat Kevlar?



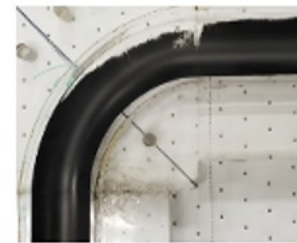
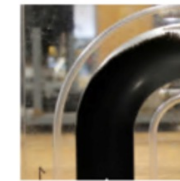
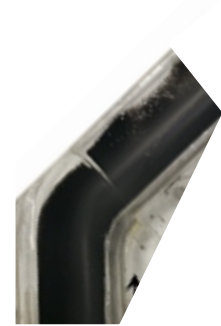
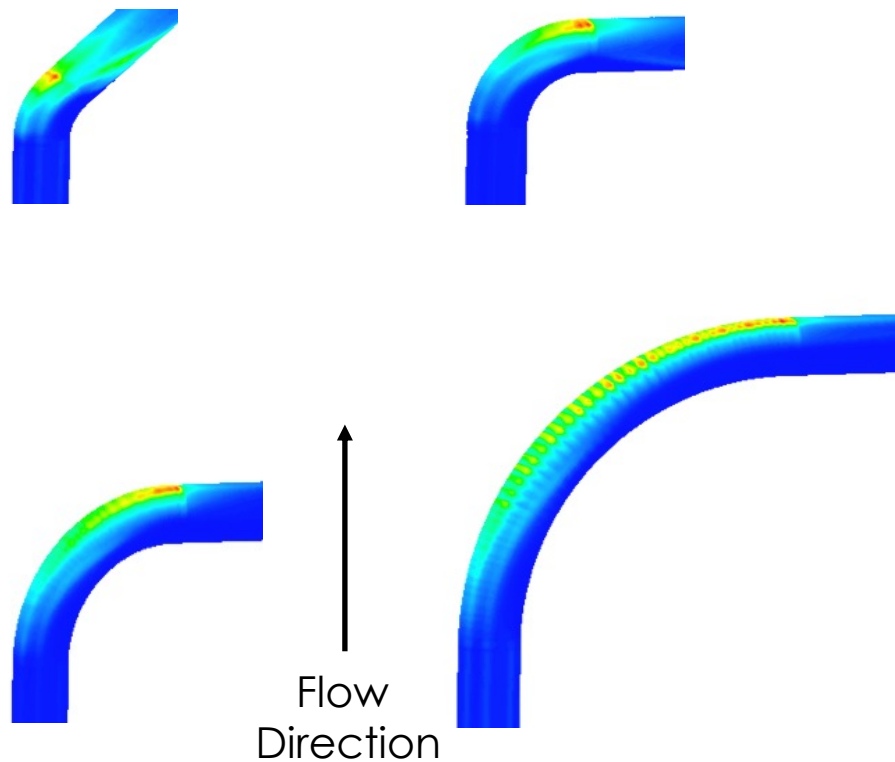
Compared to a standard Kevlar vest, 40 wt.% SNK gives a 20% mass advantage = 32 7.62x51 mm bullets!

The Effect of Solid Particle Erosion on Different Bends with Various Elbow Curvature Radii

Faris Bilal (TU), Thiana Sedrez, and Siamack Shirazi

Content for the online/live

one-minute presentation on April 3, 2021



Flow Direction



Why thermo-acoustics?

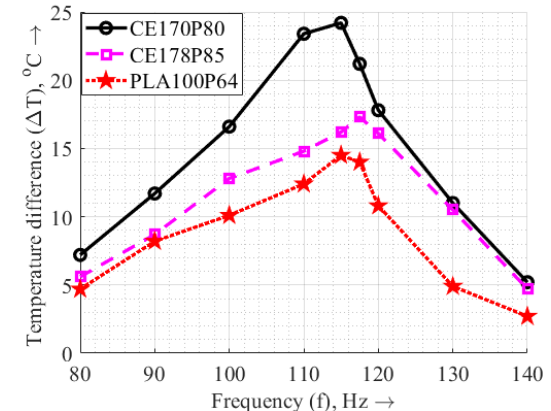
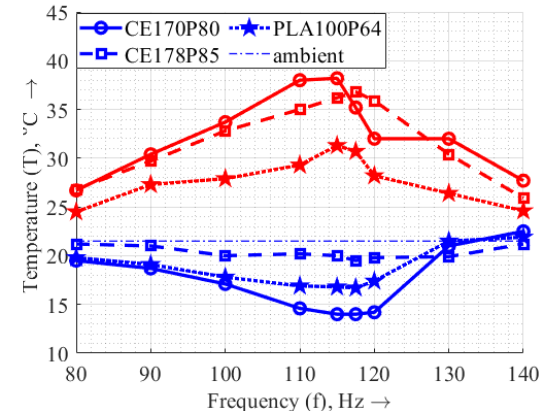
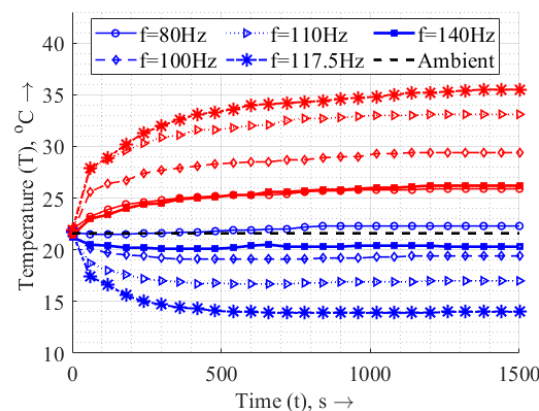
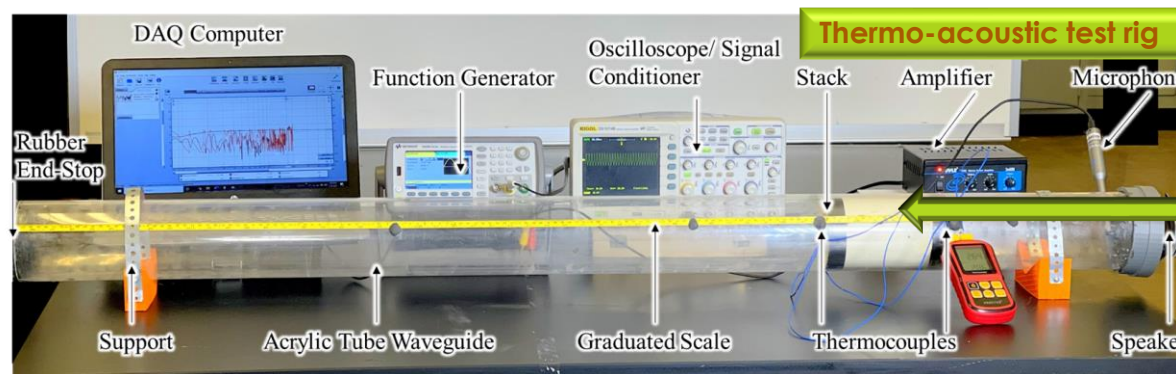
- Instability due to acoustic waves inducing oscillations in a porous stack, the ends of which manifest a temperature gradient [1]
- No combustion – Green energy
- No moving parts – Robust, durable design

Objectives

- Assess performance of additively manufactured polymer stacks vs ceramic stacks
- Determine influence of stack material, length, porosity, pore geometry and location on performance
- Correlate experimental data vs simulations using DeltaEC [2]

Experimental parameters

- Mean pressure, $P_m = 1 \text{ atm}$
- Mean temperature, $T_m = 21.5 \text{ }^\circ\text{C}$
- Resonator length, $L_R = 1524 \text{ mm}$
- Speaker SPL = $\sim 90 \text{ dB}$



Results

- Temperature gradient of **21.5 °C** at 117.5 Hz for the **ceramic stack**, CE170P80 and **14.5 °C** at 117.5 Hz for the **PLA stack**, PLA170P64
- **PLA stack** is observed to give **comparable performance** to the ceramic stack

Acknowledgements

- NSF RII Track-4 Grant No. 2033399
- Ray and Linda Booker Fellowship

[1] Rott, N. Zeitschrift für angewandte Mathematik und Physik ZAMP, Vol. 20, No. 2, pp. 230–243, 1969.

[2] Ward, B., Clark, J., Swift, G. DeltaEC, Version 6.4b2.7 Users Guide, 2017.

Introduction

Blast wave-induced damage to the inner ear is difficult to examine non-invasively. Finite element (FE) modeling provides a useful way to quantify the response of the inner ear to pressure waves. The current model changed the two-chambered straight cochlea of the previous model to a more anatomically accurate spiral shape.

Methods

1. Current FE model of the human ear consists of the ear canal, middle ear, and spiral cochlea with two chambers separated by the basilar membrane (BM).
2. A blast waveform was applied at the ear canal entrance, and the resulting pressures in the ear were calculated using a coupled Fluent and Mechanical simulation in ANSYS.

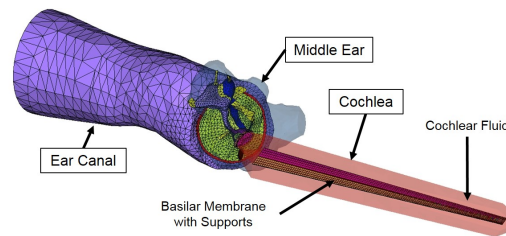
Conclusions

The low frequency BM displacement and transverse BM displacement observed only in the spiral cochlea model are caused by the spiral shape of the cochlea.

Work supported by DOD W81XWH-14-1-0228

Results

Previous FE Model



Current FE Model

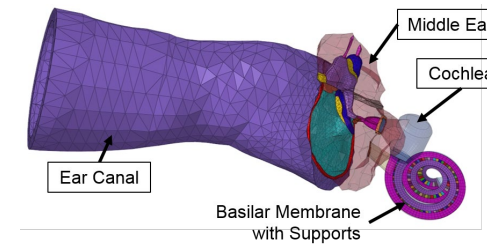


Fig 1. FE model of human ear with uncoiled two-chambered cochlea (left). FE model of human ear with spiral two-chambered cochlea (right).

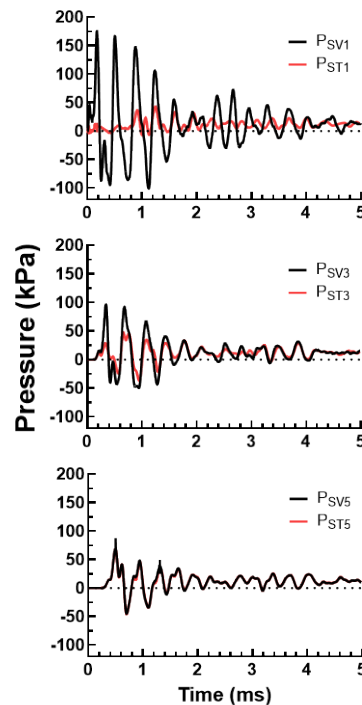


Fig 2. Cochlear pressures recorded in the scala vestibuli (black) and scala tympani (red) at 2.5, 18.0, and 28.25 mm from the base of the cochlea, respectively. Location of pressure monitors in the cochlea (bottom).

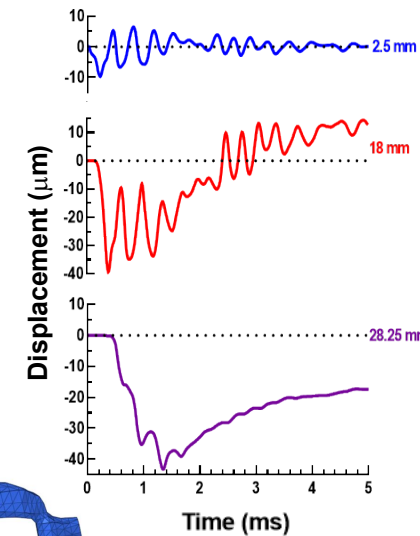
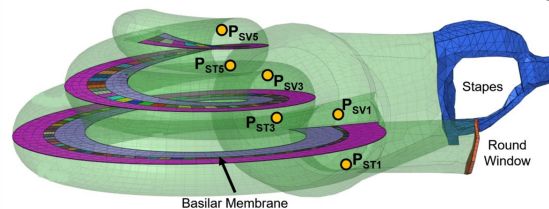


Fig 3. Basilar membrane (BM) displacement at 2.5, 18.0, and 28.25 mm from the base of the cochlea, respectively.

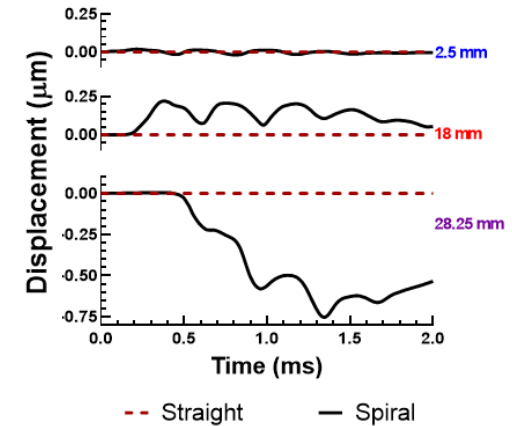


Fig 4. Basilar membrane (BM) transverse displacement in previous (dotted) and current (solid) model at 2.5, 18.0, and 28.25 mm from the base of the cochlea, respectively.

Inflow Analysis for Multi-Rotor Systems

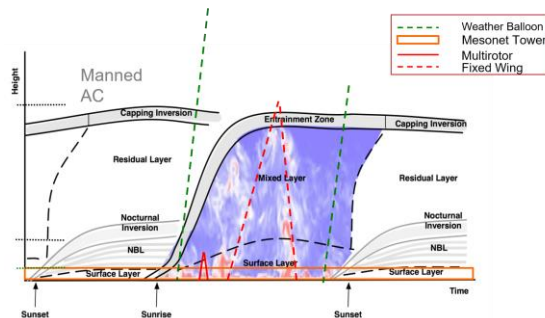
James Brenner(OSU)

Project Description



- The goal is to improve mapping of the lower level of the boundary layer which is where most weather activity starts.
- Using small multi-rotor systems equipped with weather sensors to gather data
- Sensitive sensors can be heavily affected by rotor wash
- This creates the need to analyze the flow-field of multi-rotors to determine the optimal sensor placement
- Conducted a Particle Image Velocimetry (PIV) experiment using a water-tunnel, examined flow for dual and quad rotor systems.

Mapping the ABL

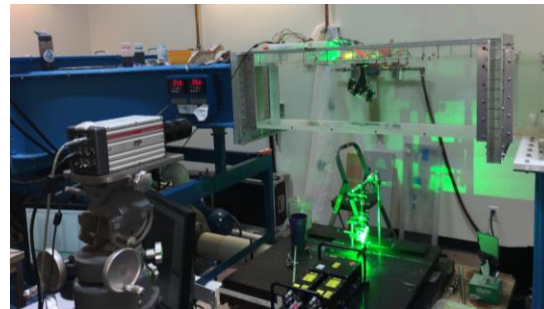


Experimental Setup

Quad Rotor Plus

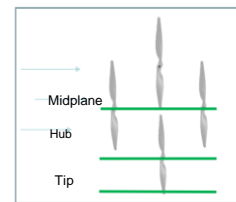


OSU Water Tunnel With PIV



Laser Planes Positions: Top to Bottom

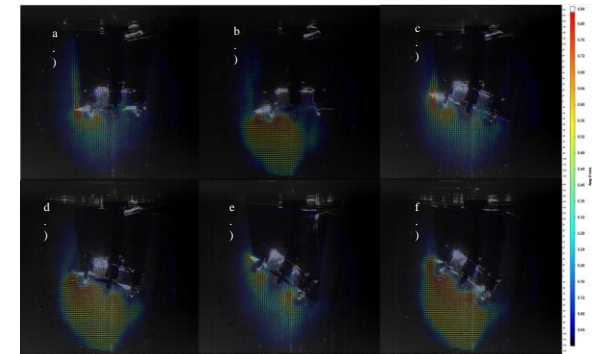
Quad Rotor Plus: Midplane, Hub, Tip



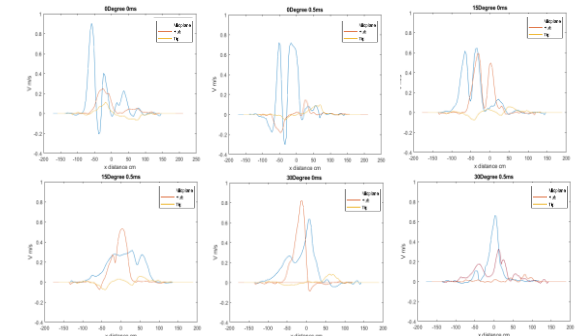
- 1/4 scaled down from DJI Phantom
- Quad-Frame diameter = 4in
- Propellor diameter = 3 in
- Circumference = 7 in
- Quad Rotor in the plus configuration

Results

Velocity Flow-Field Quad Rotor Midplane



Vertical Velocity Profiles Quad Rotor



Conclusions & Future Work

- Small dead region above rotor hub
- Optimal sensor placement is center of multi-rotor or outside of the flow-field
- In-flight testing comparison with system and tower comparison

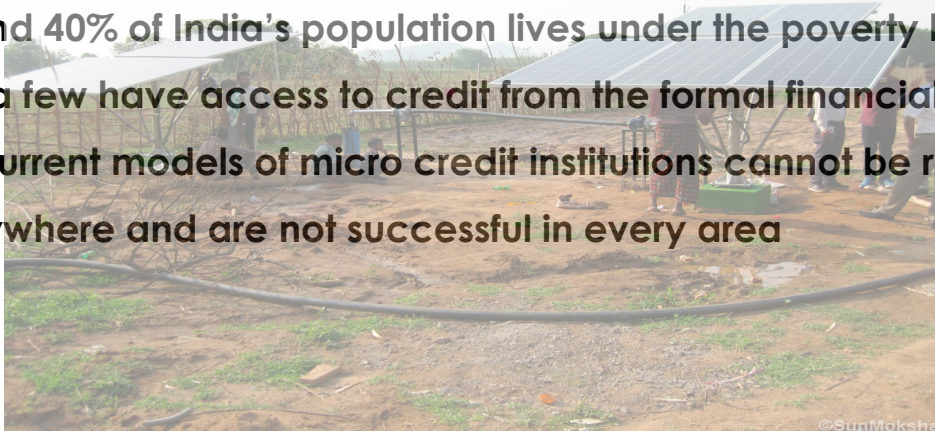
Promote Financial Inclusion in Small Villages in India

Allana Calvano, Lin Guo, Janet K. Allen, and Farrokh Mistree

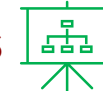
Background



- Around 40% of India's population lives under the poverty line, and only a few have access to credit from the formal financial sector.
- The current models of micro credit institutions cannot be reproduced everywhere and are not successful in every area



Questions



- How to create a business model that accounts for different villages and adapts to each culture?
- How to evaluate how much does the micro loan contribute to each villager's economic status?

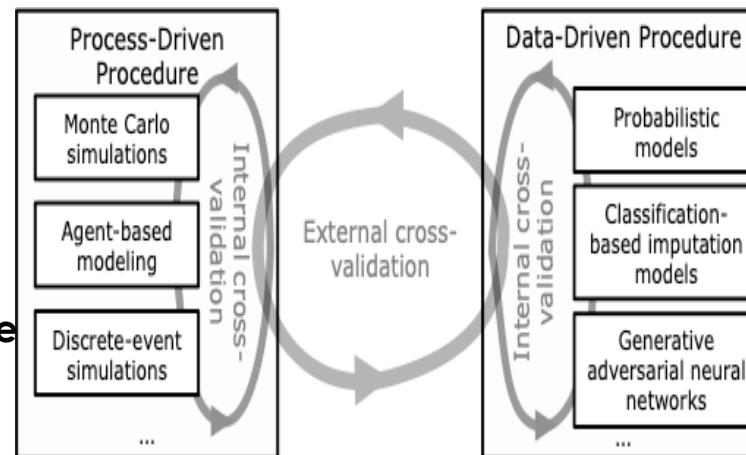


Method



Build a micro credit business model, focusing on:

- How to evaluate villagers' payment ability
- How to design the loan cycle and payment frequency



Results & Analysis

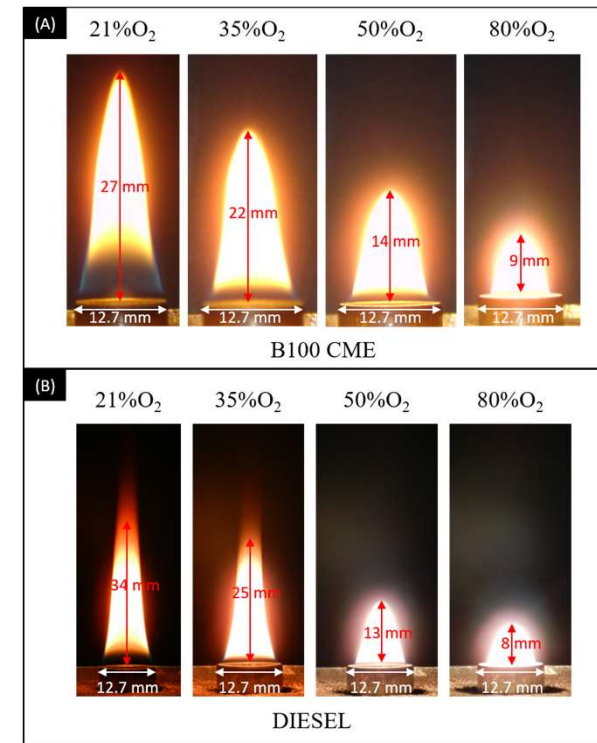
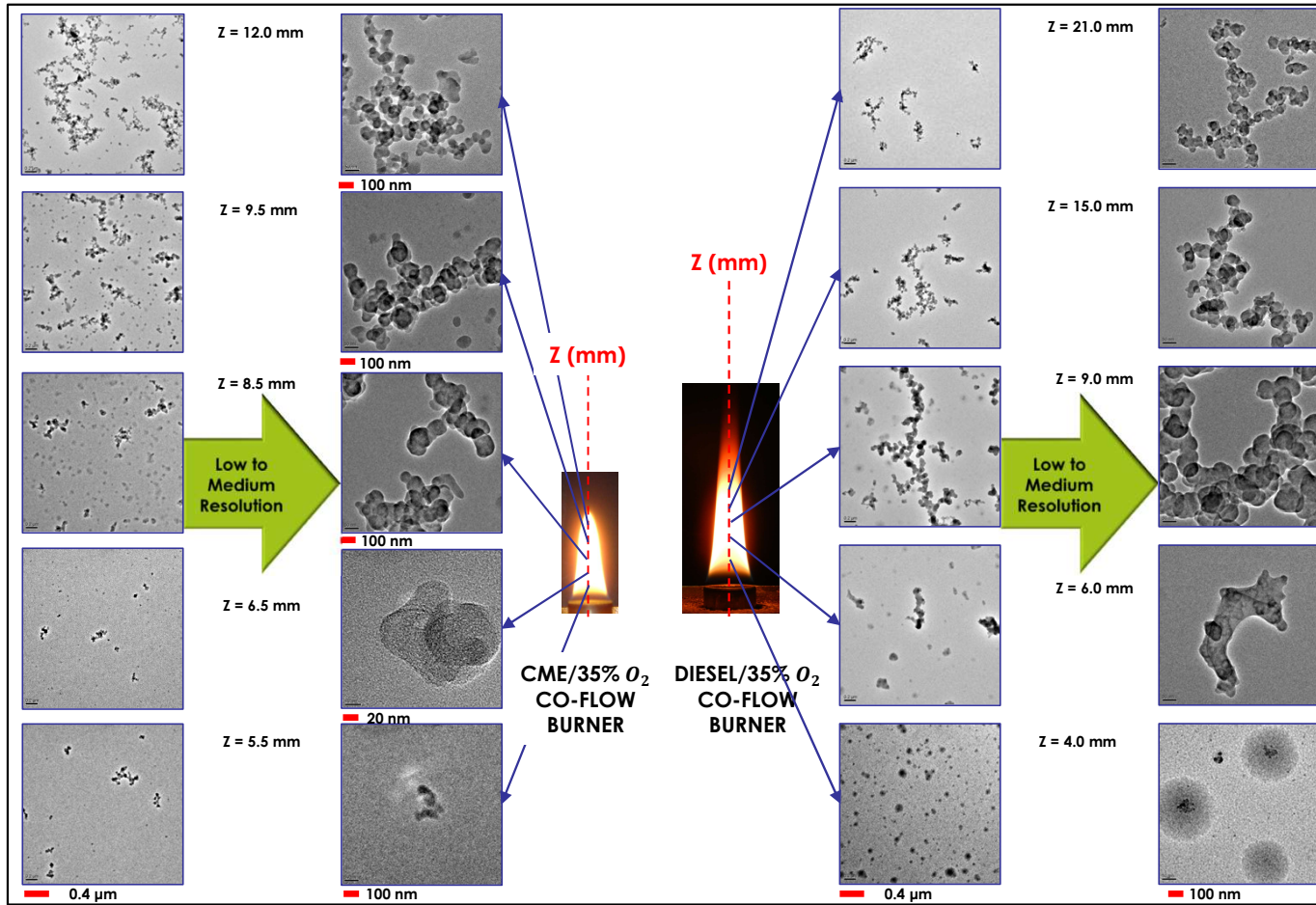


- A standardized data preprocessing method to quantify villagers' payment ability
- A product family of micro loans supporting Agriculture 4.0



Soot Formation in Biodiesel-Oxygen Enriched Air Laminar Diffusion Flames

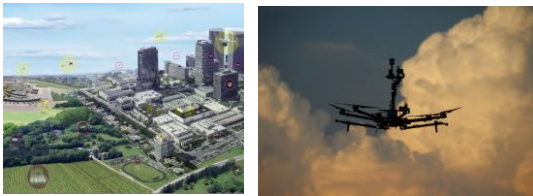
Stephanie Prado Carbonell (OU) and Wilson Merchan-Merchan (OU)



Introduction

1) Motivation

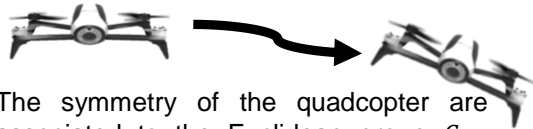
- Improve quadcopter state estimation and flight performance
- Atmospheric measurements for environmental studies and meteorology



2) Four approaches for wind estimation

- Mounting sensors on aircrafts
- Static mapping method
- Machine Learning method
- Model-based method

3) Symmetry and Lie group



The symmetry of the quadcopter are associated to the Euclidean group $G = SE(3)$ which consists of rotations and translations in dimension 3 represented as (x_g, q_g) .

Problem Formulation

1) Quadcopter system dynamics with wind drag model

$$\begin{aligned} \dot{x} &= q * v * q^{-1} + Cd \\ \dot{v}_r &= v_r \times \omega + q^{-1} * A_{gr} * q - \frac{1}{m} f_c b_3 + \frac{1}{m} f(v_r) \\ \dot{q} &= \frac{1}{2} q * \omega \\ \dot{d} &= Ad \end{aligned}$$

States:

- x - position
- v_r - relative velocity
- q - unit quaternion matrix
- d - disturbance

where * is quaternion multiplication

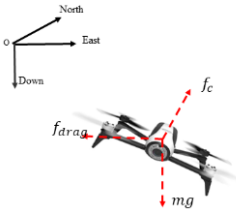
Inputs:

- ω - angular velocity
- f_c - control thrust
- D - drag coefficient matrix

Drag model

$$f_{drag} = f(v_r) = -\frac{1}{2} \rho D |v_r| v_r$$

$$D = \begin{pmatrix} D_x & 0 & 0 \\ 0 & D_y & 0 \\ 0 & 0 & D_z \end{pmatrix}$$



Wind model

$$\dot{d} = Ad, v_w = Cd$$

Measurements Sensor model

$$y = \begin{pmatrix} x \\ a \\ q^{-1} * B * q \end{pmatrix} \quad \begin{aligned} y_{x_m} &= x + \sigma_x \\ y_{a_m} &= a + \sigma_a \\ y_{b_m} &= q^{-1} * B * q \end{aligned}$$

We assume quadcopter is equipped with a GPS, a 3-axis accelerometer and gyroscope, and a magnetometer.

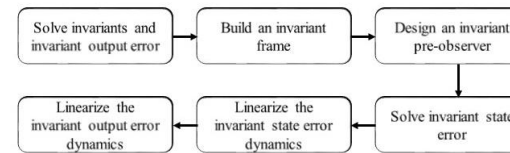
IEKF Design

1) Invariance of the dynamics and equivariance of measurements

$$\varphi_g(X) = \begin{pmatrix} x + x_g \\ q_g * v_r * q_g^{-1} \\ q * q_g^{-1} \\ d \end{pmatrix}, \quad \psi_g(U) = \begin{pmatrix} q_g * \omega * q_g^{-1} \\ q_g * f_c b_3 * q_g^{-1} \end{pmatrix}$$

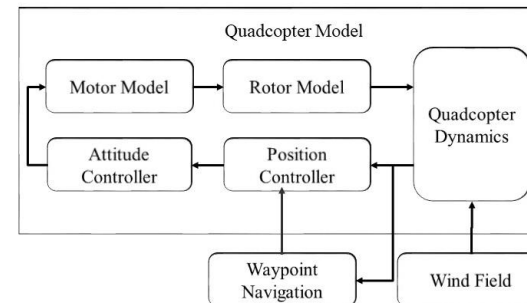
The system is invariant and measurements are equivariant with respect to the above transformations.

2) How to design an IEKF?

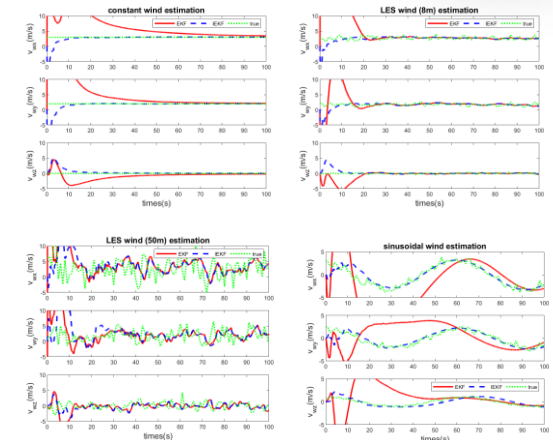


Simulation Results

1) Quadcopter Simulink model



2) Wind estimation



The simulation results show that **the estimation performance of IEKF converges more quickly and produces less error during the transient part.**

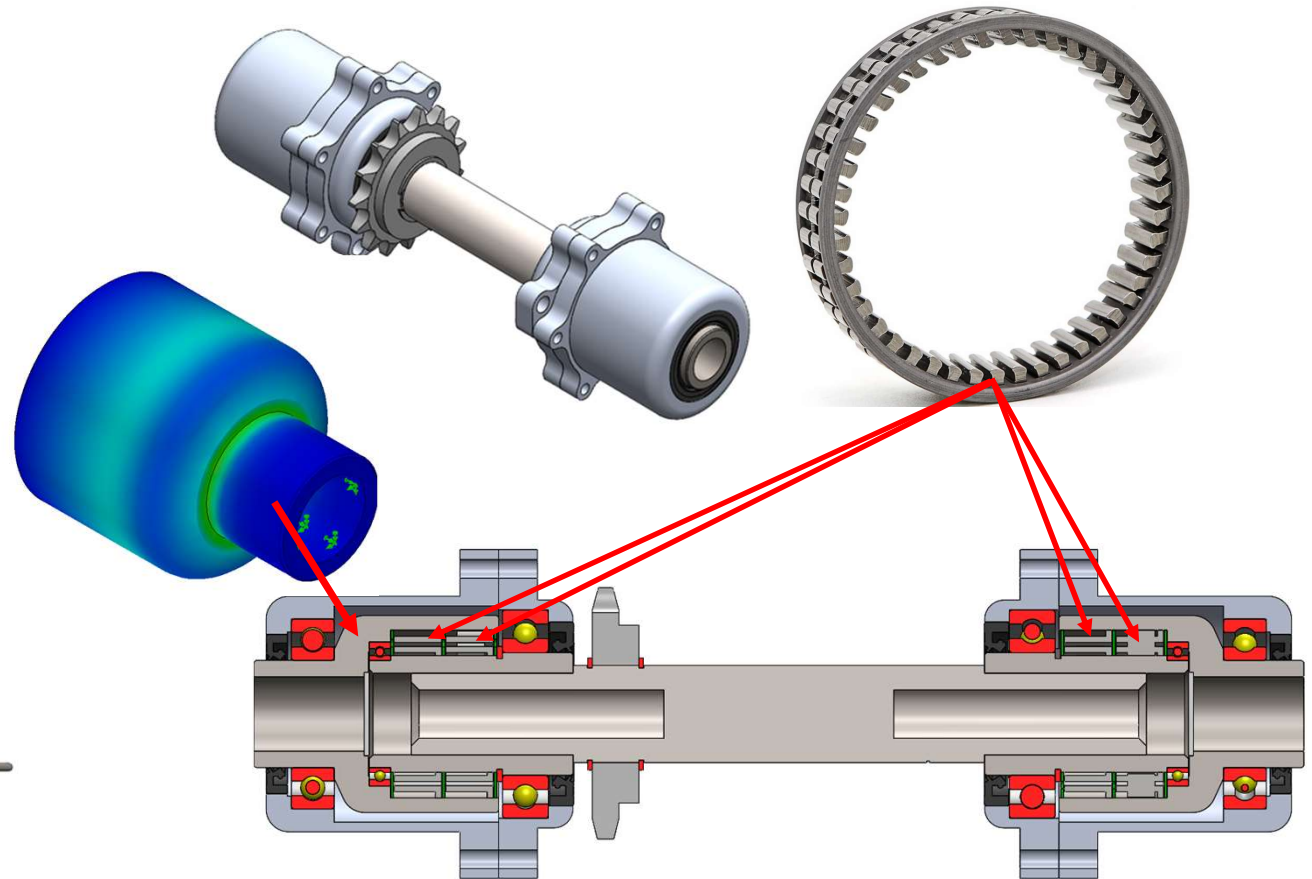
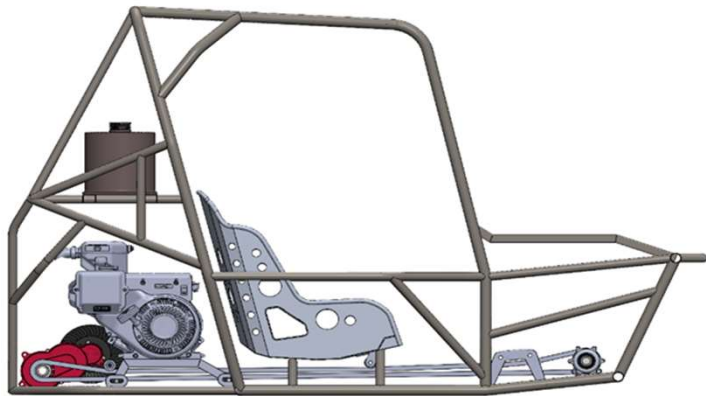
Future Work

Future works includes

- ❖ Examining the robustness of the IEKF against uncertainties in drag model.
- ❖ Experimental validation on a real quadcopter platform.

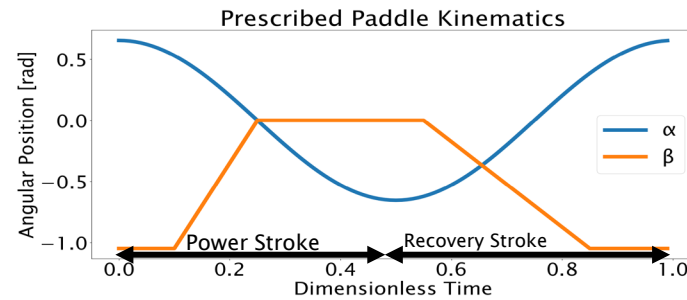
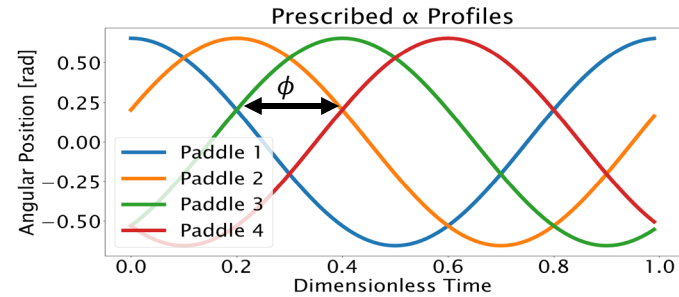
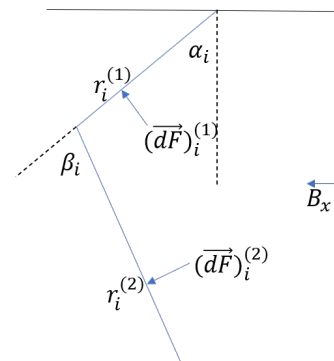
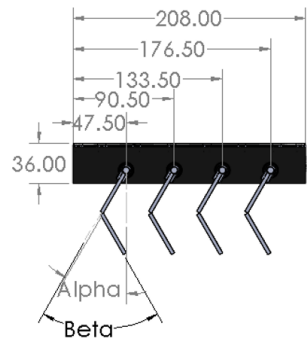
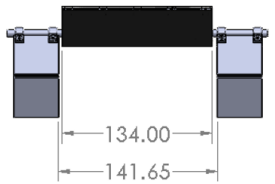
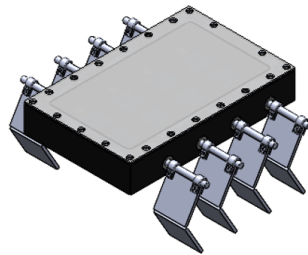
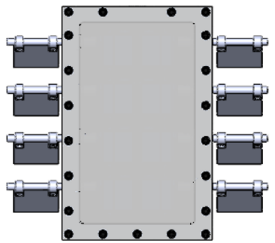
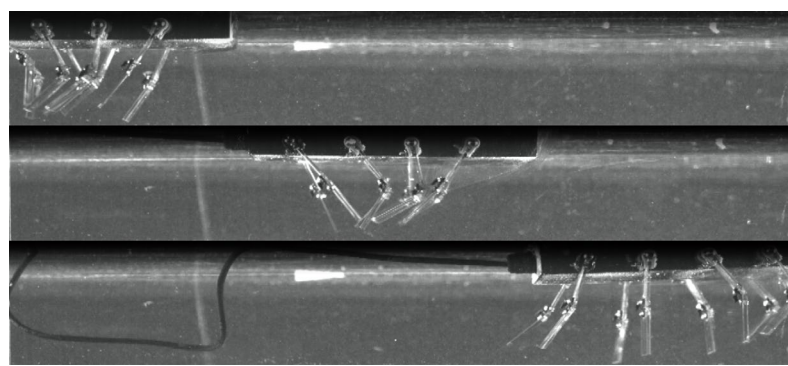
Front Differential Research Project — Sooner Off-Road Team

Brenden Chenoweth, Joseph Grimes



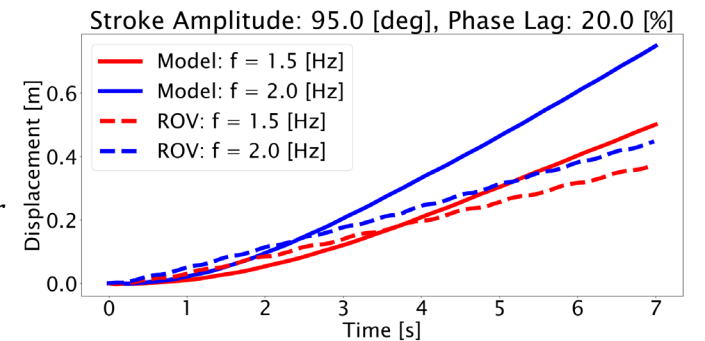
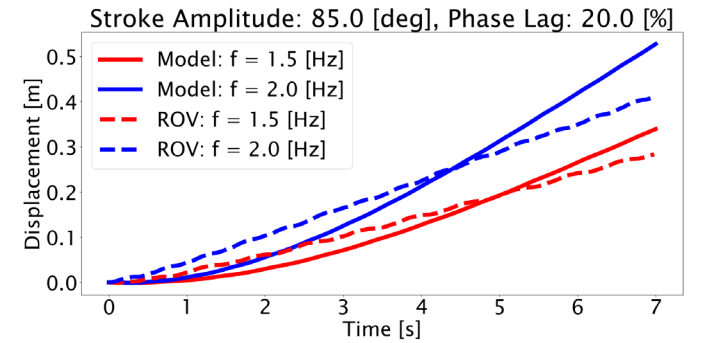
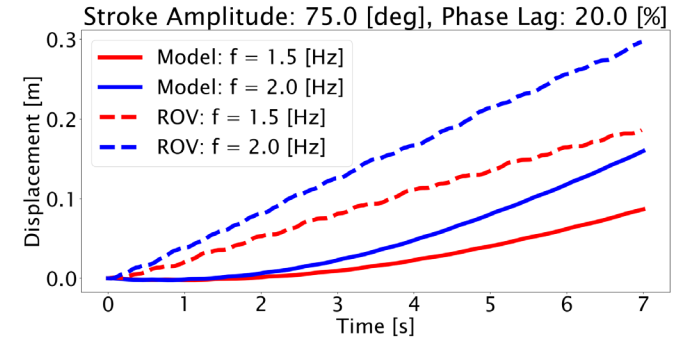
A Newtonian Model of Drag-Based Metachronal Swimming

Diego Colón (OSU), Mitchell P. Ford (OSU), and Dr. Arvind Santhanakrishnan (OSU)



$$\ddot{x} = \vec{F}_{ba}(\dot{x}) + \sum_i \sum_j (\vec{F}_i^{(j)}(A, f, \varphi, t))_x$$

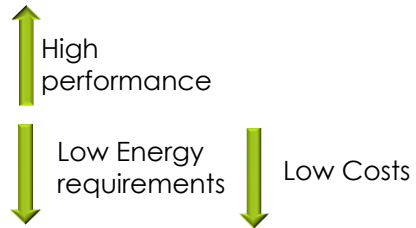
$$d\vec{F}_i^{(j)} = -\frac{1}{2} C_d \rho \omega (\vec{\omega}_i^{(j)} \times \vec{r}_i^{(j)}) \left| \vec{\omega}_i^{(j)} \times \vec{r}_i^{(j)} \right| dr$$



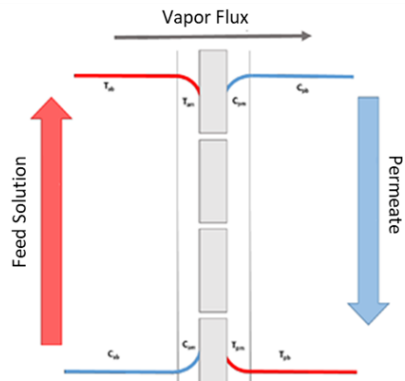
Membrane Distillation Process and High Salinity Water Desalination

Bruno da Silva, Khaled Sallam, Cristiano Borges and Fabiana da Fonseca

High Salinity Water desalination challenges

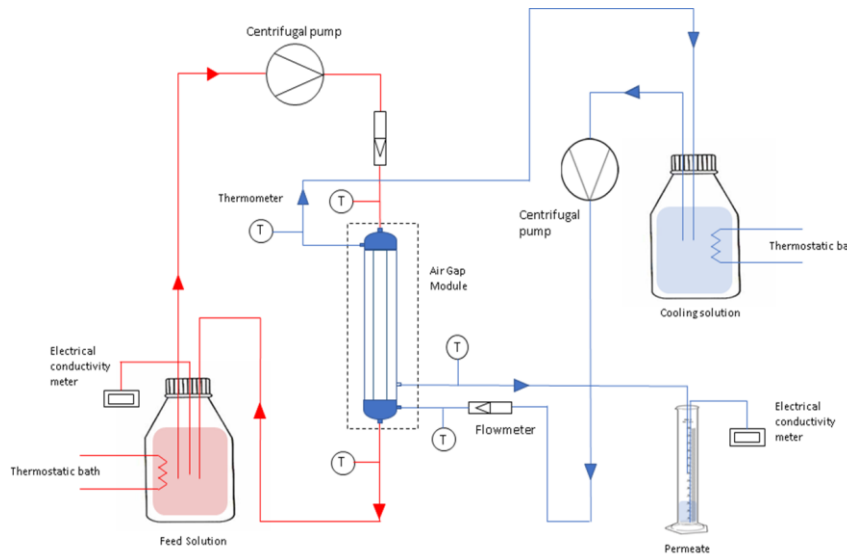


Membrane Distillation



What about the Energy ?

- Renewable Heat resources
- Solar Energy
 - Geothermal Energy
 - Waste Energy



Operational Parameter Evaluated

- Salt concentration (Raw seawater and NaCl solution 70 ppt)
- Feed temperature (Min: 55°C Max: 70°C)
- Cooling temperature (Min: 15°C Max: 25°C)
- Feed flow rate (Min: 40L/h Max: 120 L/h)
- Water quality (Salt Rejection)

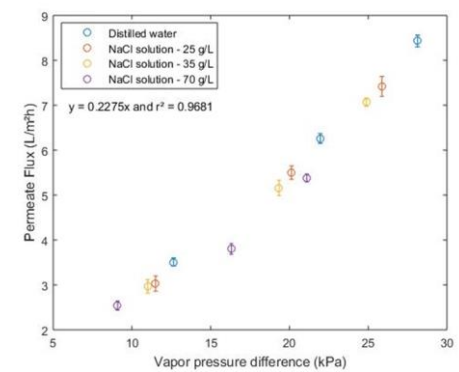
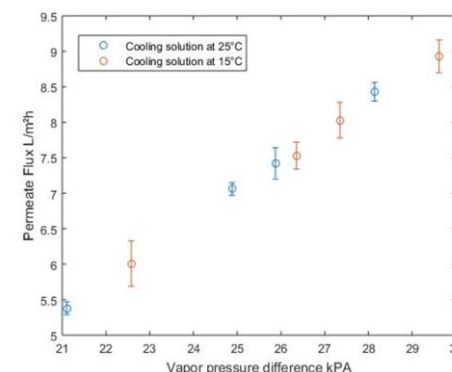
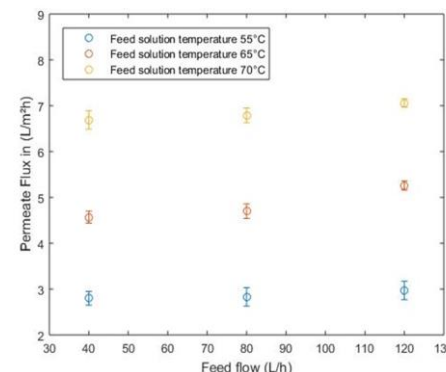
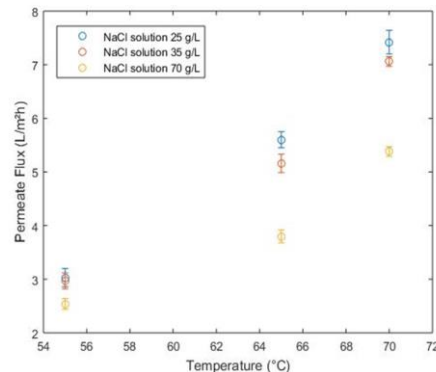
- ↓ Low concentration sensibility
- ↑ High temperature sensibility

Global Salt rejection on NaCl solutions

99.9%

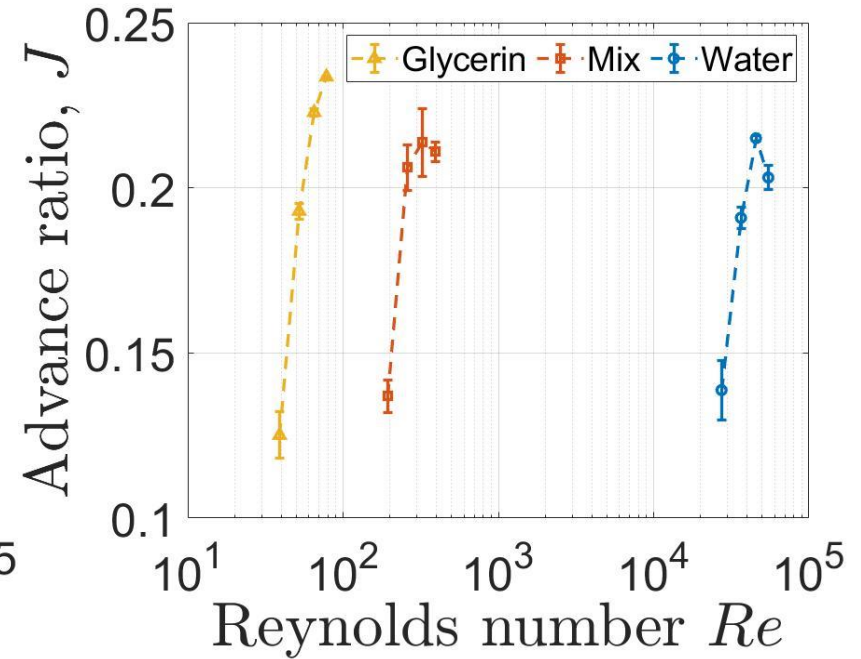
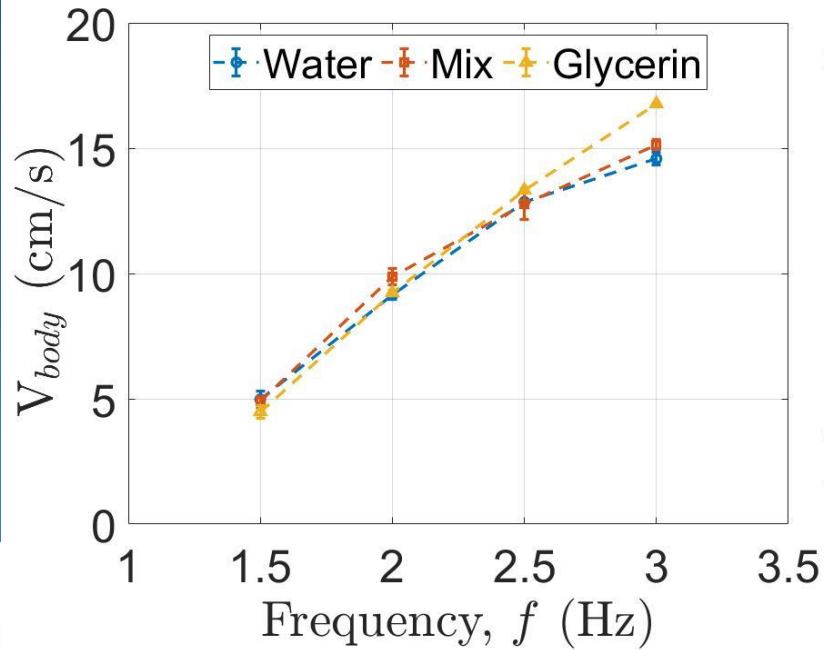
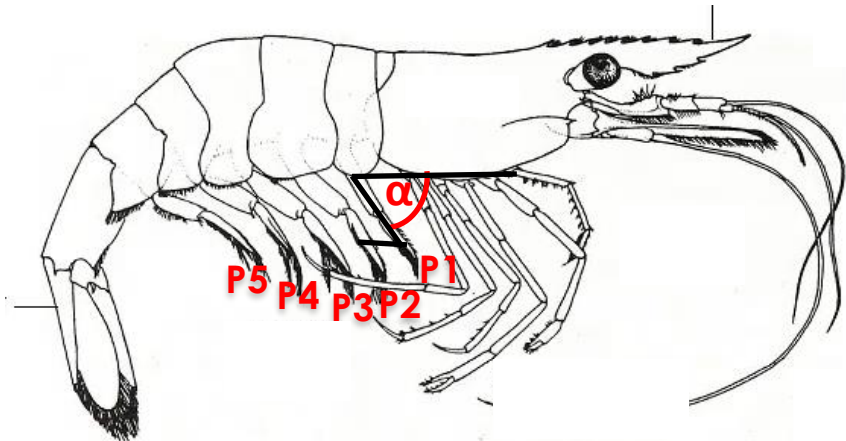
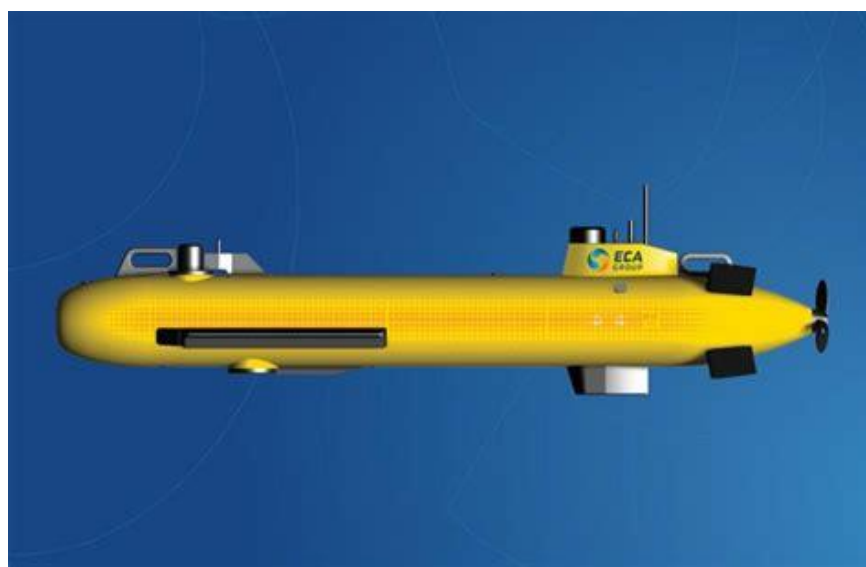
Global Salt rejection on raw seawater

98.5%



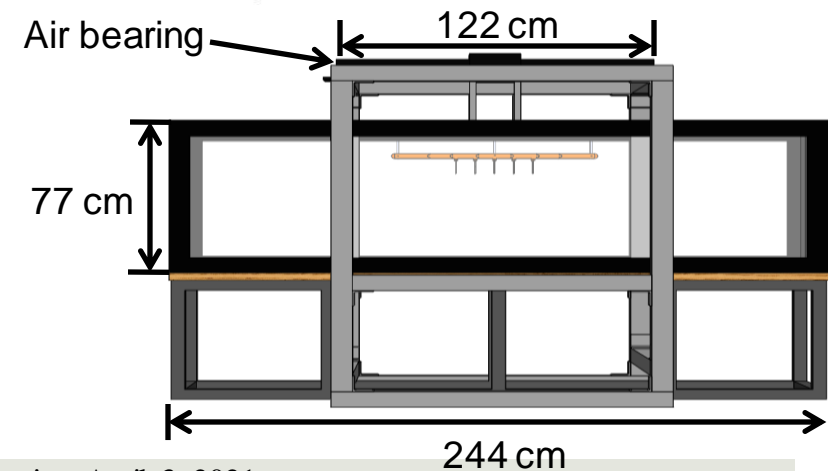
Reynolds Number Dependence on Metachronal Swimming Performance

Erika DiLuca (OSU), Mitchell Ford, and Arvind Santhanakrishnan



$$Re = \frac{2\theta fL \cdot L}{\nu} \quad J = \frac{V_{body}}{2\theta fL}$$

V_{body} = swimming speed
 θ = stroke amplitude (radians)
 L = length
 ν = kinematic viscosity
 f = frequency



This work was supported by the Lew Wentz Foundation at Oklahoma State University (Wentz Research Scholarship to E.D.) and the National Science Foundation (CBET 1706762 to A.S.).

Active Throttle Control in Small Hybrid Unmanned Aircraft

Carson Elmore (OSU), Dr. Kurt Rouser, Ph.D (OSU), and Jonathan Burgess (OSU)

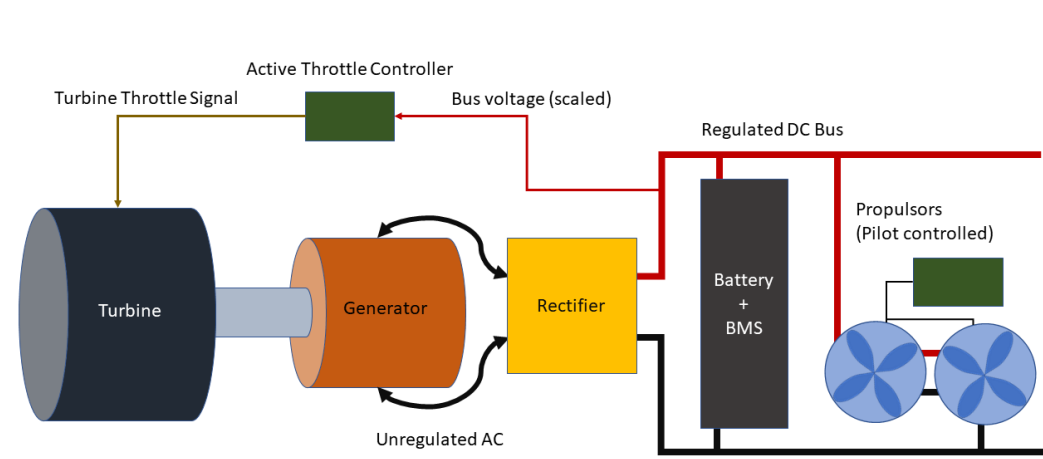
Background

Characterize hybrid turboelectric systems to establish advantages and trade-offs.

- Range improvement over battery UAS
- Distributed propulsor layouts
- Determine safety requirements

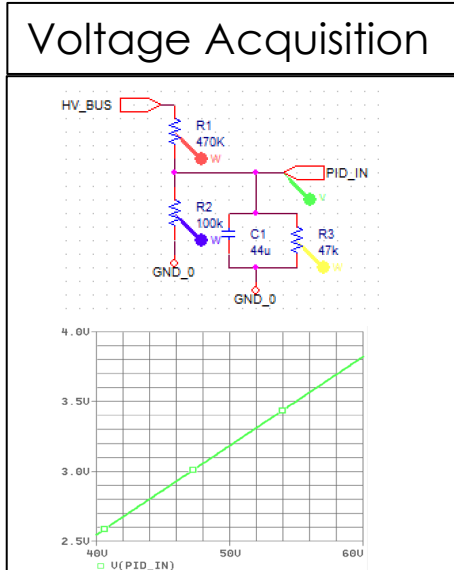
Goal

Our completed active automatic throttle control allows the pilot to control one or more electric propulsors while the turbine provides consistent high-amperage power.



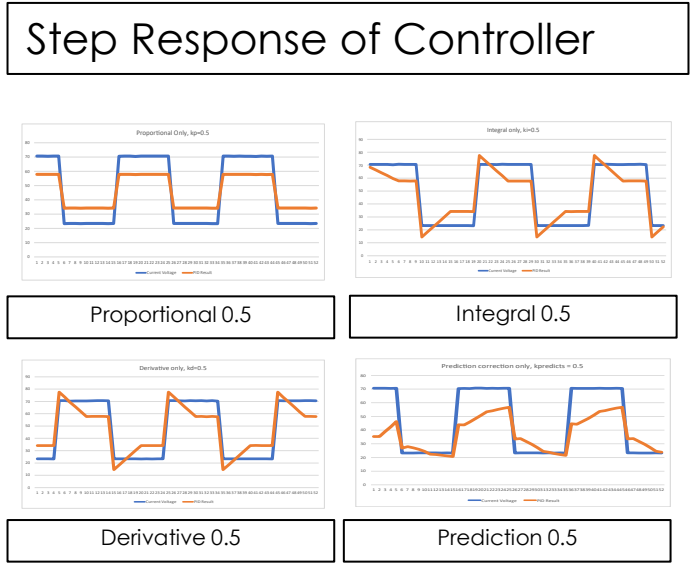
Method

Divided voltage from target bus to TTL levels (Linear in target range)
 Programmed PID controller with adjustable history length
 Controller uses executives to handle safety monitoring and turbine control at separate rates
 Matches turbine response rate (2Hz)



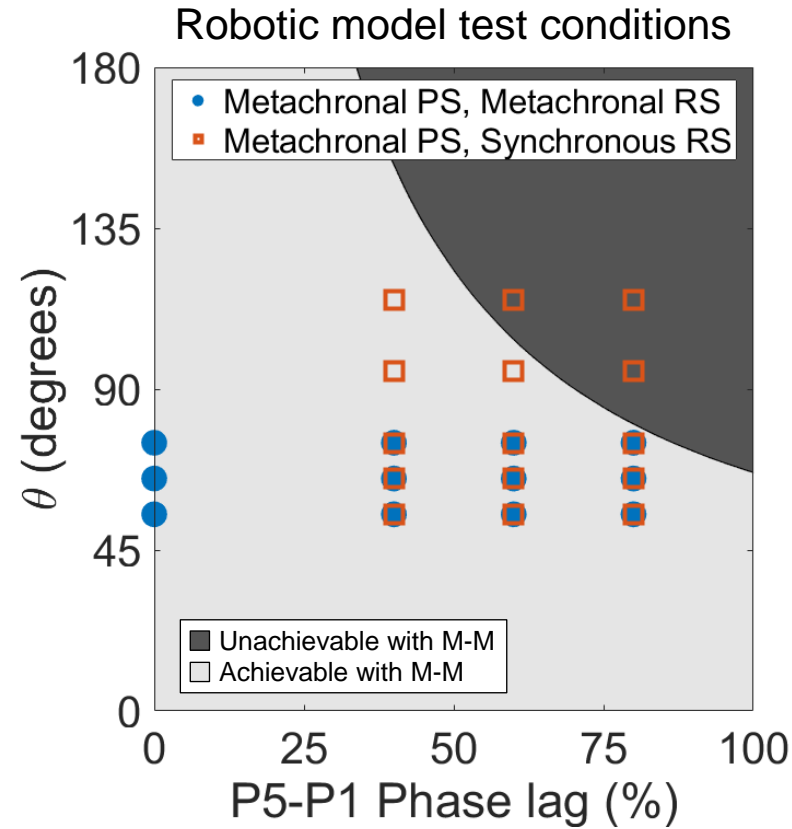
PID Parameters

The controller stores old values of error and their integrated trend to compute an output. It also compares the last prediction to the actual value to improve accuracy. History is weighted by distance to improve response.

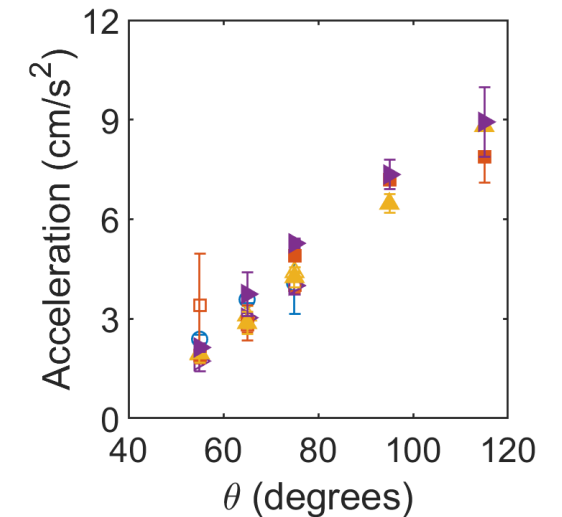
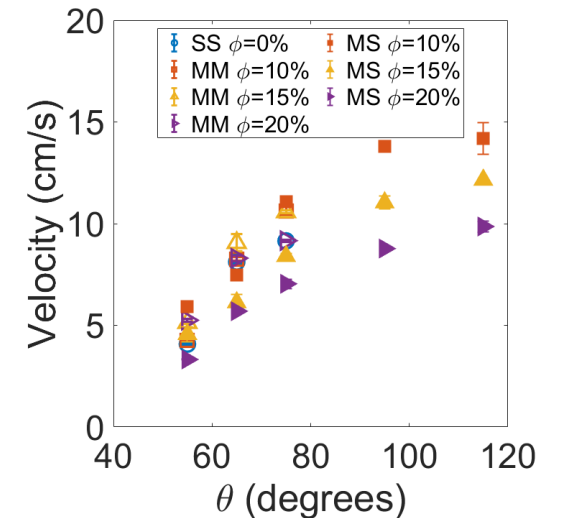


Metachronal, Synchronous, and Hybrid Kinematics in Aquatic Paddling

Mitchell Ford (OSU), Erika DiLuca, and Arvind Santhanakrishnan

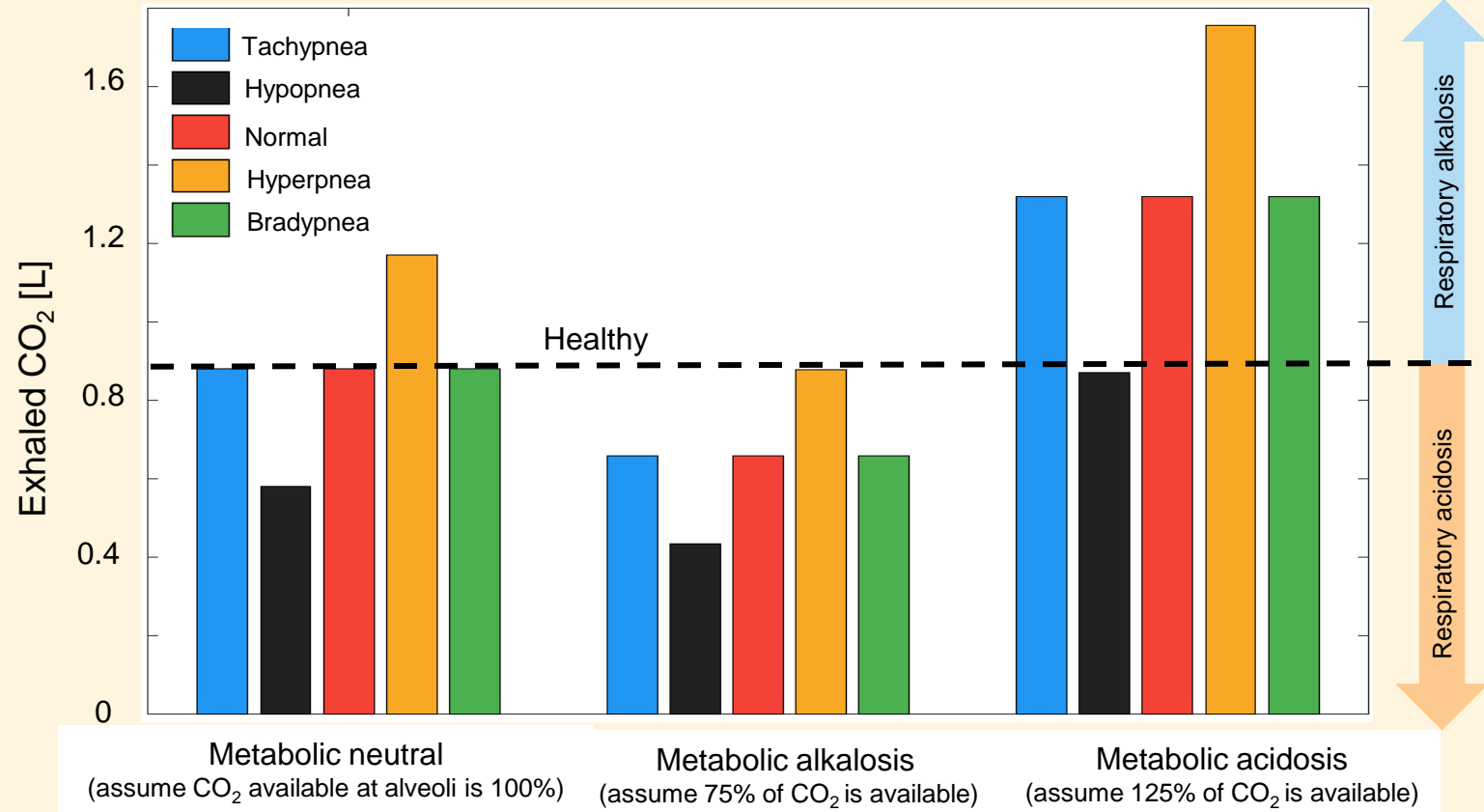
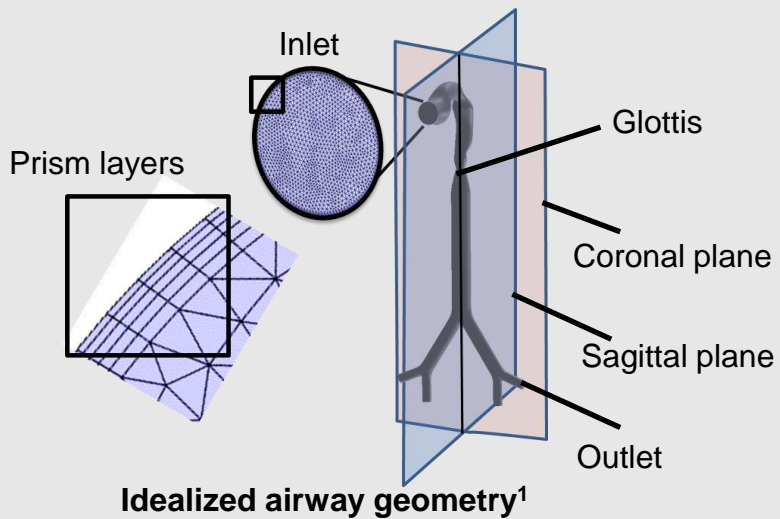
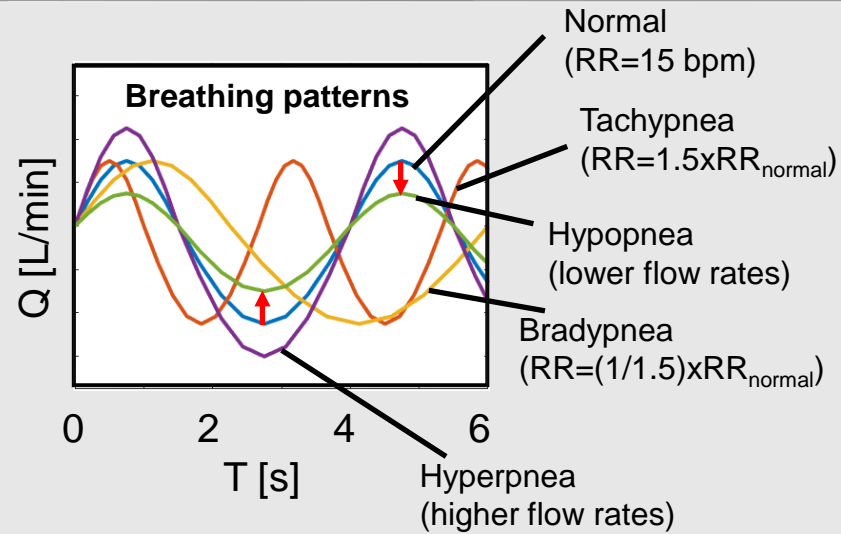


PS = Power stroke ϕ = Phase lag (adjacent paddles)
 RS = Recovery stroke θ = Stroke amplitude
 SS = Synchronous stroke P1 = First paddle
 MM = Metachronal stroke P5 = Last paddle
 MS = Metachronal PS Synchronous RS



Fluid Dynamics of Abnormal Breathing Patterns in Idealized Human Airways

Manikantam Gaddam (OSU) and Arvind Santhanakrishnan



RR=respiratory rate, T=breathing time=60/RR, Q=air flow rate, bpm=breaths per minute

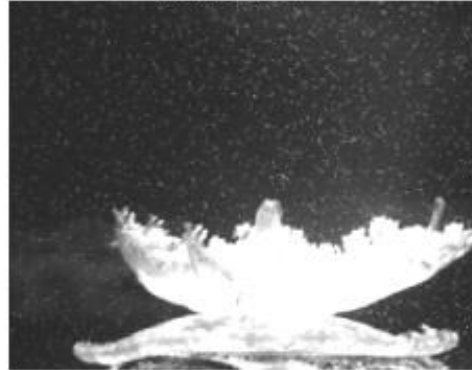
¹Feng et al. (2016), *J. Aerosol Sci.*, 96, 96-123.

Feeding Currents of Upside-Down Jellyfish

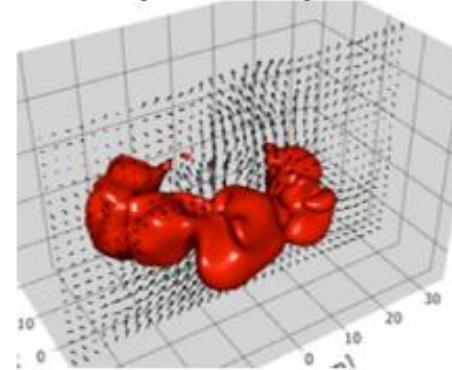
Nicolas George, Manikantam Gaddam and Arvind Santhanakrishnan



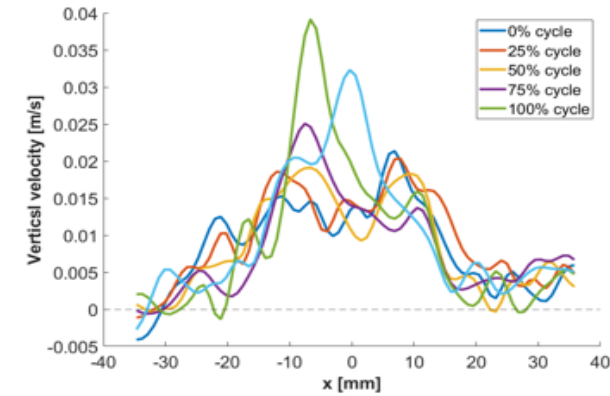
Raw Data



Isovorticity on velocity vector field

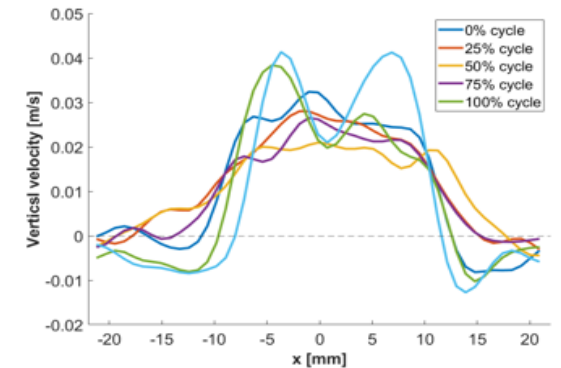


Back view with oral arms
 $y/d=0.8$ above medusa

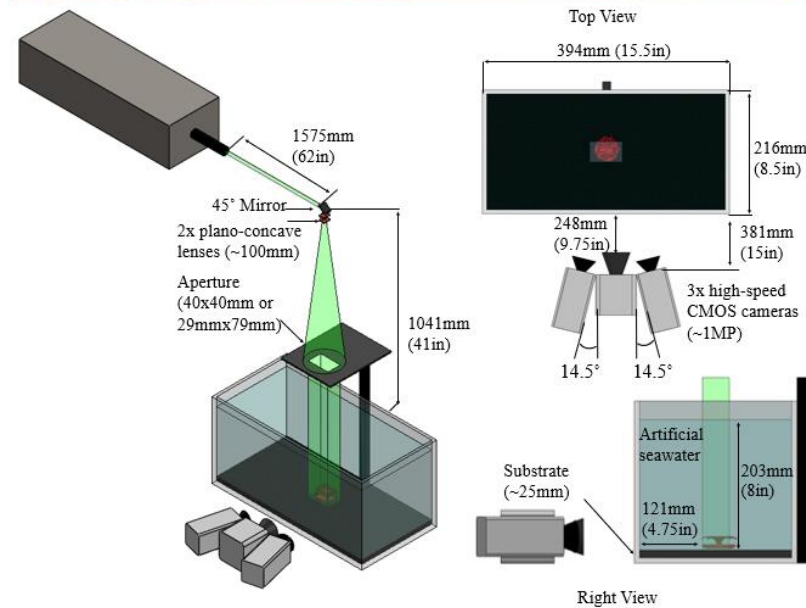
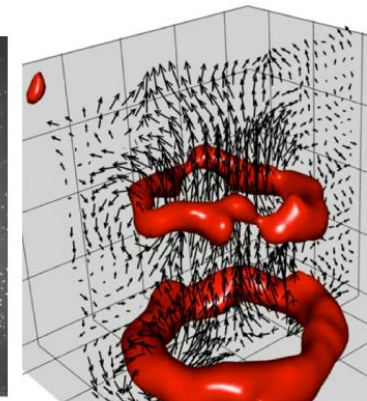


$d=5$ cm bell diameter

Without oral arms
 $y/d=0.8$ above medusa



$d=2$ cm bell diameter



Supported by NSF CBET 1916061

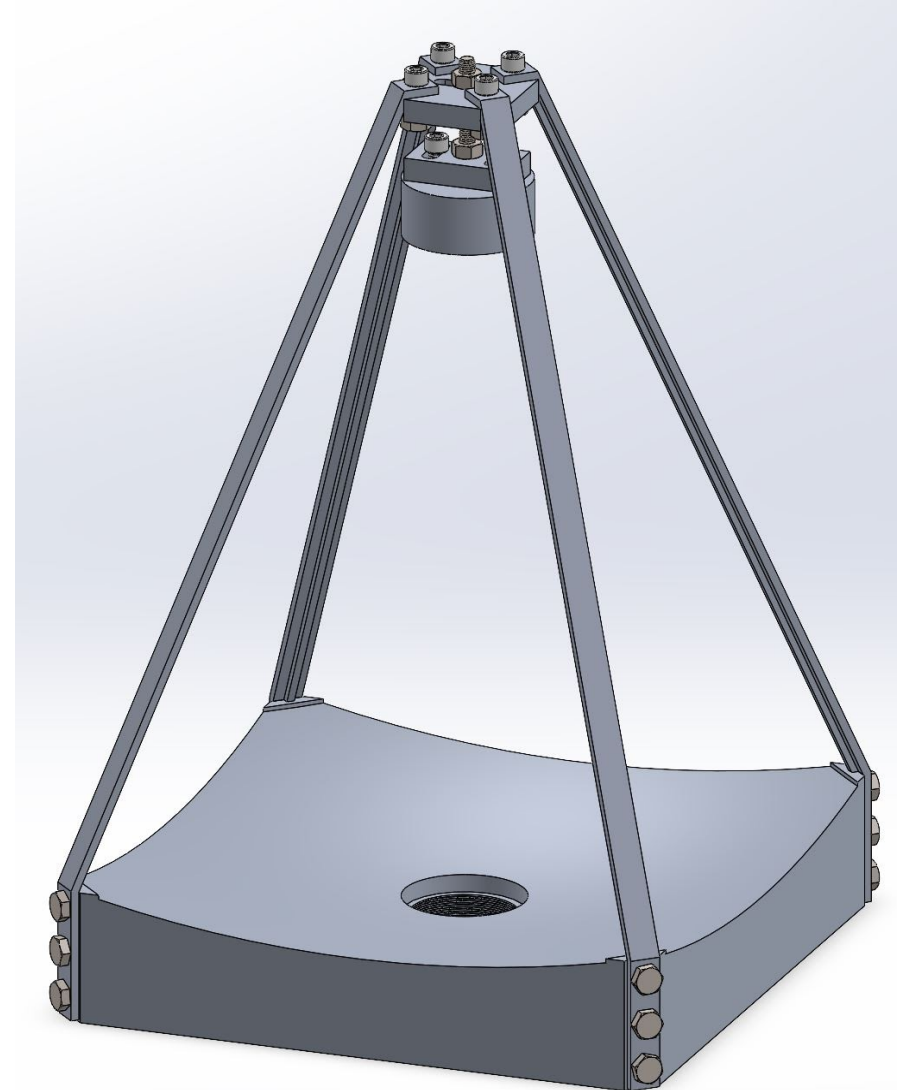
LuXsine Solar Heater

Isaac Fulton (ORU), Michael Guffey, Blake Jackson, and Samuel Nelson

The LuXsine solar heater is a solar energy technology that provides effective and efficient conversion of solar flux into mechanical heat energy.

The apparatus is designed as a two-mirror system that reflects and concentrates solar flux into a piping system which allows the solar flux heat energy to be transferred to a thermal fluid. The fluid can then be used in all manner of ways, such as heating a house.

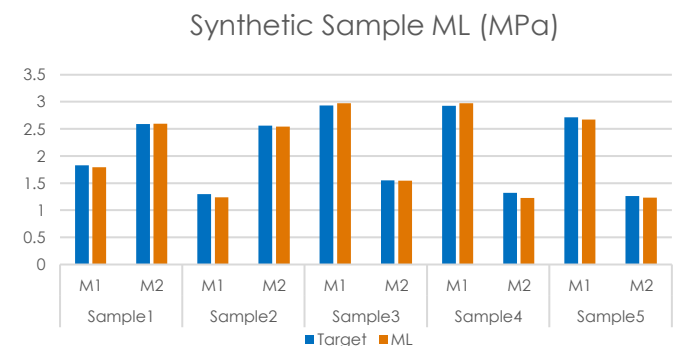
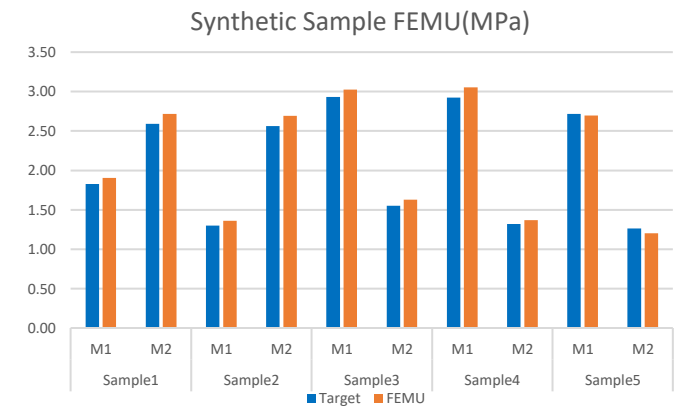
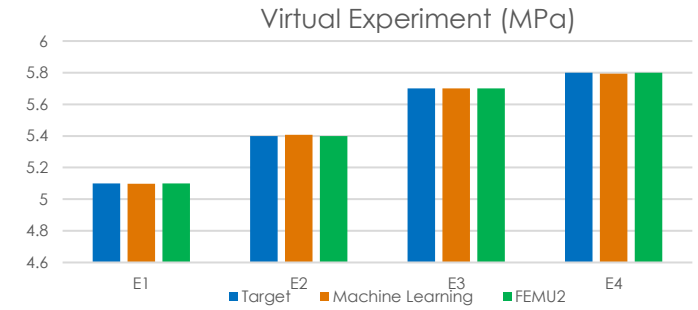
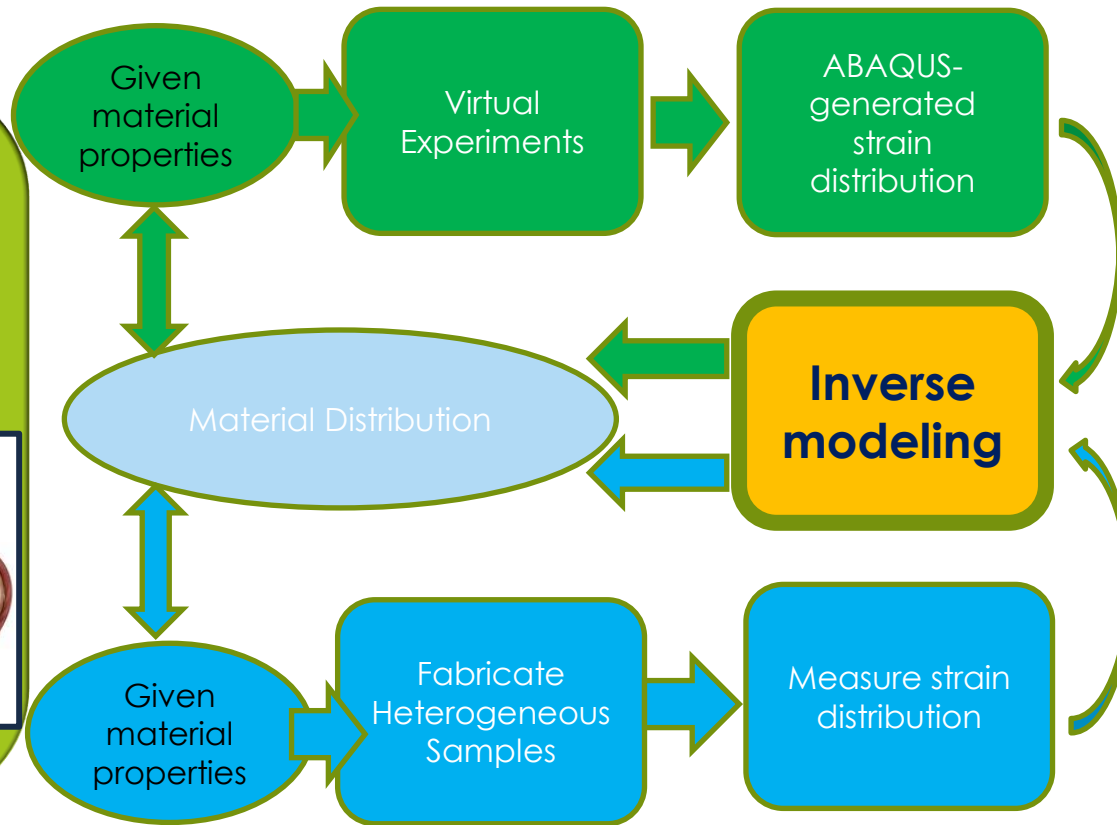
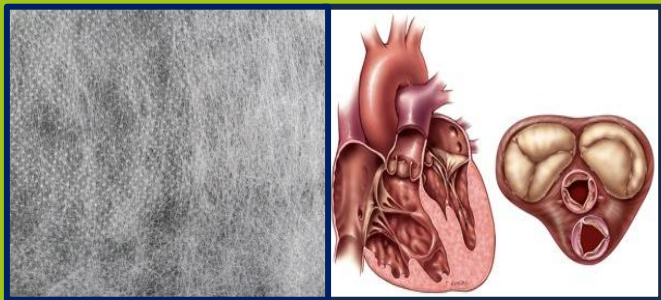
This project is for a senior design capstone class at Oral Roberts University in conjunction with LuXsine Energy Company.



Mechanical Characterization of Linear Elastic, Heterogeneous Membranes by Inverse Modeling and Full-Field Strain Measurements

Yuan Zhang(OSU), Shudao Wang and Lin Guo.

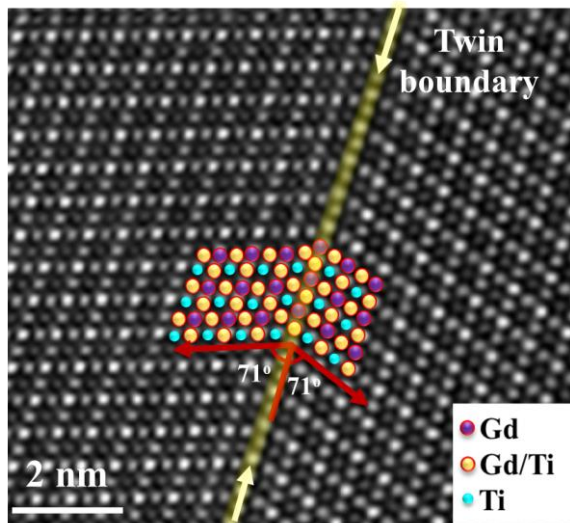
Goal
To characterize the mechanical behaviors of heterogeneous membrane.



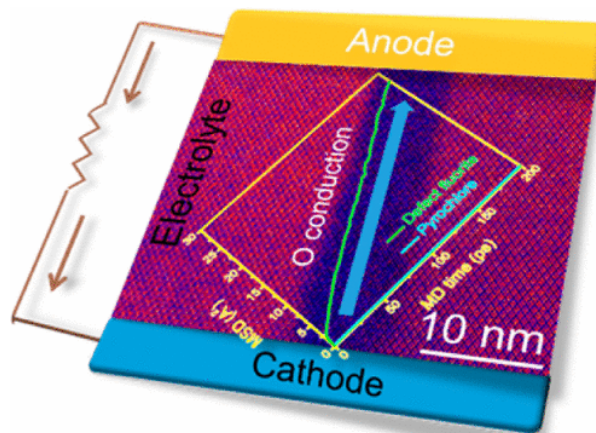
$\Sigma 3$ Twin Boundaries in $Gd_2Ti_2O_7$ as pathways for fast oxygen migration

Ashish Kumar Gupta (OSU), Gaurav Arora, Dilpuneet S. Aidhy and Ritesh Sachan

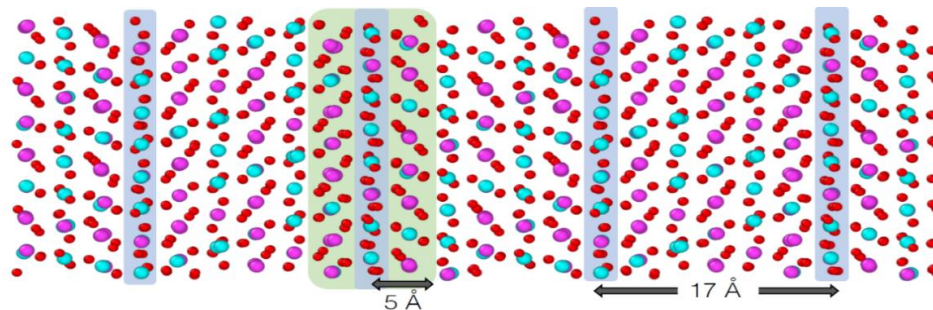
Identifying materials with fast-ion transport for energy conversion and storage applications in hybrid-electric systems



Atomic resolution image of $\Sigma 3$ Twin Boundary in $Gd_2Ti_2O_7$

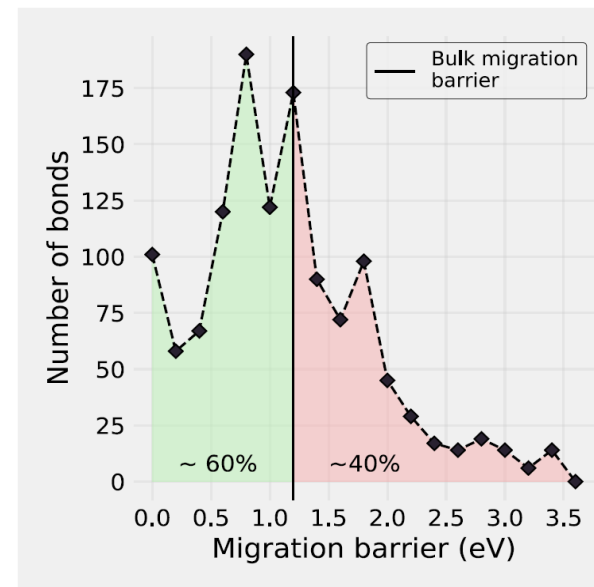


Schematic showing $\Sigma 3$ TB as a pathway for fast ionic conduction



Reconstruction of $\Sigma 3$ TB using MD simulations

Direct observation of atomic scale twin boundary defect promoting fast ionic conduction



Mean migration barrier was reduced by 25% at $\Sigma 3$ TB as compared to bulk



Ashish K. Gupta, et. al, " $\Sigma 3$ Twin boundaries in $Gd_2Ti_2O_7$ pyrochlore: pathways for oxygen migration", ACS Appl. Mater. Interfaces 2020, 12, 45558–45563



Impact of Asset Management In A Green Supply Chain (SC)

Sara Hajjhashemi, Reza Alizadeh, Janet K. Allen, Farrokh Mistree .

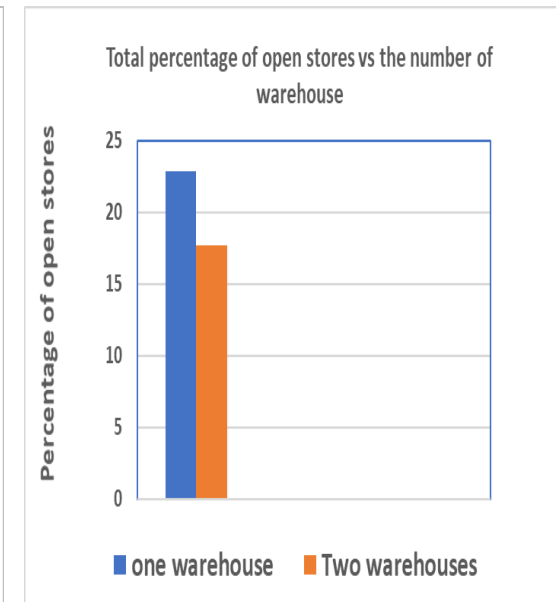
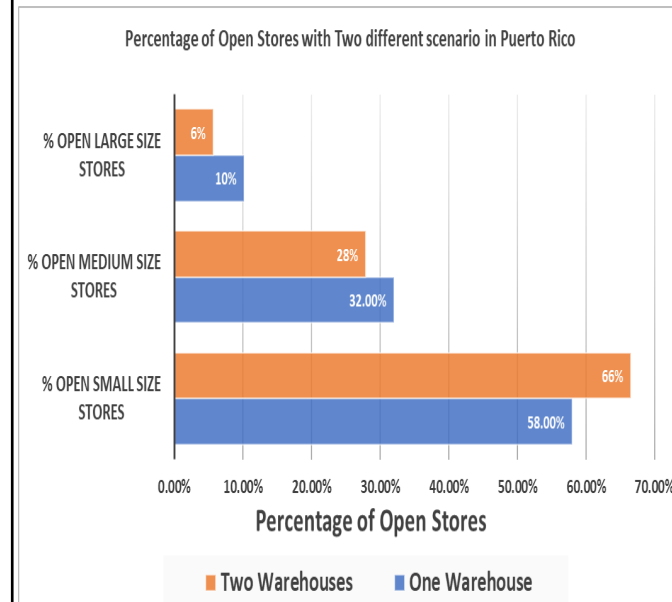
Background

- Companies such as Walmart, may develop SC by cost minimization, but they ignore green house gas (GHG) emissions which is huge threat to the environment.
- We are showing them how they could minimize the GHG emissions and cost of the system simultaneously.
- They generate about 30% of GHGs in their transportation.
- We are offering them a system that minimize operating and emissions cost simultaneously along with **asset management** to reduce their footprint in environment.



Results & Analysis

- We found that GSC has more small stores closer to the customers, because customers' cars create more GHG than supplier's trucks.
- Having **more warehouses** and **less stores** mitigate GHG significantly. Therefore, changing the business models through asset management make the SCs greener.

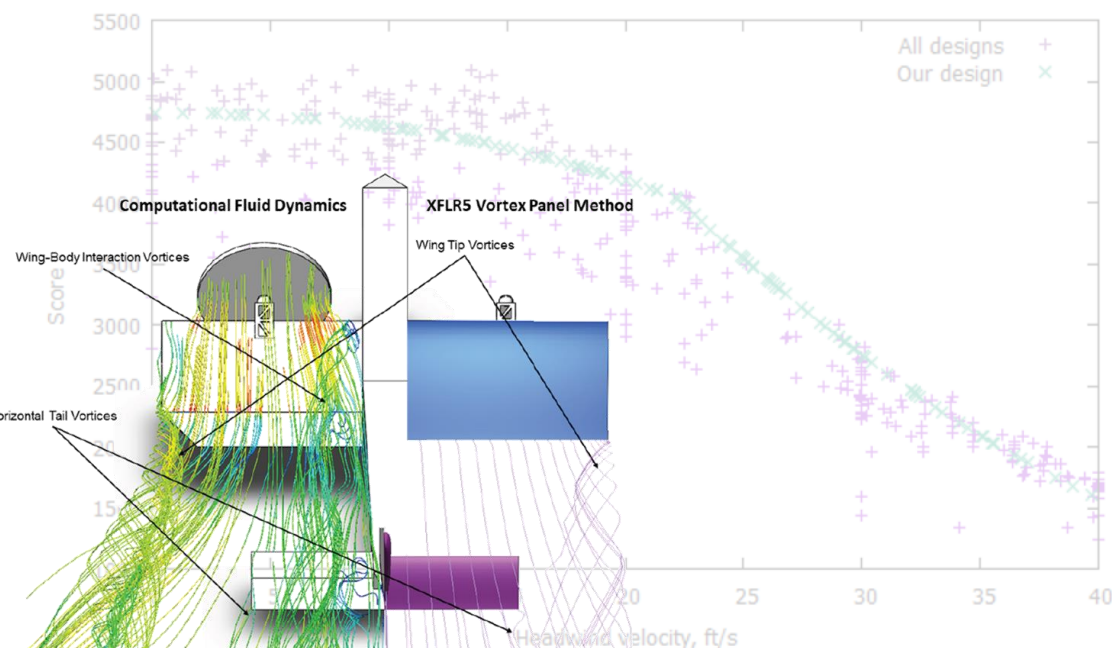
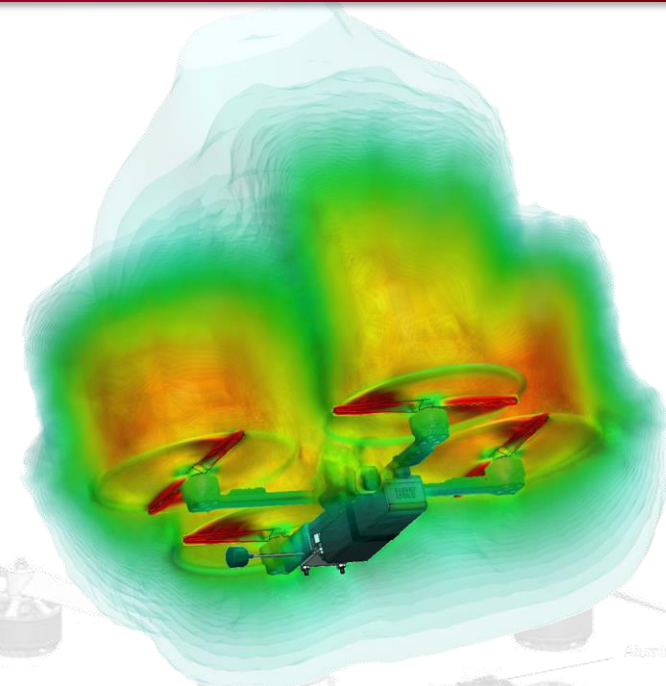


Integration of Advanced Computational Tools in Aerospace Capstone

Dr. Thomas C. Hays (OU), Nigh Herndon, Tyler Swisher

- Ray Tracing / Rendering
- Vortex Lattice Aerodynamics
- Computational Fluid Dynamics
- Finite Element Analysis
- Optimization
- Electric Propulsion Modelling

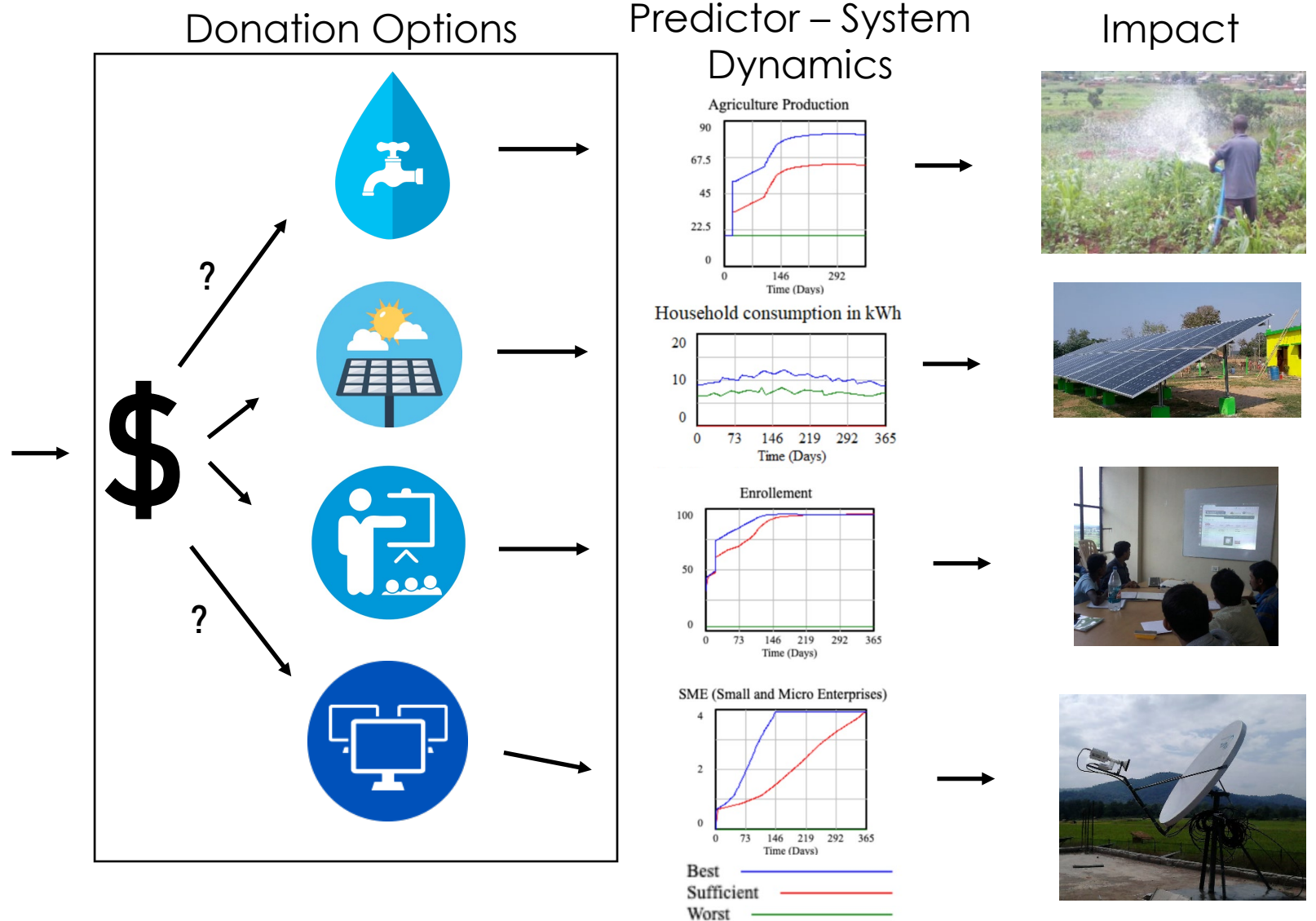
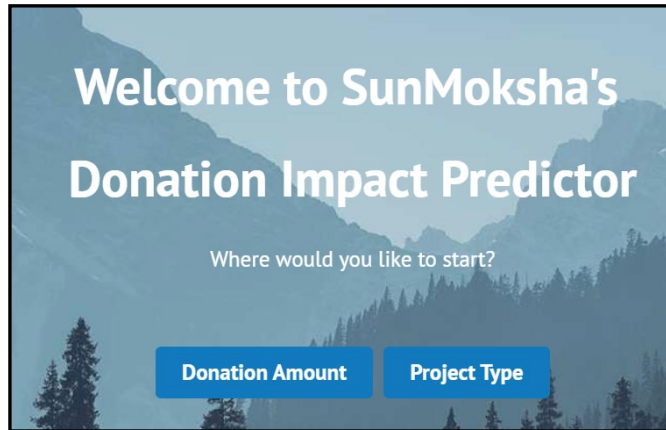
Affordable multicore consumer GPU's, CPU's, and software to utilize that calculation horsepower have enabled aerospace capstone students to create high-end engineering studies on low cost machines. This presentation reviews how some motivated students have used those tools to improve their designs and education in aerospace capstone.



Crowdfunding for Sustainable Development in Rural India

Julia Henry, Janet K. Allen, and Farrokh Mistree

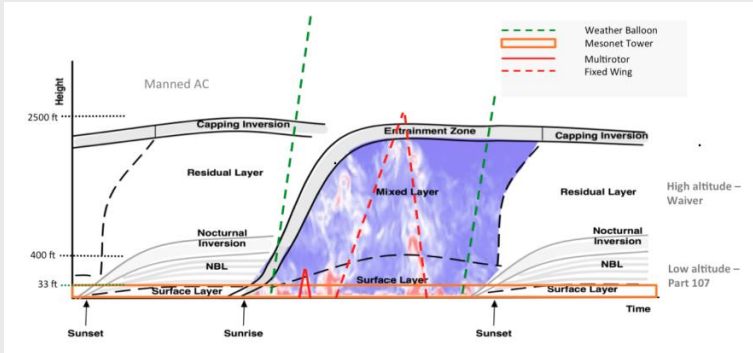
Objective:
Help a small donor
decide how distribute
a donation



An Experimental Approach to Correcting Airspeed Measurements From Unmanned Aerial Vehicles

Kyle Hickman(OSU), Jamey Jacob

Motivation: Need a reliable and accurate windspeed measurement from UAS



Solution: Experimentally corrected systems

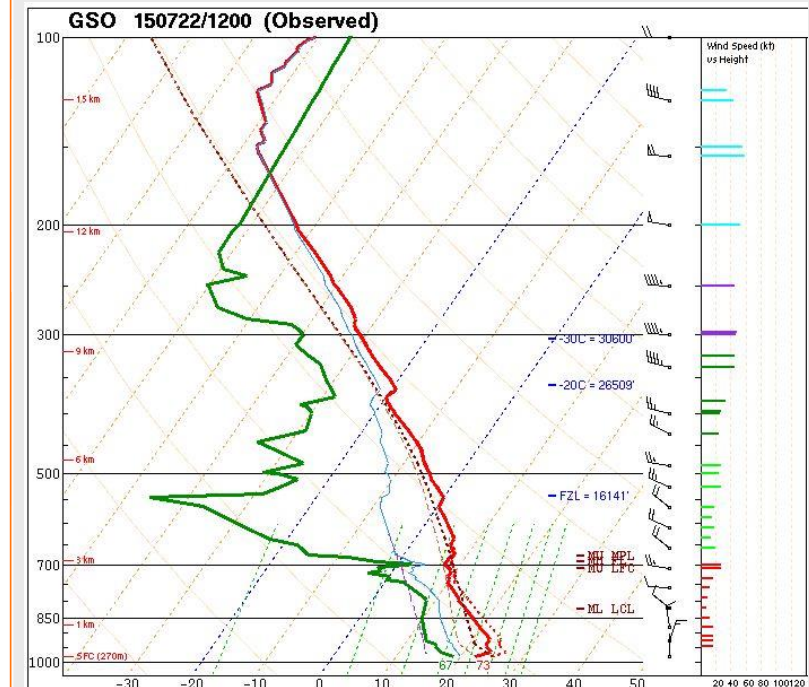
Fixed Wing Mounted 5HP



Multi-Rotor Anemometer



Future Work: Integration and Validation

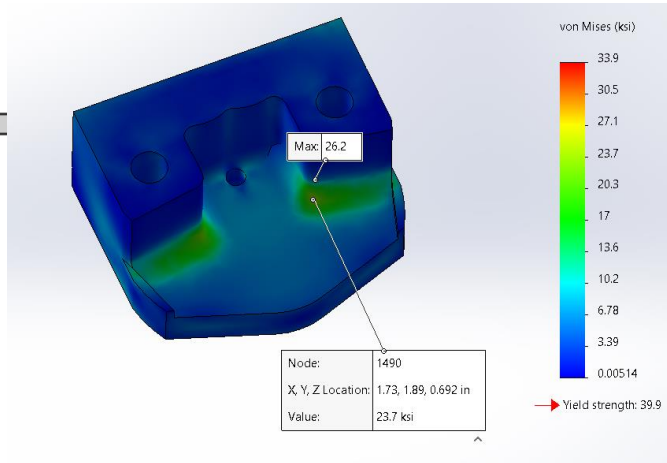
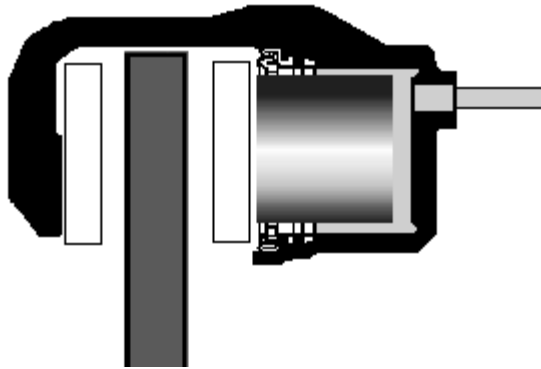


Want to be able to prove

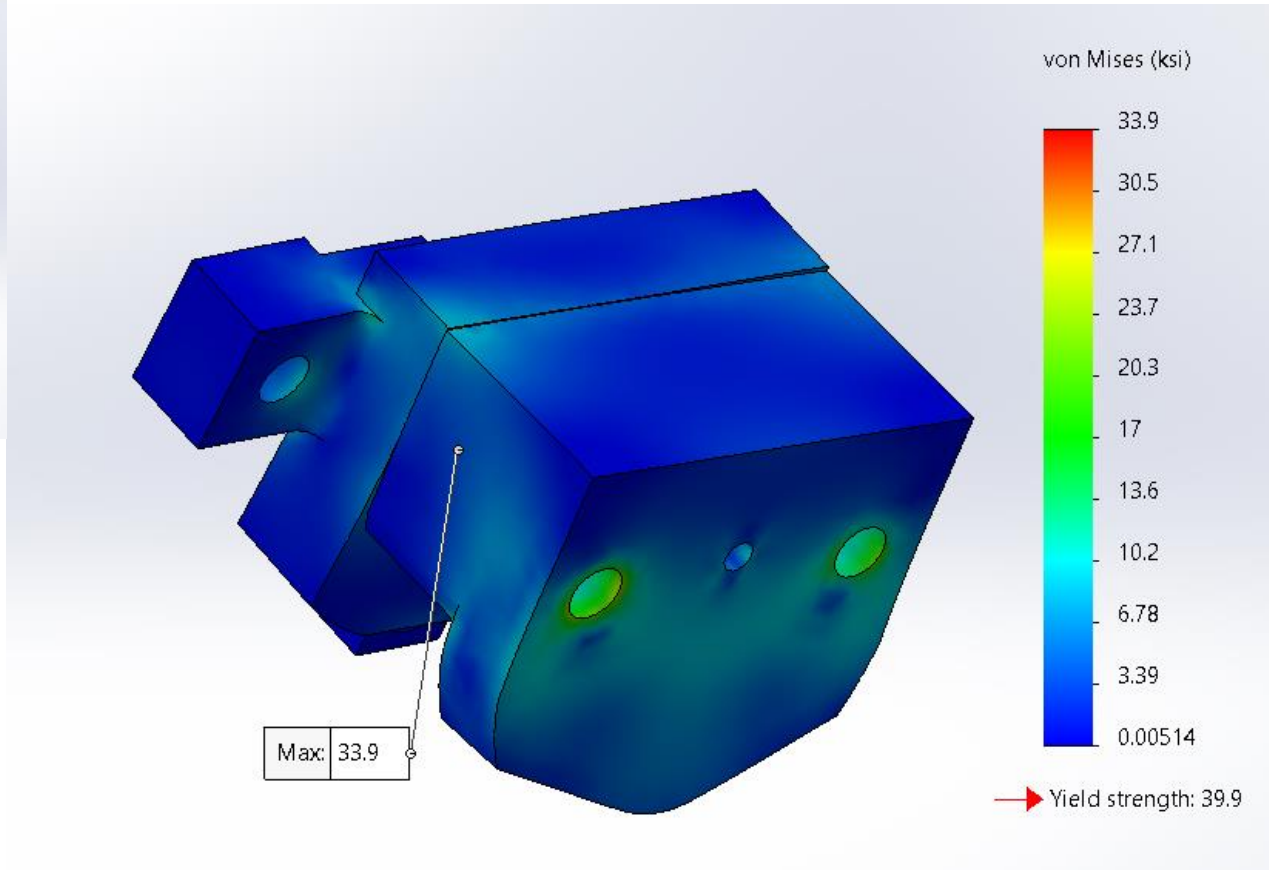
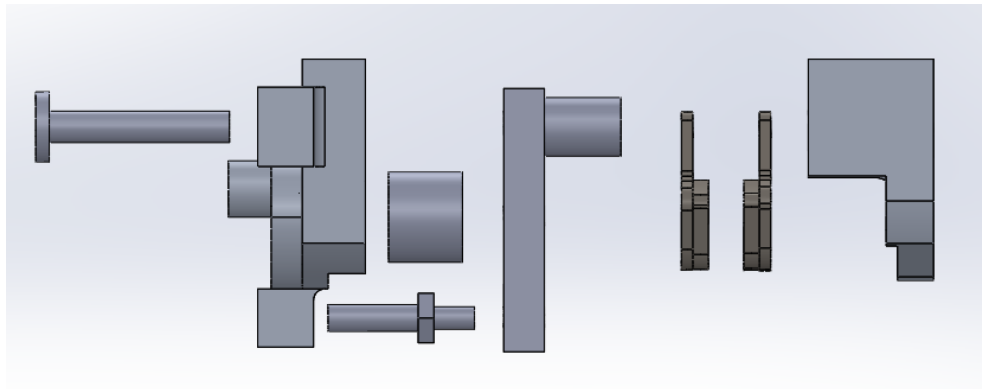
- Data is accurate enough for weather research purposes
- Data use is beneficial for weather modeling

Floating Brake Caliper Research Project

Chayton Hogue (OU)



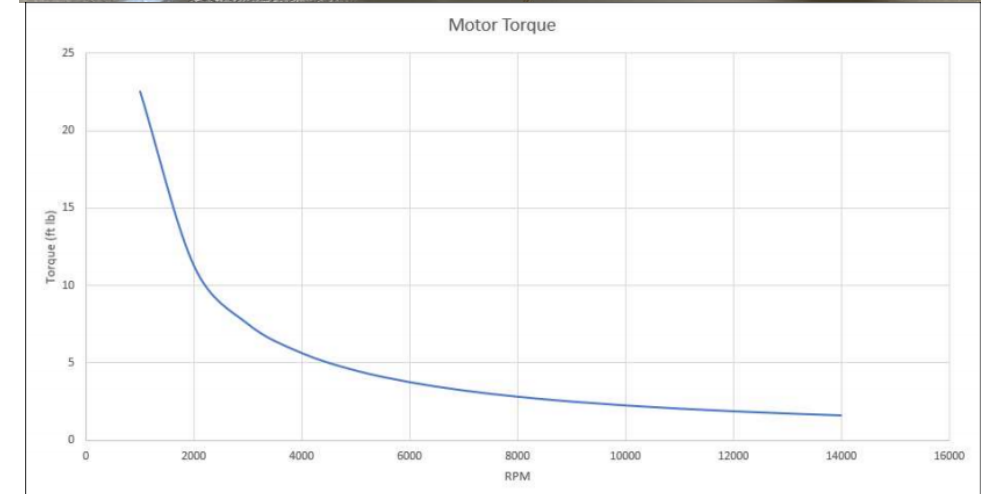
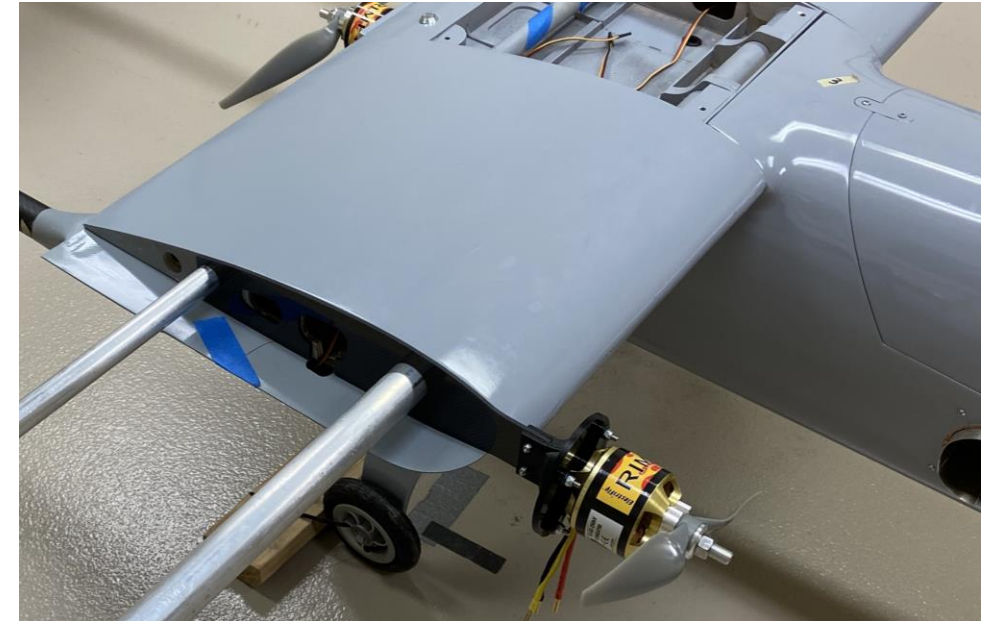
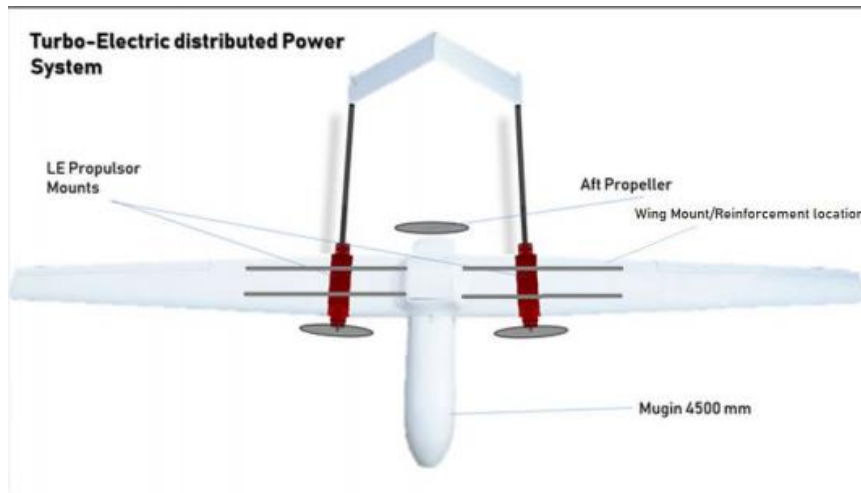
www.quora.com/What-is-the-difference-between-fixed-and-floating-caliper.



Distributed Power Turbo-Electric Unmanned Air Vehicle

Chase Holland, Dr. Kurt Rouser, and Johnathan Burgess

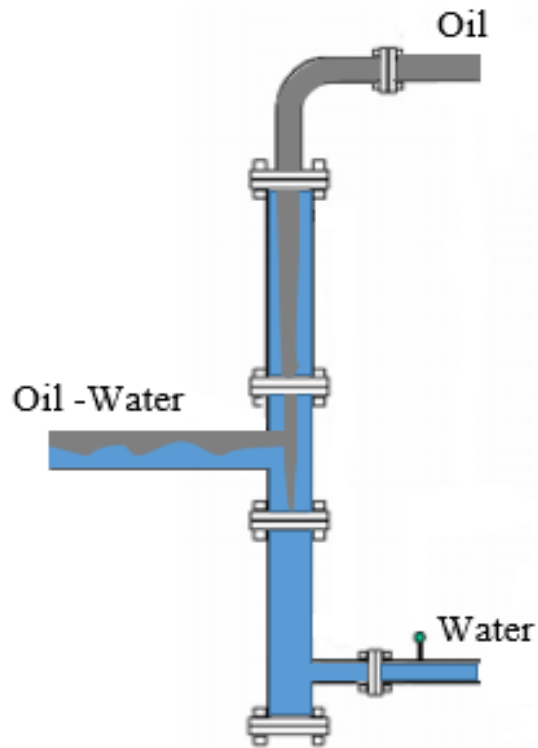
- ❖ Great power density and versatility of battery with energy density of hydrocarbon
- ❖ Increased the propulsive efficiency with added leading-edge motors
- ❖ PLA 100% infill motor mount & Carbon-Fiber wing bracket



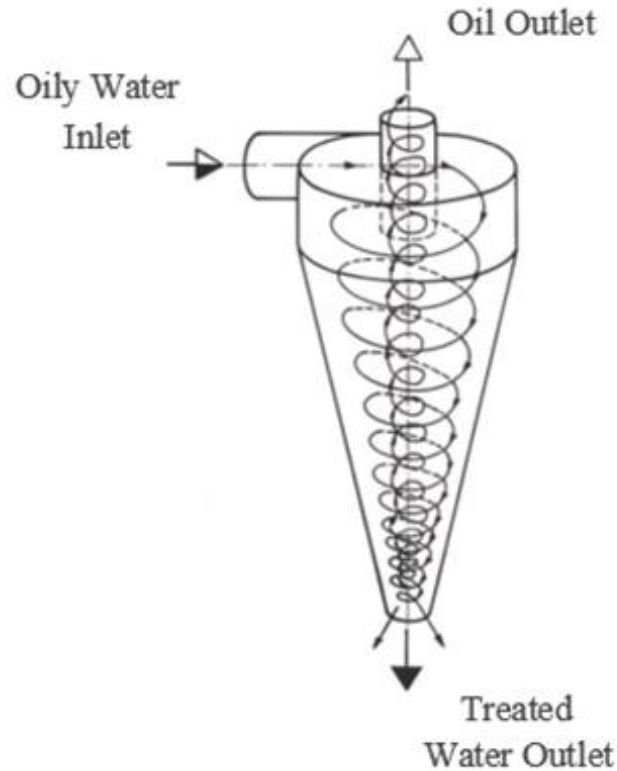
Produced Water Polishing Utilizing Integrated Compact Separator System

Lucas Hornbrook (TU), Dr. Ovadia Shoham, and Dr. Ram Mohan

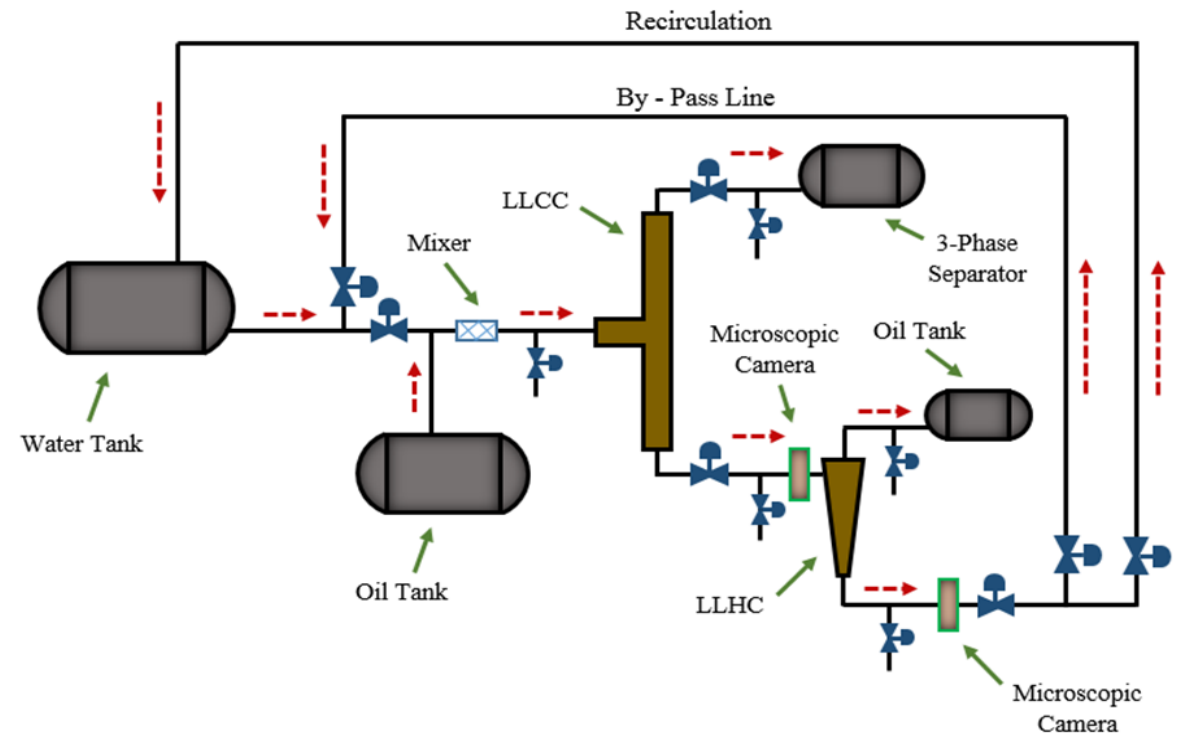
1. LLCC[®] Schematic



2. LLHC Schematic



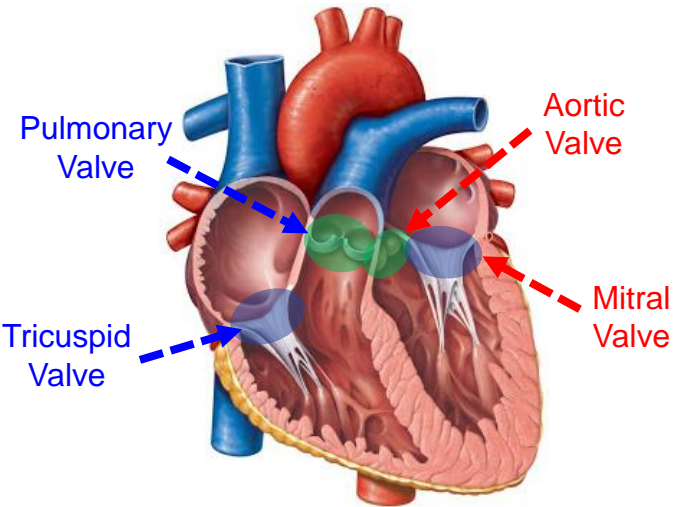
3. Test Section Schematic



Biomechanical and Microstructural Characterizations of Four Heart Valve Soft Tissue Leaflets

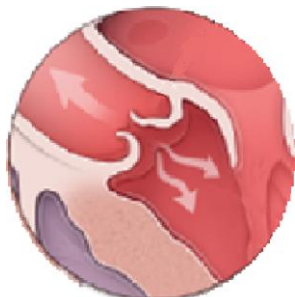
Luke Hudson (OU), Arshid Mir, Harold Burkhart, and Chung-Hao Lee

Heart Valve Anatomy & Disease



MV: ~7.8 million

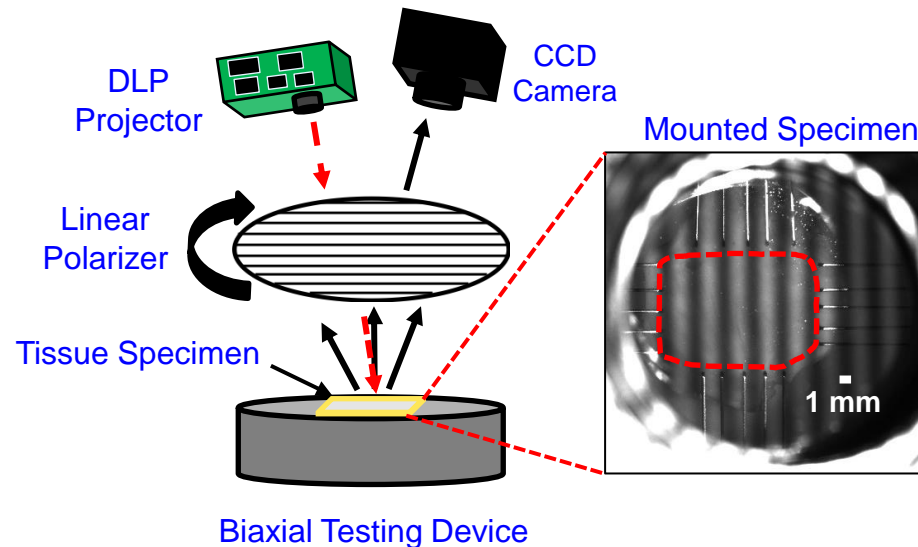
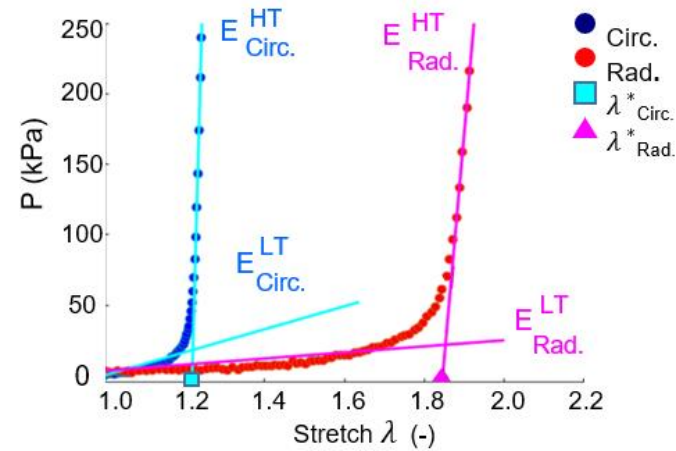
TV: ~1.6 million



AV: ~1.5 million

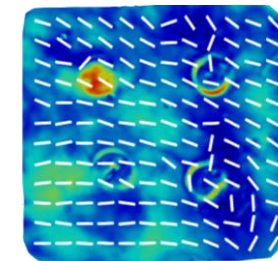
PV: 5-10% of CHD

Opto-Mechanical Testing



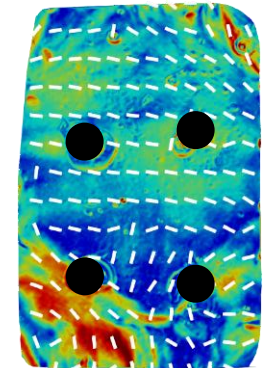
Key Findings

Zero stress
Zero Deformation

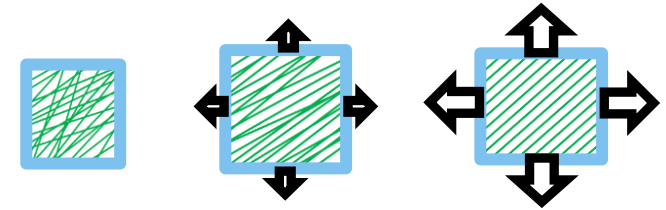


$\theta_{\text{fiber}} = 154.9^\circ \pm 20.5^\circ$
 DOA = 0.053 ± 0.015

Peak Equibiaxial Loading



$\theta_{\text{fiber}} = 162.5^\circ \pm 26.8^\circ$
 DOA = 0.072 ± 0.023

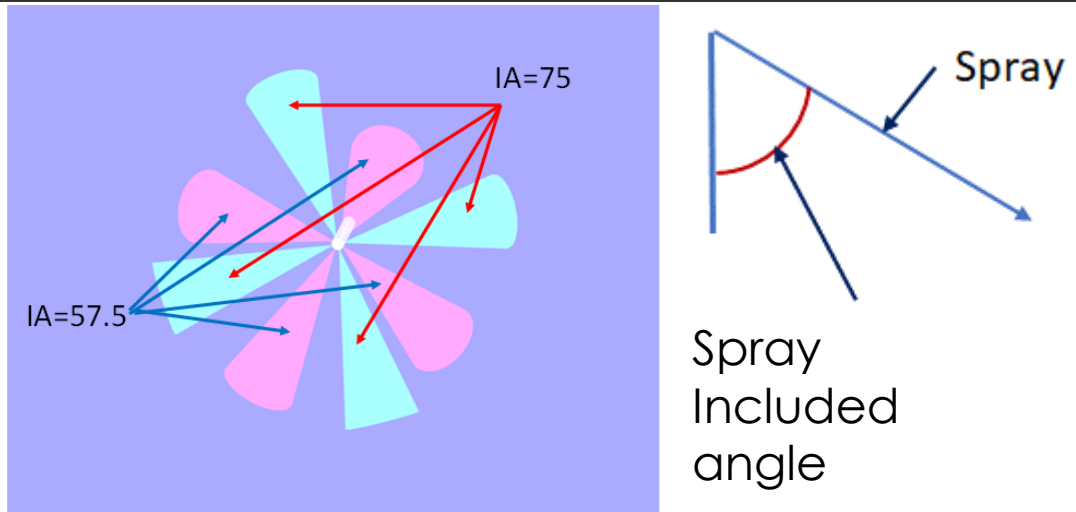


Differences in mechanical properties due to anatomical location (left vs. right side of the heart)

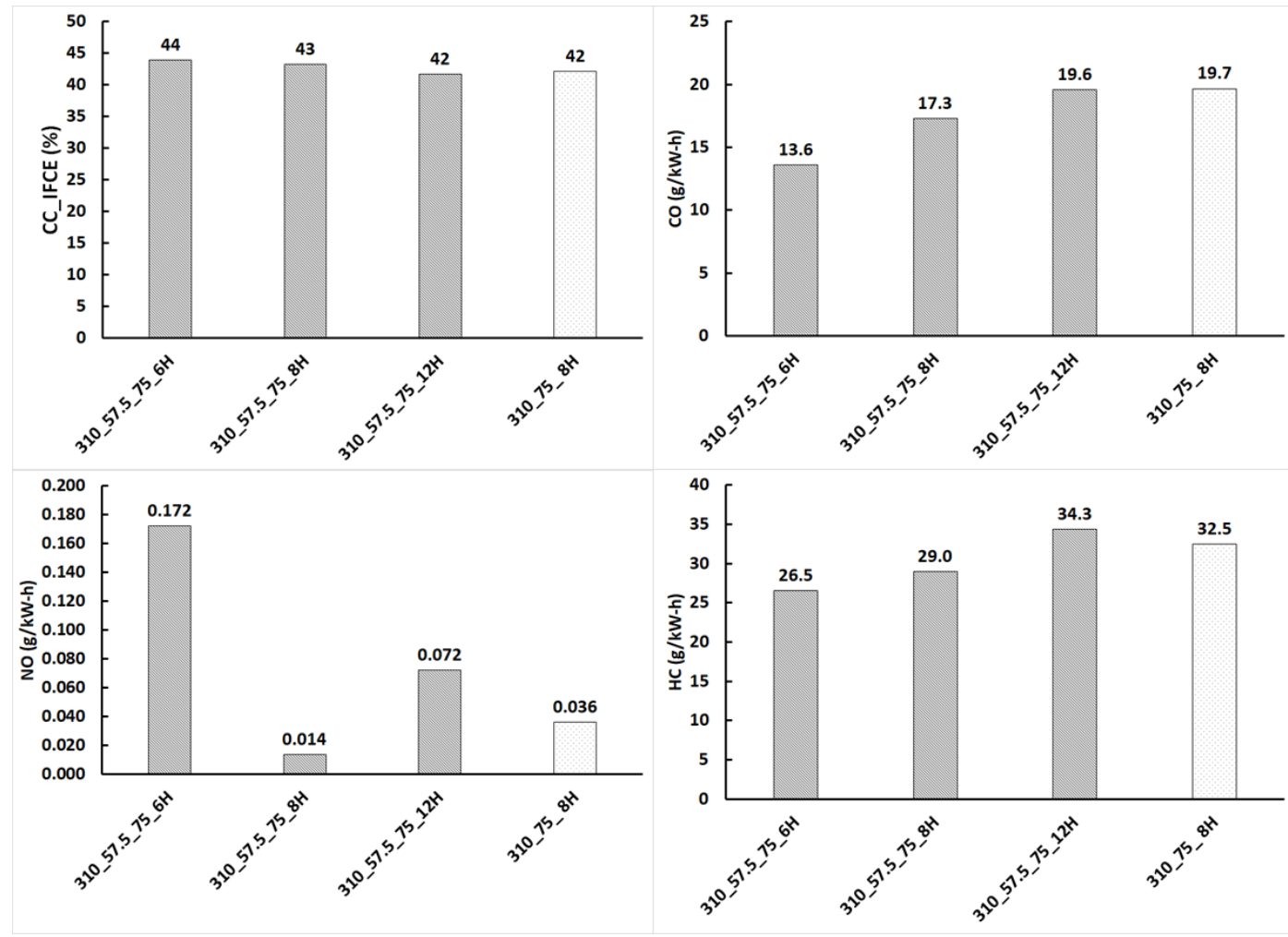
Collagen fiber architecture is dynamic and load-dependent

Strategies for the reduction of hydrocarbon and carbon monoxide emissions in dual fuel engines

Prabhat R. Jha (OU), Kalyan K. Srinivasan (UA), and Sundar R. Krishnan (UA)



- Spray targeting can be utilized to simultaneously reduce HC and CO emissions and increase closed cycle indicated fuel conversion efficiency



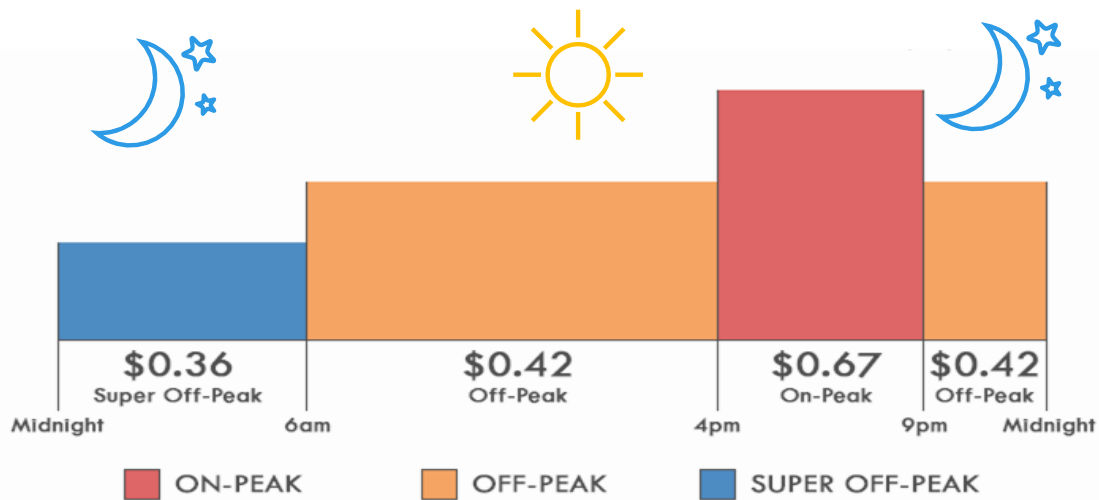
Design of a Home Energy Management System (HEMS)

Yilin Jiang (OU), Li Song, Janet K. Allen, and Farrokh Mistree

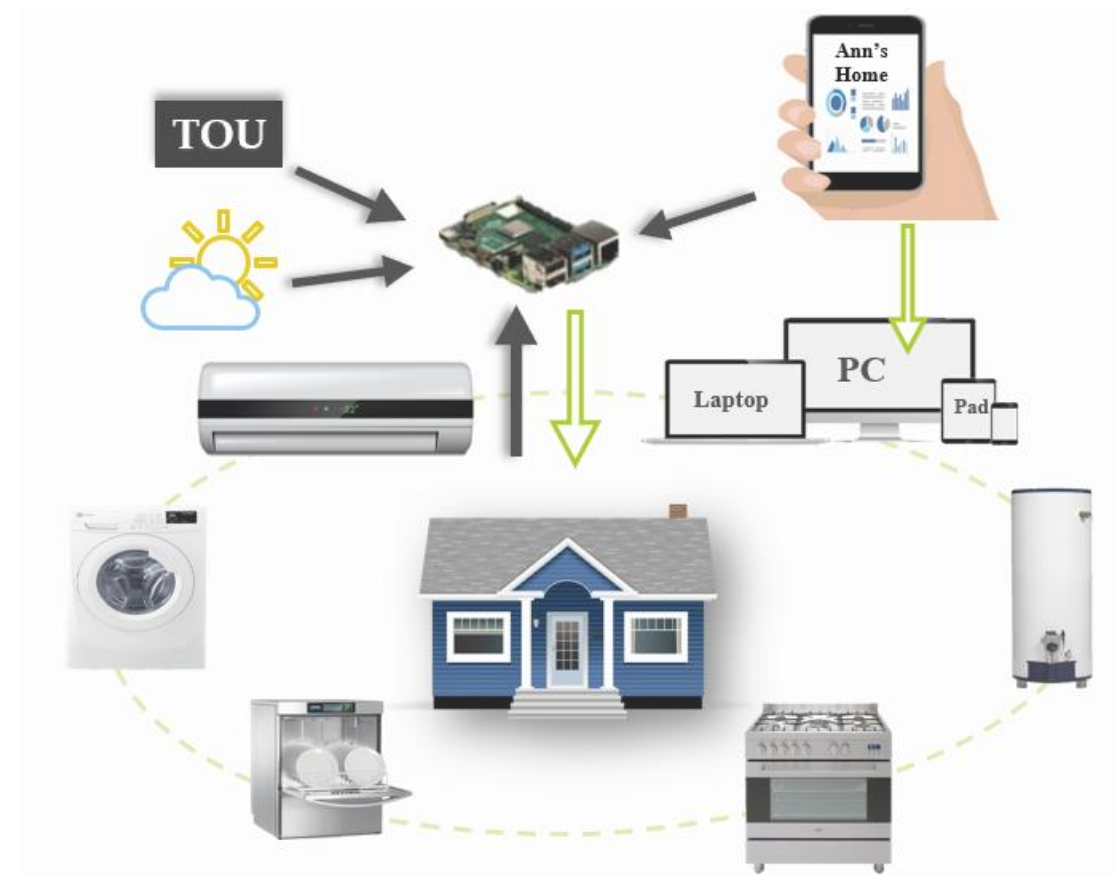
Goal

- Minimize cost of electricity while maintain the satisfactory comfort and convenience for the homeowners 😊
- Reduce the peak load for the company 😊

Time of Use (TOU)



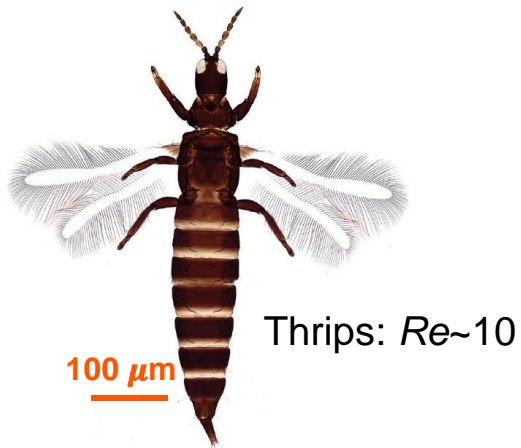
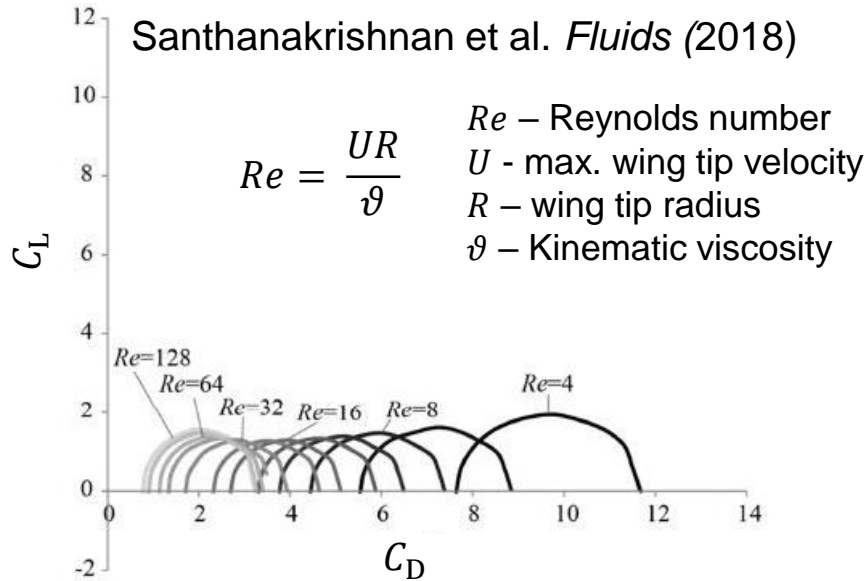
Smart Home



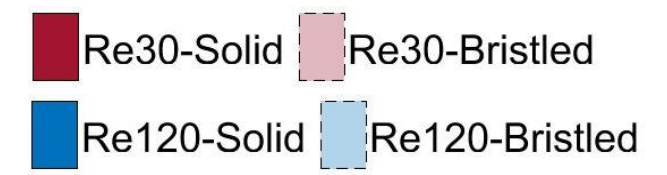
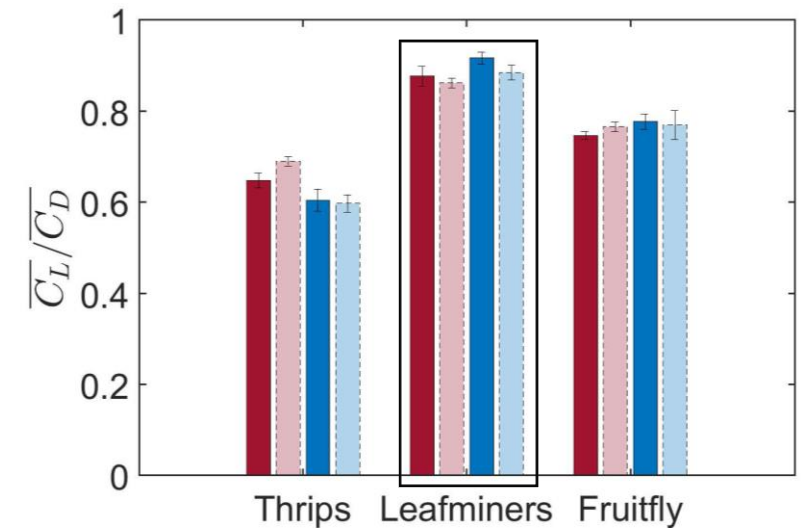
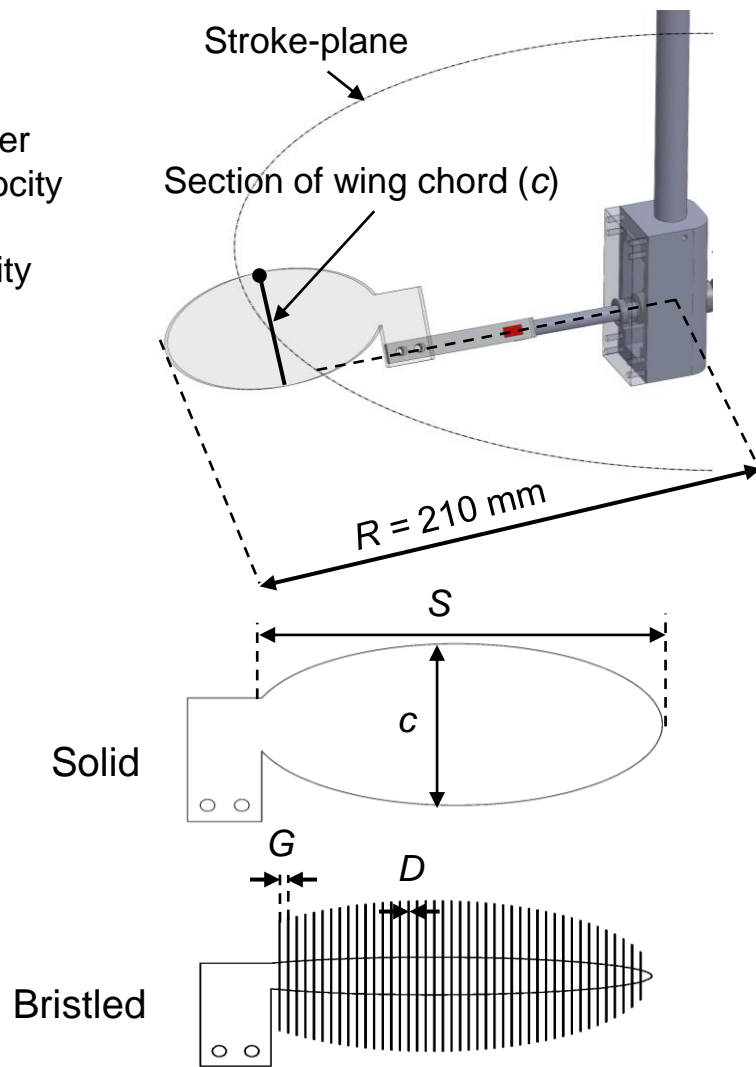
Paper Jiang, Y., Song, L., Allen, JK and Mistree, F., 2021, "Home Energy Management System (HEMS): Coupled Flexible Load Management in Homes," ASME IDETC 2021, under review

Three-dimensional flapping flight of tiny insects using bristled wings

Vishwa Kasoju(OSU) and Arvind Santhanakrishnan



Thrips image taken from Tyagi et al. (2018)

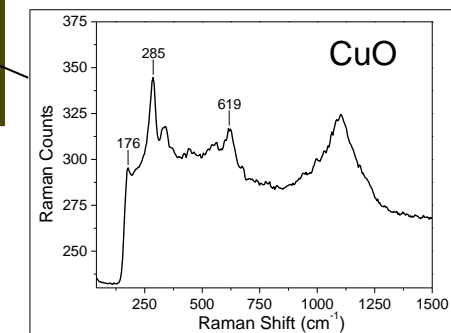
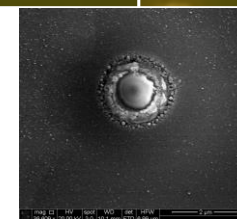
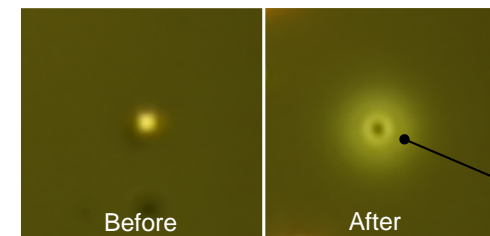
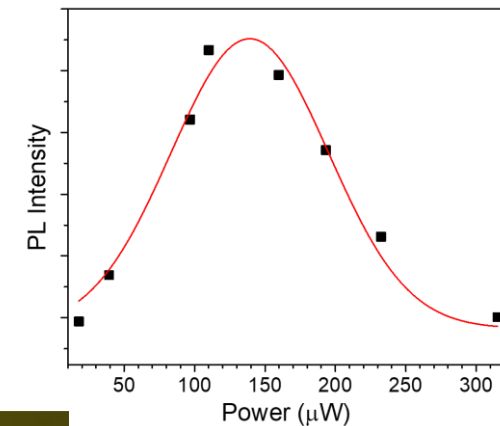
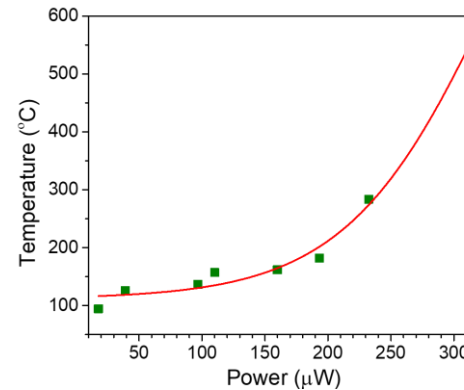
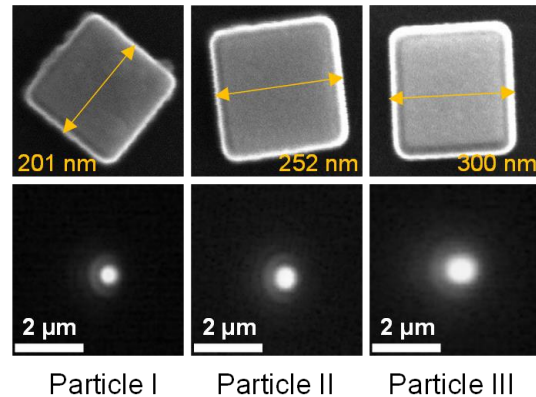
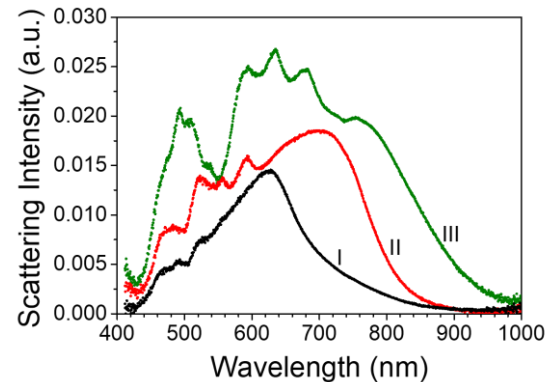
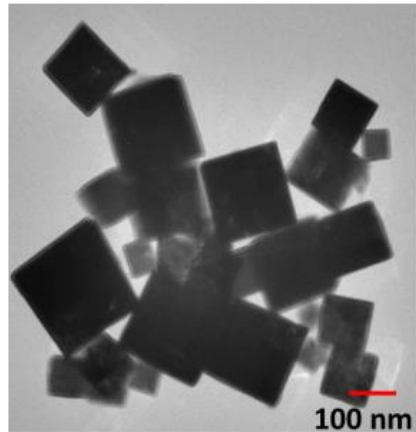


Chord (c) – 45 mm, Span (S) – 90 mm, Gap width (G) – 2.032 mm, Bristle diameter (D) – 0.2032 mm

Explosive Oxidation of Submicron Cu_2O Cubes with Low Power Laser

Nishan Khatri (OSU), Matthew Green, Marimuthu Andiappan and A. Kaan Kalkan

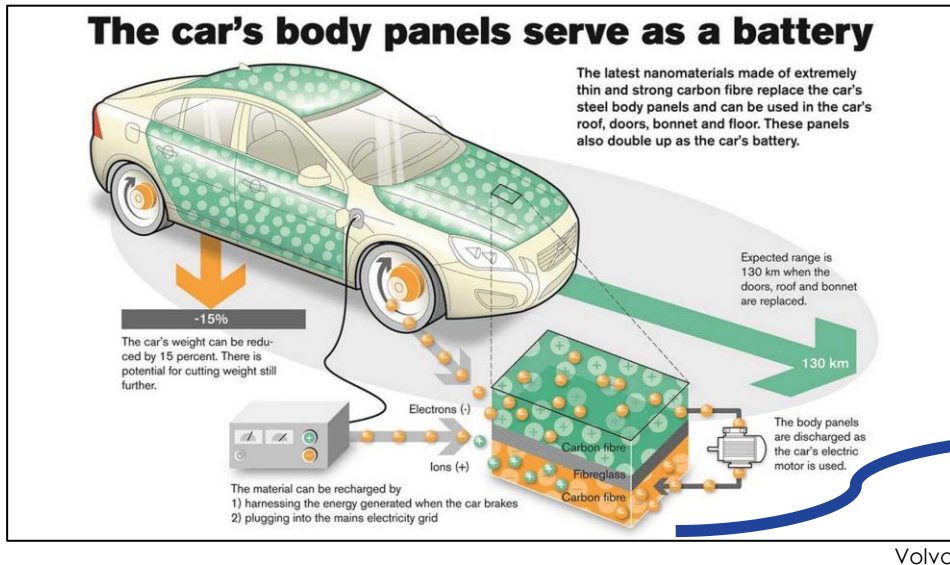
- ❑ Dielectric resonances in submicron Cu_2O cubes lead to enhanced photothermal heating.
- ❑ This enhanced photothermal heating can cause explosive oxidation of the Cu_2O cubes to CuO .
- ❑ The photothermal heating quenches the defect photoluminescence through exciton dissociation with increased laser power (before any oxidation). Photoluminescence is restored if laser power is lowered.



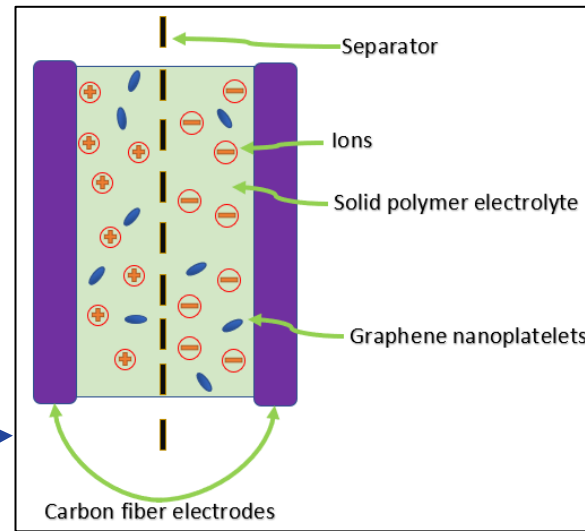
In situ measurement of AC conductivity to quantify alignment of graphene nanoplatelets (GNPs) in epoxy

Sai Tharun Kotikalapudi (OSU) and Raman P. Singh

1) Introduction



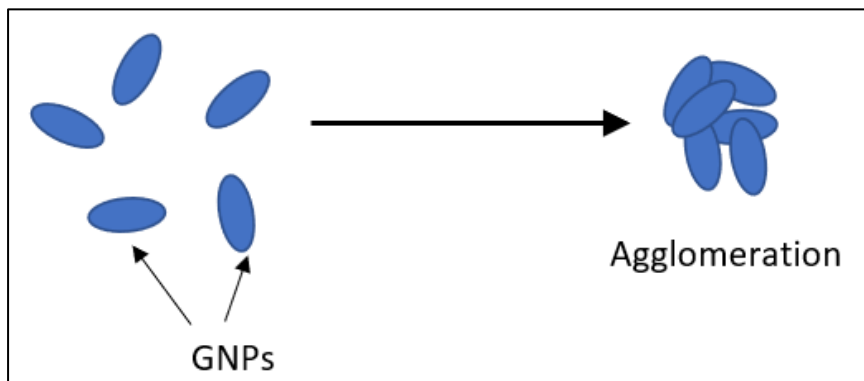
2) Structural battery



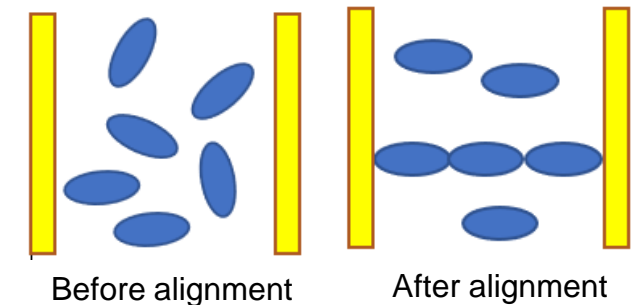
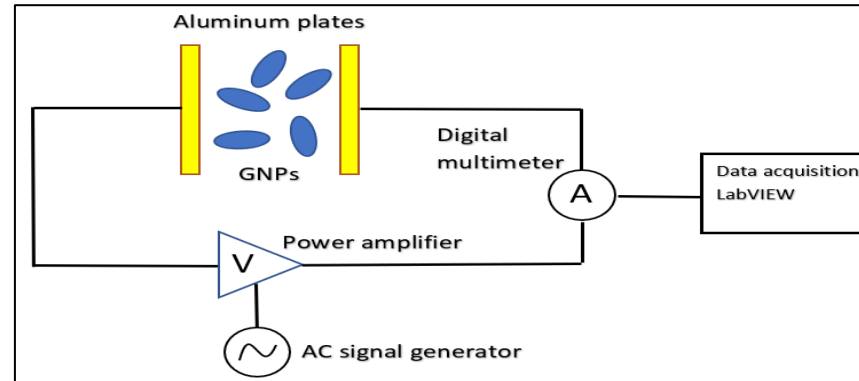
Notes

- Battery needs to provide strength while storing charge
- Solid electrolytes are not effective as liquid electrolytes
- Graphene is an amazing electrical, thermal and ionic conductor and strongest material in the world
- Graphene is added to improve ionic conductivity
- But graphene tends to agglomerate
- Solution is alignment using AC fields
- Prevents agglomeration and adds **directional properties**

3) The problem



4) Solution



Tunable Performance Metrics for Acoustic Liners

William Kresl (OSU), James M. Manimala

Motivation

- Current liners for ultra-high bypass ratio turbofan engines are impractical for low frequency ($\sim < 1000$ Hz).
- Can **Tunable Performance Metrics (TPMs)** be developed to automate selection of optimal designs of new low-frequency liner concepts such as **Folded Core Liners (FCL)** for various noise profiles?



TPMs

Baseline (LFP):

$$\frac{BM}{G} * 100$$

Cubic Lower Bound (CLB):

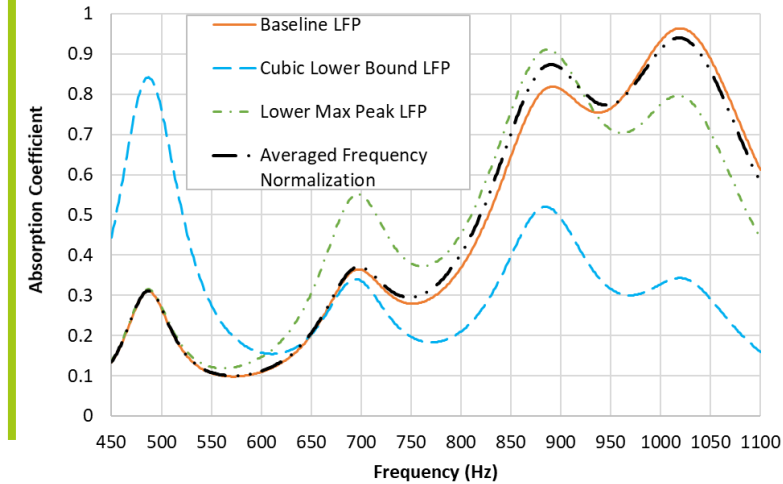
$$\frac{BM}{G^3} * 10^8$$

Lowest Freq. Max Peak (LMP):

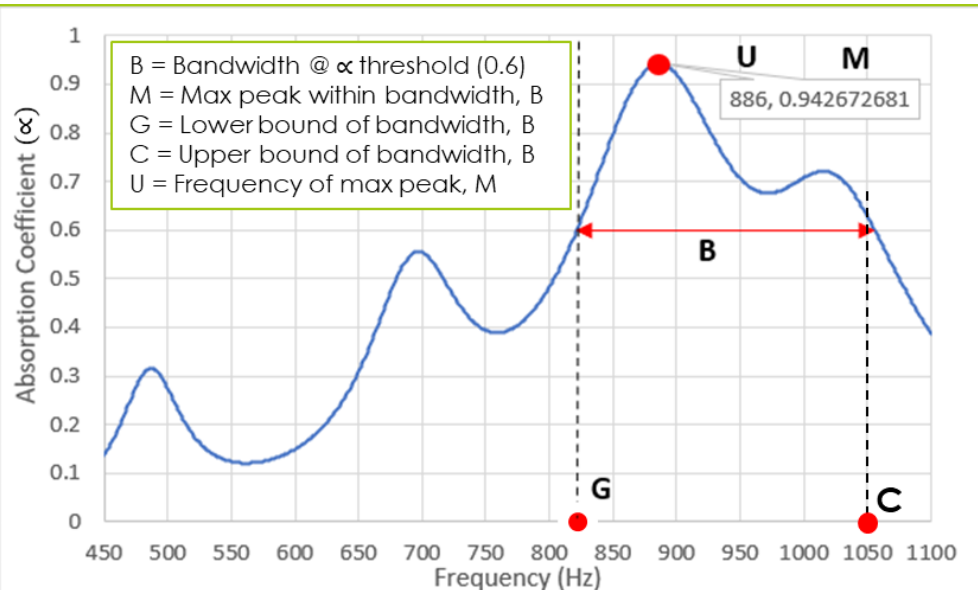
$$\frac{BM}{UG} * 10^4$$

Averaged Freq. Norm. (AFN):

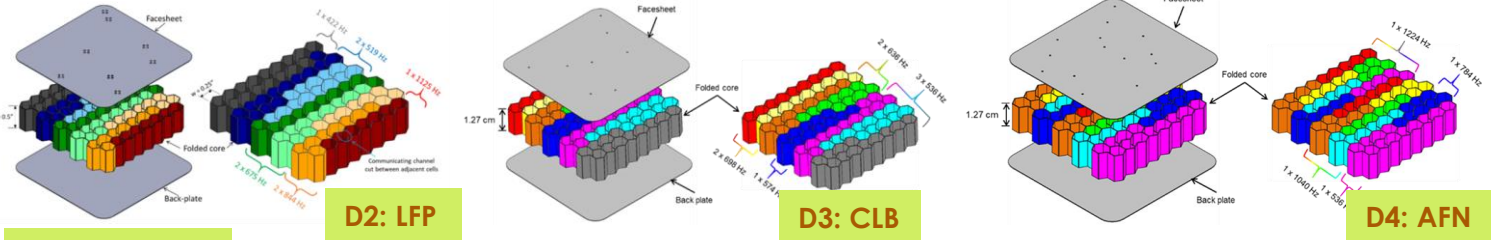
$$\frac{\int_G^C \alpha(f)}{C-G}$$



Absorption Spectral Parameters



Some Optimized FCL Designs using TPMs



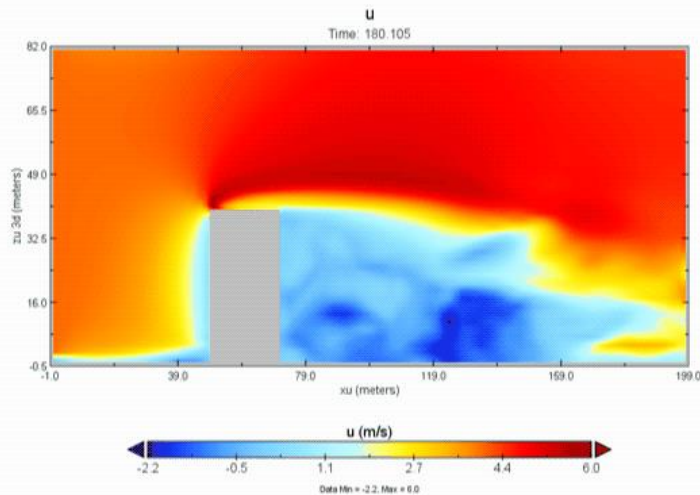
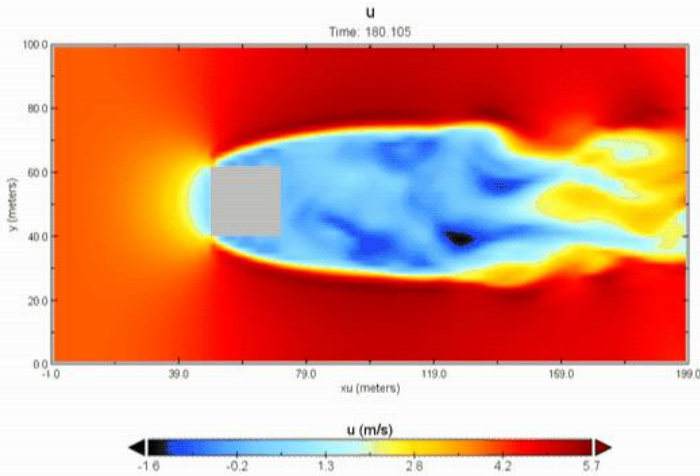
Conclusions

- Optimized designs to address **LF tones** or **broadband noise** could be identified using automated tools using TPMs
- TPMs that also **include structural parameters** related to mass, volume, stiffness or strength could provide a more holistic means of evaluating liners

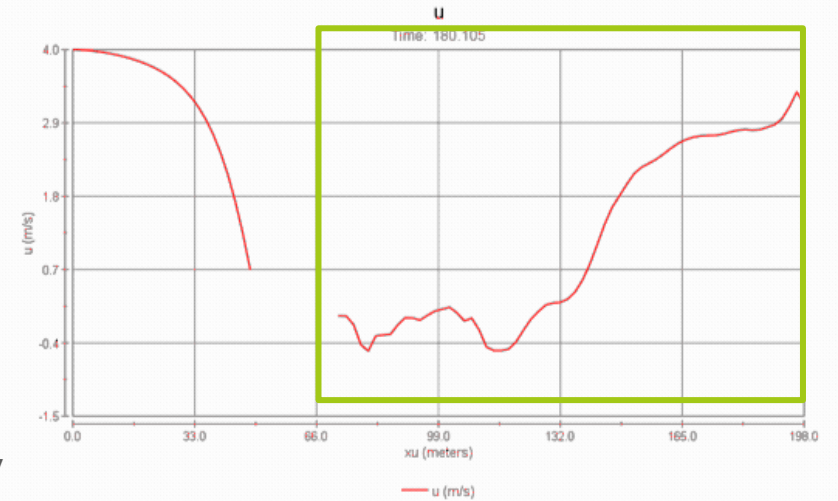


Large-Eddy Simulation Around Buildings in Crosswinds for Unmanned Air Systems

Tyler Landua (OSU), Rohit K. S. S. Vuppala, Dr. Kursat Kara

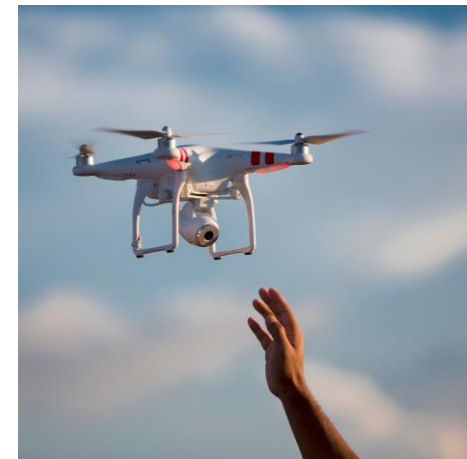


- Shown to the left are the U-velocity plots of the tall building in my analysis.
- Blue and black areas indicate negative velocities which are creating vortices behind the structure.



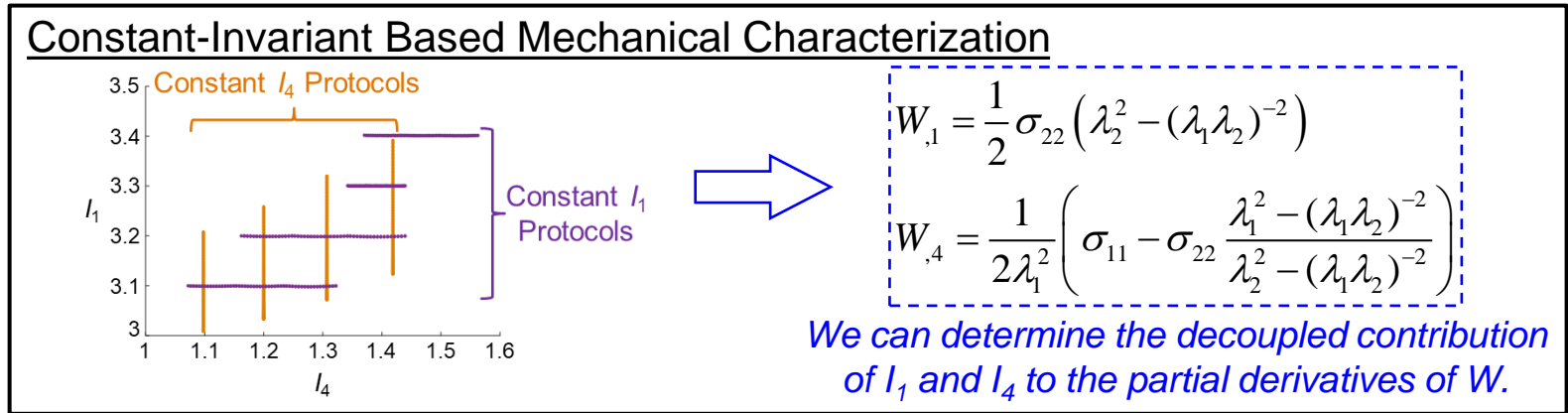
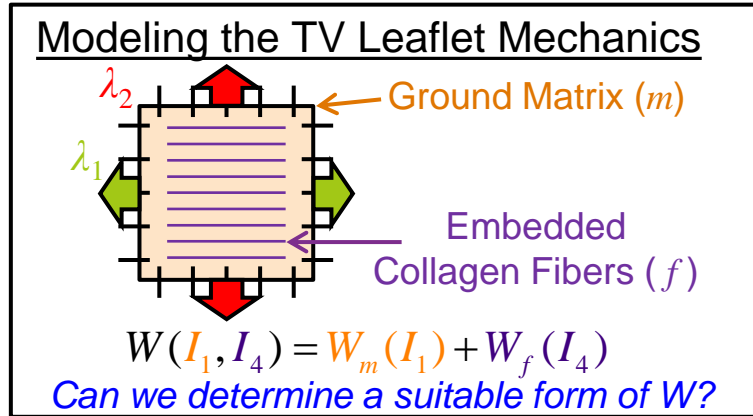
- Above and right is the plot of the U-velocity through the plane in the center of the tall building with respect to x-distance.
- Heavy flow variation can be clearly seen in the boxed area (note that this only shows results in one time frame, but the actual U is constantly changing).
- This region would be extremely difficult to fly a UAS through and could cause an accident to occur.

Conclusion: A solution to aiding the control and stability of UAS in complex flows must be developed before UAS are introduced to urban environments to reduce the chance of accident or damage.



Determination of a Strain Energy Density Function for the Tricuspid Valve Leaflets Using Constant Invariant-Based Mechanical Characterizations

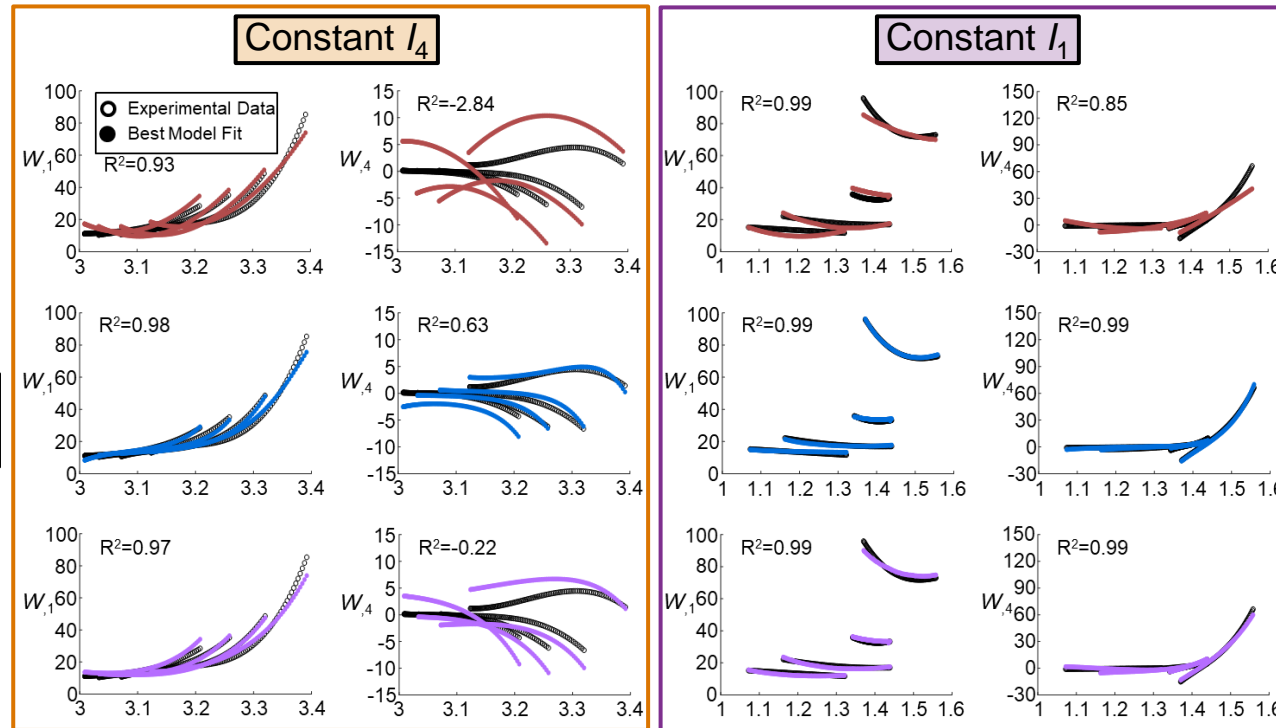
Devin W. Laurence (OU) and Dr. Chung-Hao Lee (OU)



$$W_{poly} = \sum_{i+j=1}^3 C_{ij} (I_1 - 3)^i (I_4 - 1)^j$$

$$W_{exp} = C_{00} (I_1 - 3) + \exp[W_{poly}] - 1$$

$$W_{comb} = W_{poly} + W_{exp}$$



Model	D-Optimality	Condition Optimality
W_{poly}	0	16
W_{exp}	6	0
W_{comb}	12	2

Recommendation

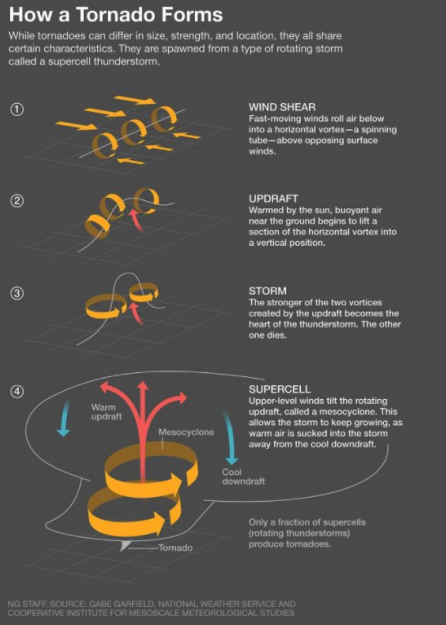
$$W_{exp} = C_{00} (I_1 - 3) + \exp[W_{poly}] - 1$$

Superb fitting & model parameter search space

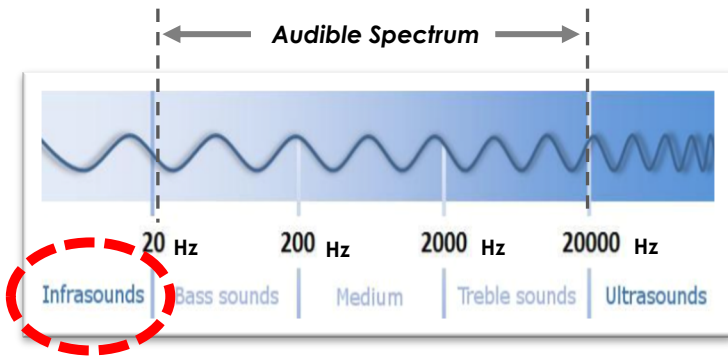
Development and Deployment of a Mobile Infrasonic Data Acquisition Unit

Bryce Lindsey (OSU), Brandon White (OSU), Dr. Brian Elbing (OSU), and Dr. Imraan Faruque (OSU)

Tornadoes



Infrasound, in the nominal range of 0.5 Hz to 10 Hz, has been an observed by-product of tornadogenesis

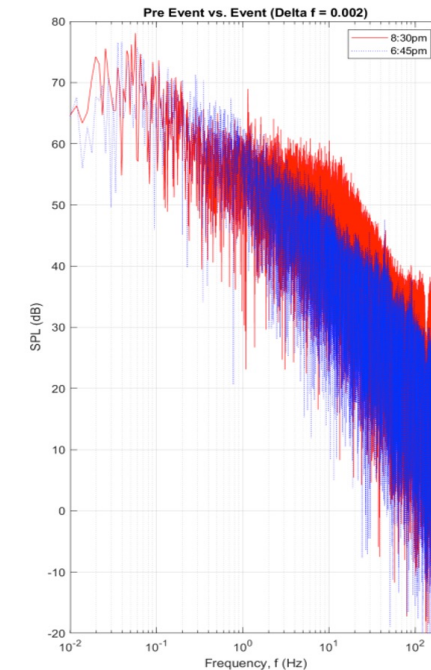


- 1) Computer/sensor box
- 2) Chaparral 24 Mic
- 3) Power Supply

A Ground-based Local Infra-sound Data Acquisition package (GLINDA) was constructed and deployed in the News 9 Storm Tracking Vehicle



GLINDA has gathered data during several storm events, including a tornado event in Lakin, KS on 21 May 2020 (pictured above)

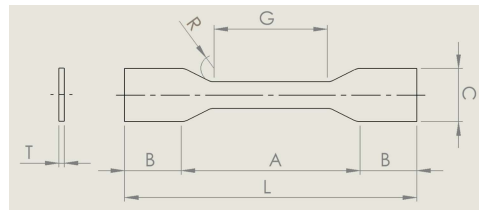
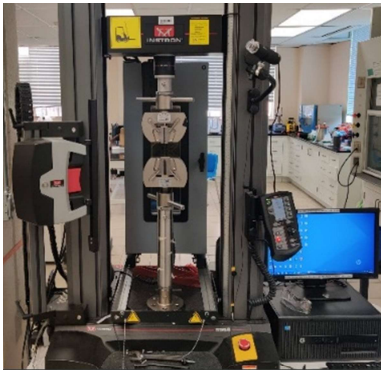


Comparing the pre-event vs event data shows a swell of infrasound during the tornadic event

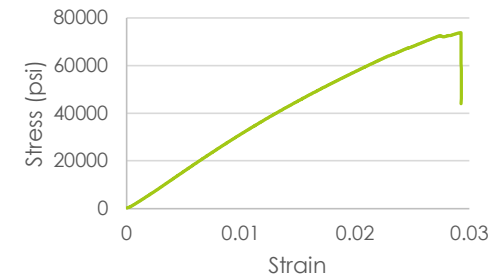
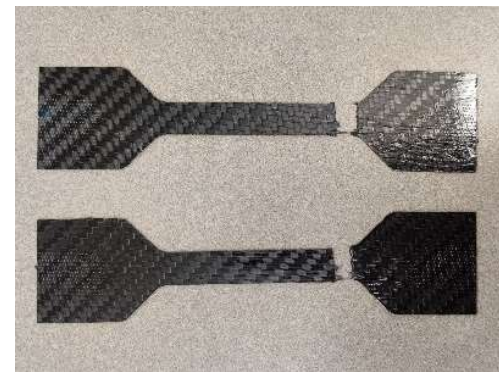
Experimental Analysis of Bonding Carbon Fiber Composite and Metal

Presenting Author (OU), Matthew Llano

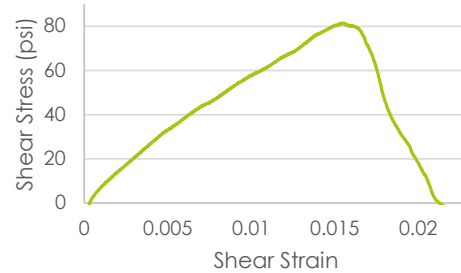
Experimental Setup



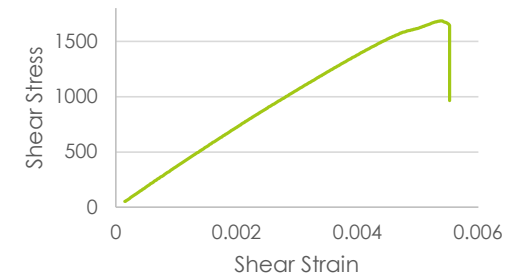
Carbon Strength



West Systems 105/206



Lord 310 A/B



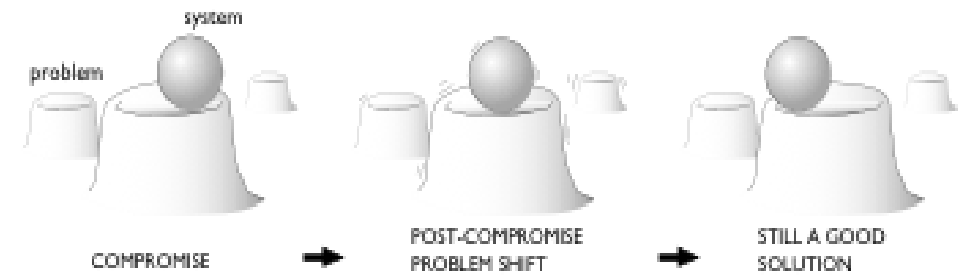
Satisficing in Engineering Design

Dylan Lloyd, Jordan Perkins, Lin Guo, Janet K. Allen, Farrokh Mistree

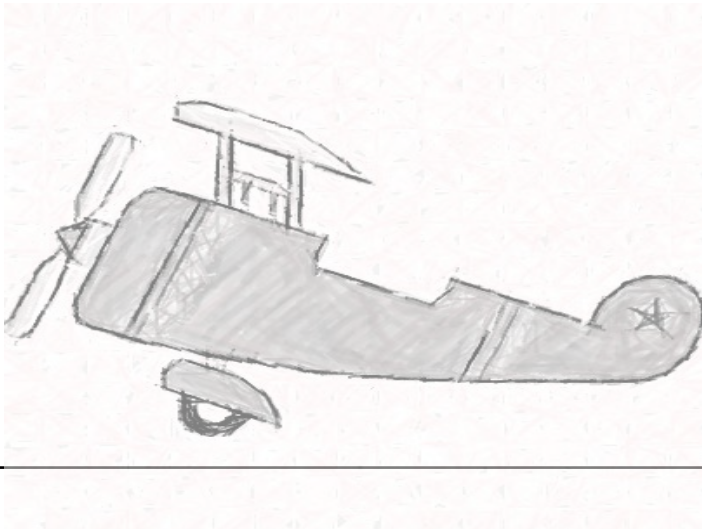
An Optimum Solution



A Satisficing Solution



Test Problem

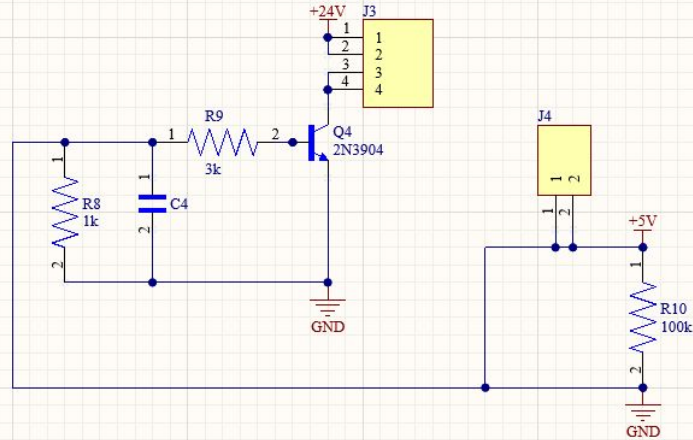


- Optimization
- Satisficing

Findings

- Optimized solutions assume there is no change in formulation
- Satisficing solutions, regardless of starting point, will be relatively close to goals

Application of a Debouncing Circuit on an Emergency Cut-off Switch

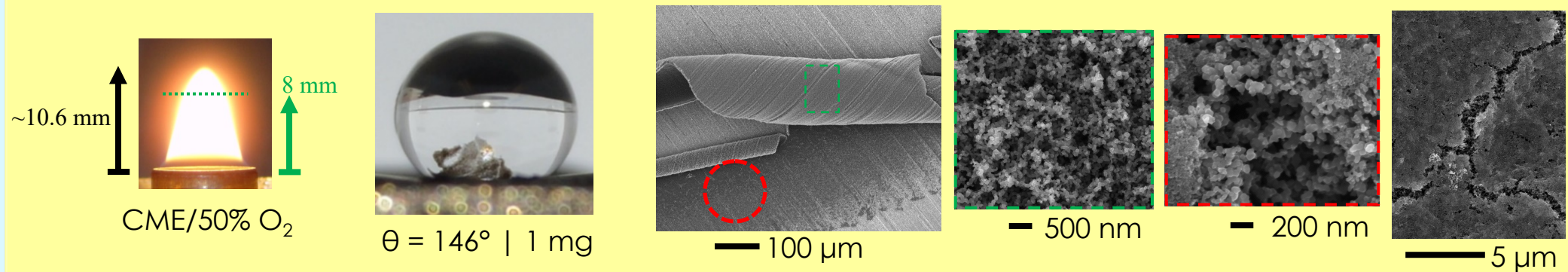
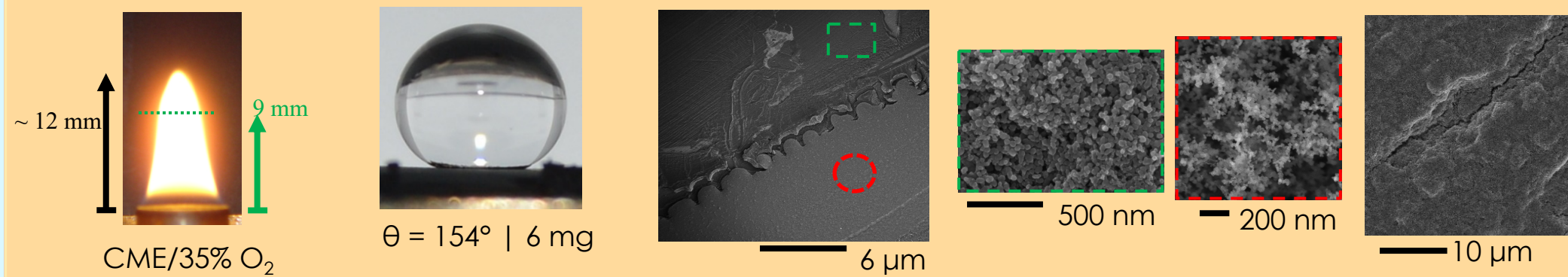
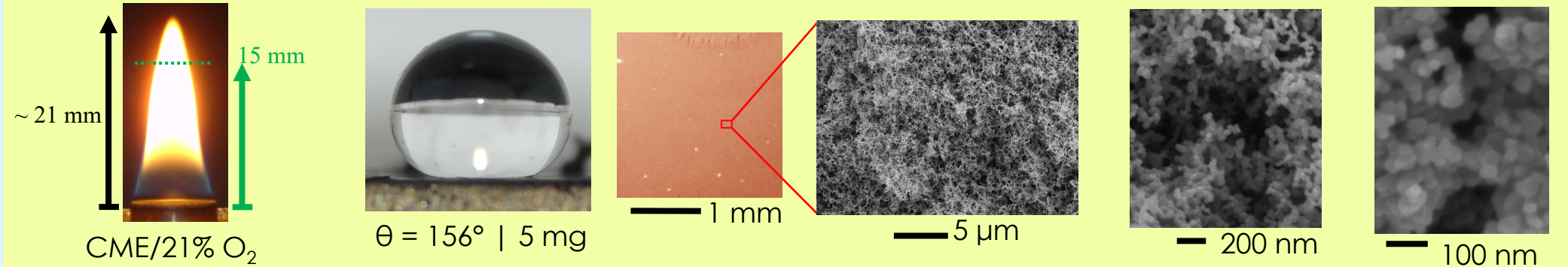
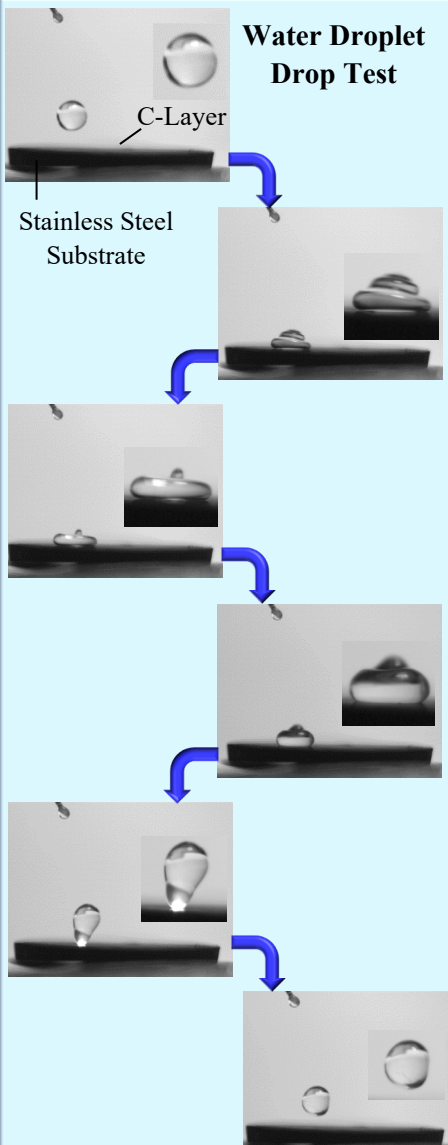


By Benjamin Weir and AJ Mallett
Oral Roberts University School of Engineering



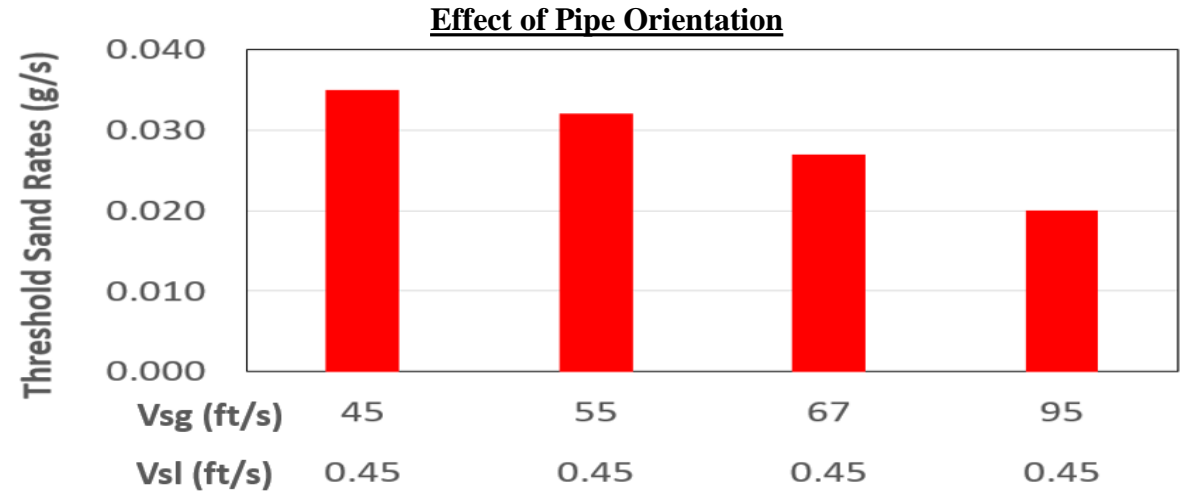
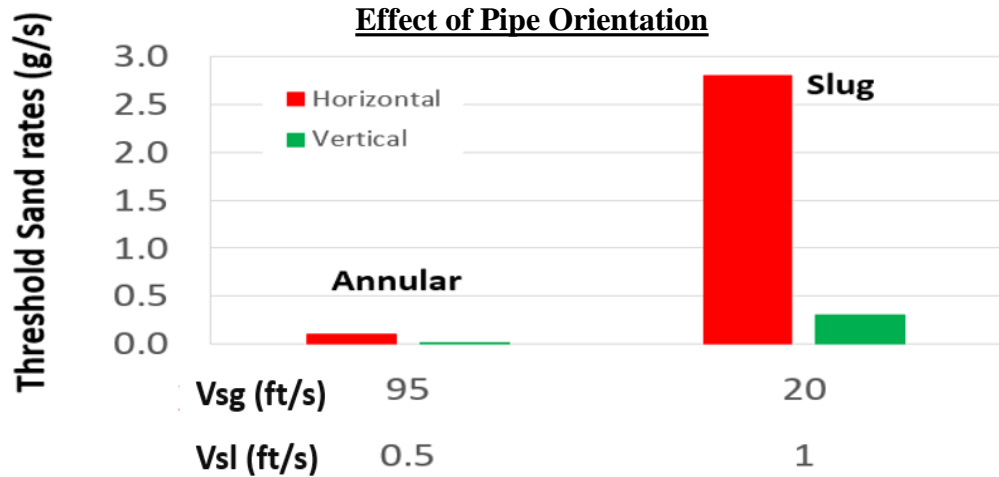
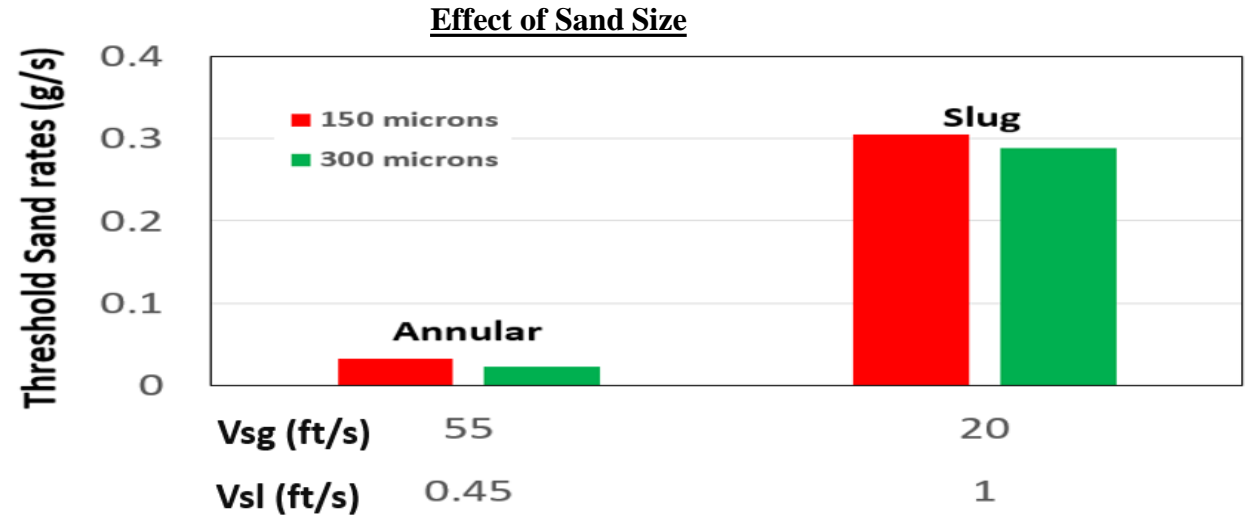
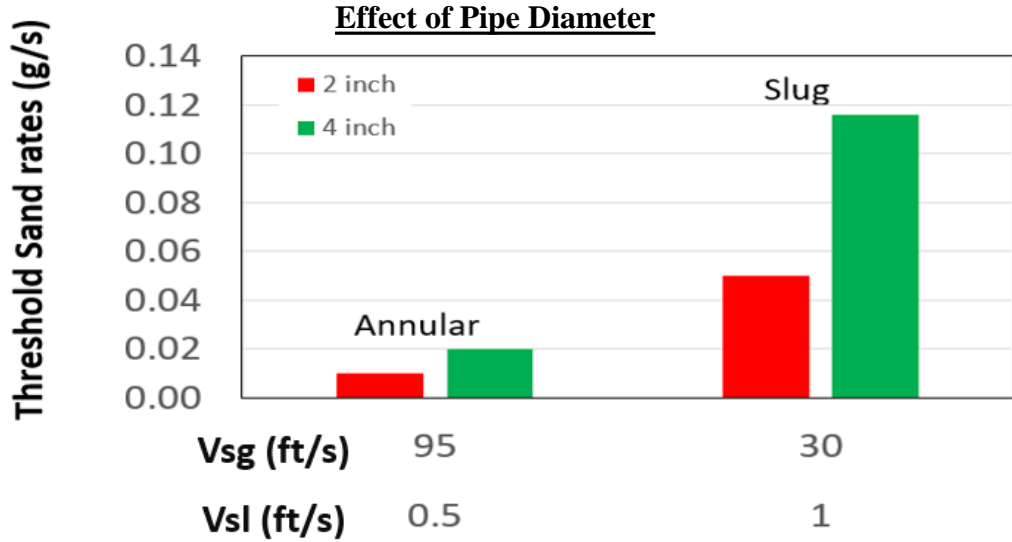
Rapid Synthesis of Carbonaceous Hydrophobic Layers via an Oxygen-Enriched Flame Deposition Process

Duncan Merchan-Breuer (School of Aerospace and Mechanical Engineering), Wilson Merchan-Merchan (OU)



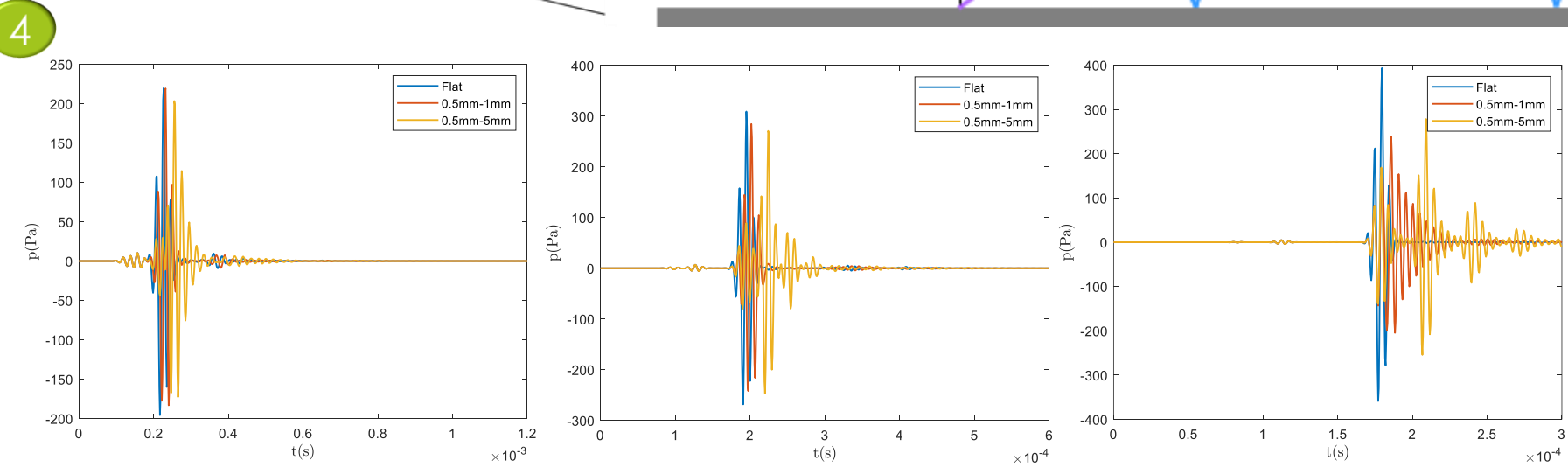
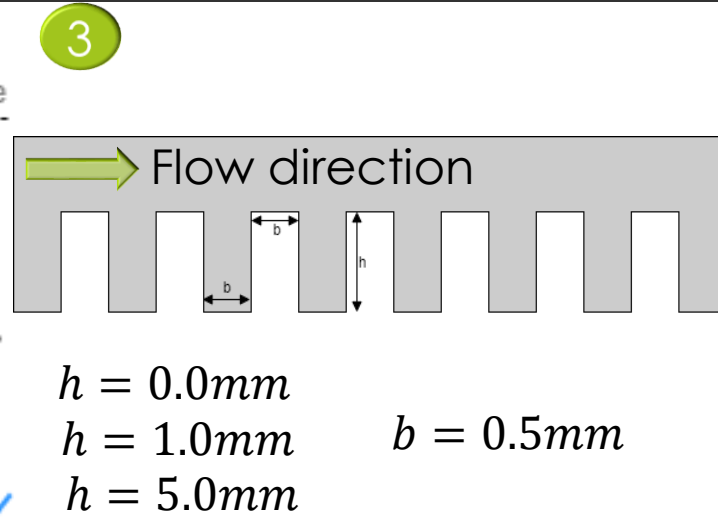
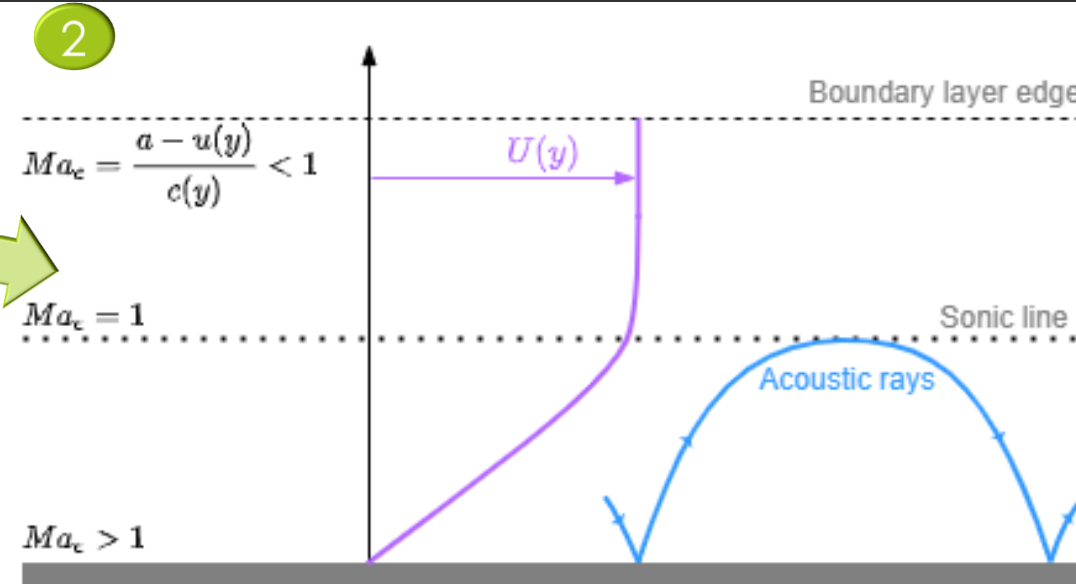
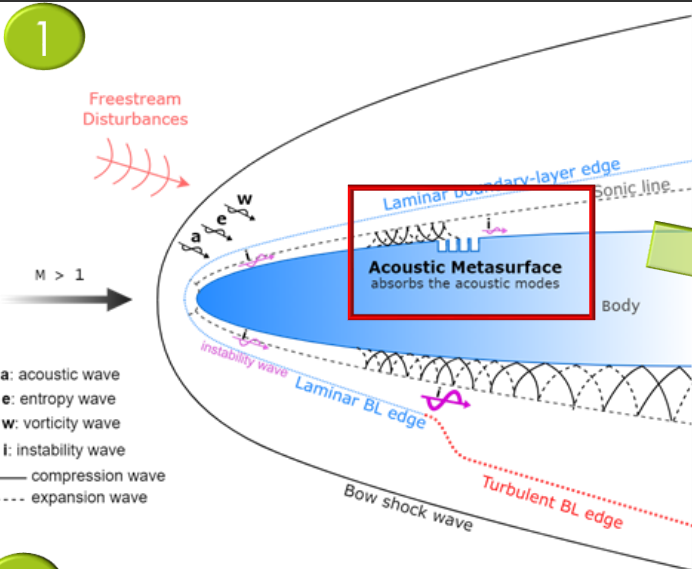
Acoustic Sand Monitors

Asad Nadeem (TU), Ahmed Nadeem(TU) and Dr. Siamack Shirazi



Stabilization of the Acoustic Mack Modes with Metasurface

Furkan Oz, Kursat Kara



Absorption Ratio			
Case	50 kHz Wave	100 kHz Wave	200 kHz Wave
Flat	0.00	0.00	0.00
1mm	0.00	0.13	0.29
5mm	0.01	0.03	0.15

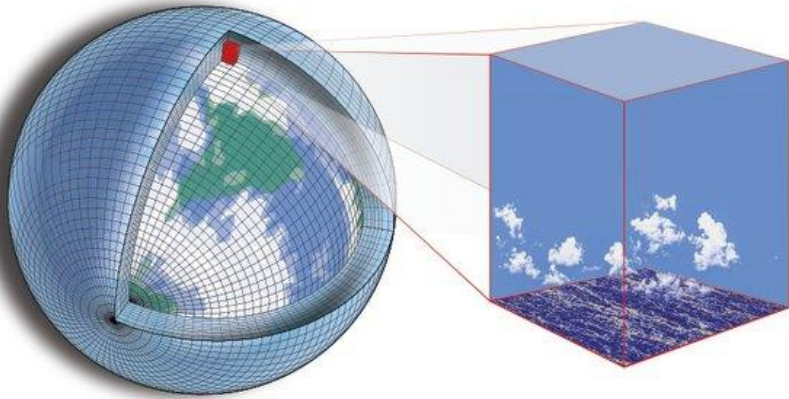
50 kHz

100 kHz

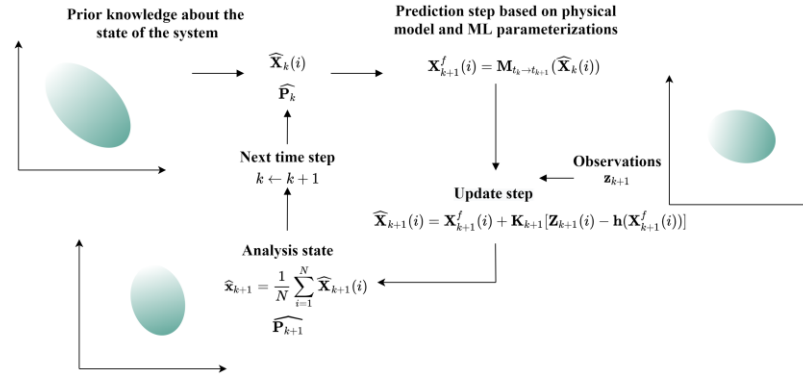
200 kHz

Deep learning approaches for subgrid scale parameterization in chaotic dynamical systems

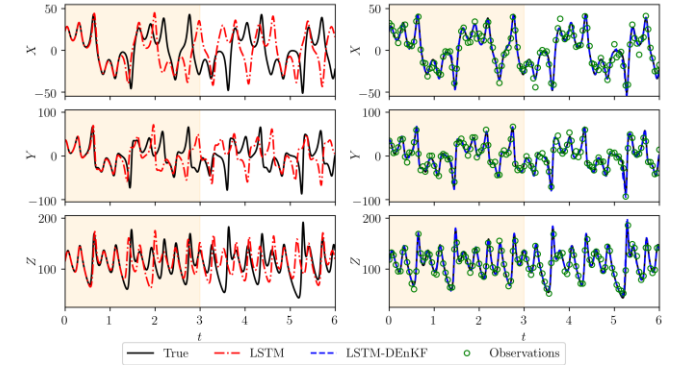
Suraj Pawar (OSU), Omer San (OSU)



Online observations collected from sensors and satellite measurements can be assimilated using sequential DA.



Missing dynamics in strongly chaotic Lorenz system is modeled using LSTM.

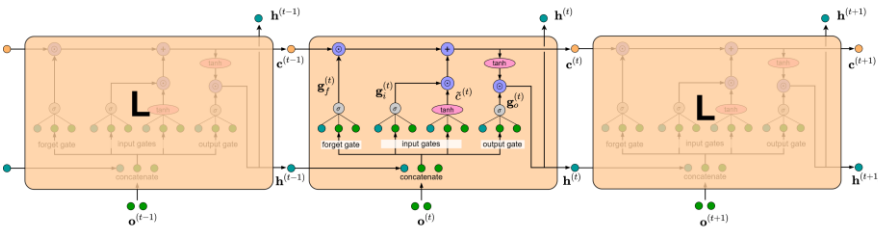


Source: Schneider et al. "Climate goals and computing the future of clouds" Nature Climate Change (2017)

Physics-based parameterization

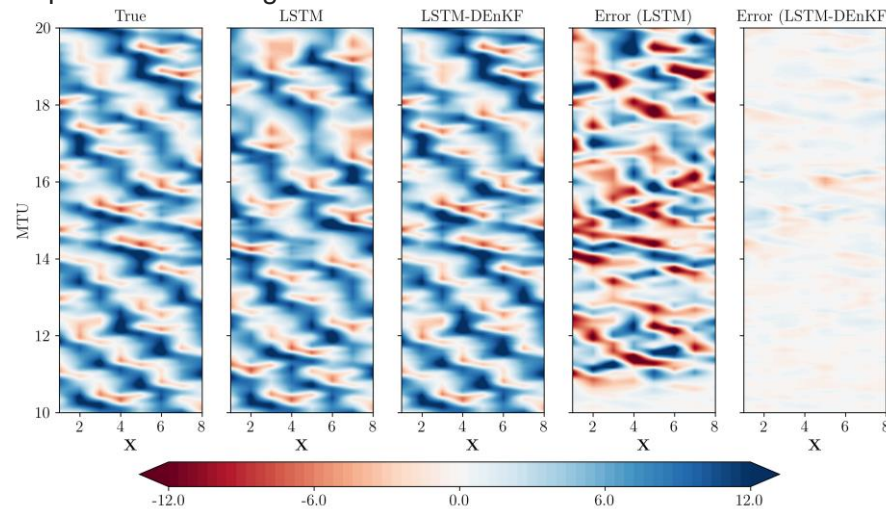
$$Y = F(X)$$

Deep learning?

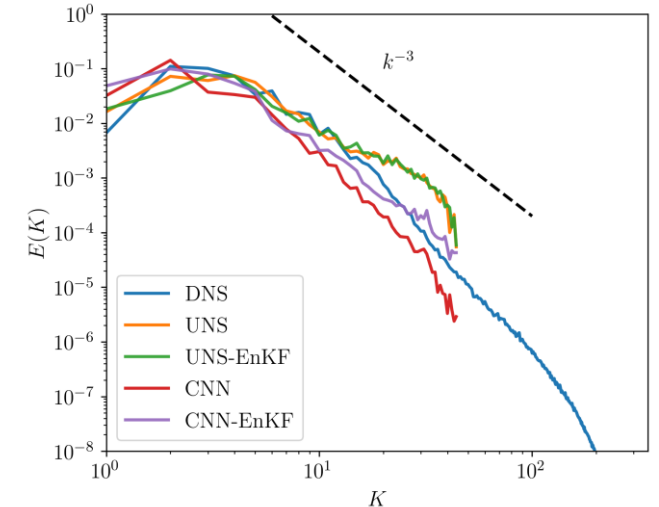


Deep learning algorithms like recurrent neural network, convolutional neural network can learn the complex spatio-temporal pattern from the data.

The DL methods can accurately model the short-term forecast of two-scale Lorenz system and the DA can further augment the prediction for longer horizon.



DL models are computationally efficient and can be stabilized in a posteriori deployment. DA improves the energy spectra for Kraichnan turbulence.

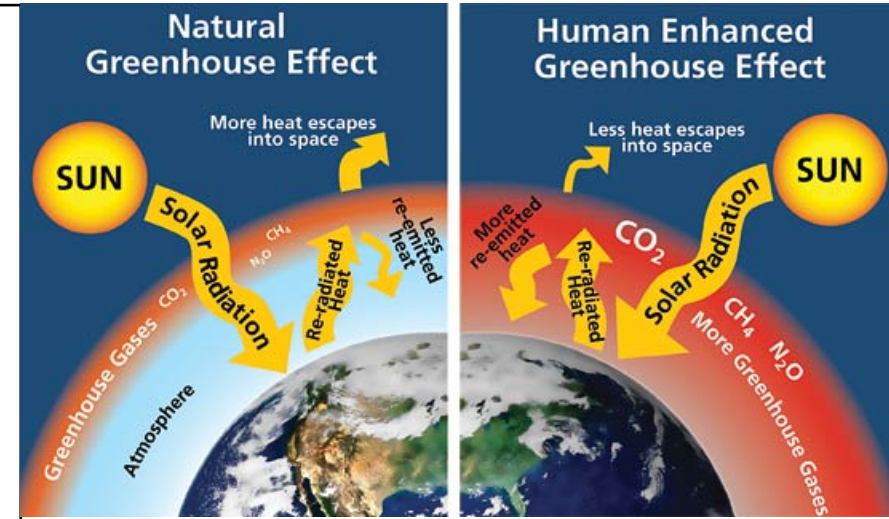


Designing Inventory Model for a Green Supply Chain (GSC) from Climate Change Mitigation Perspective

Dylan Portillo, Reza Alizadeh, Janet K. Allen and Farrokh Mistree

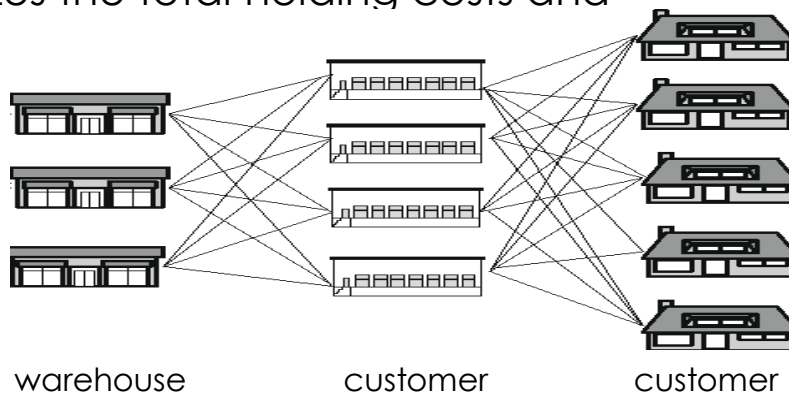
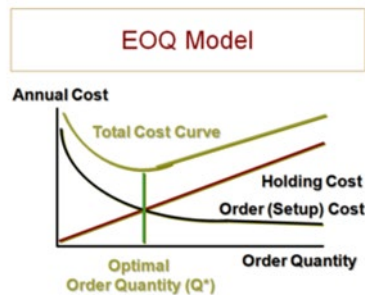
Background and Importance

- The green SC mitigates the climate change through greenhouse gas(GHG) emission reduction.
- According to the US EPA, companies with a (SC) generate about 42% of GHGs in their transportation (30%) and inventory systems (12%).
- Over-sized orders causes unnecessary costs and GHG while under-sized orders causes unmet demand, loss of reliability and customer dissatisfaction.



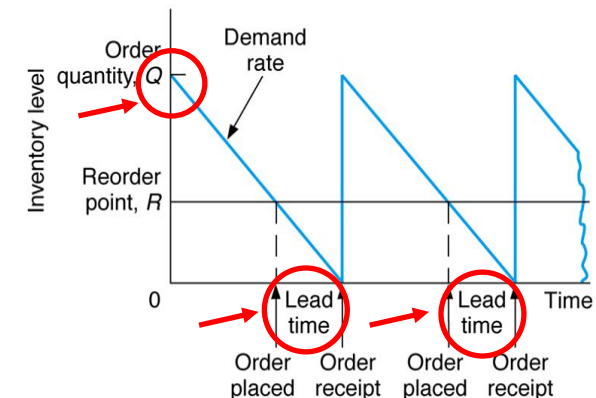
Method

Economic Order Quantity method for a multi-echelon and multi-commodity supply chain is used as the order quantity that minimizes the total holding costs and ordering costs.



Results

- Based on this model, it shows how much the store will order and when to order it.
- Finding the optimal order point and time will help to cut the cost and emission.



Data Curation for Fail-Safe Healthcare Networks

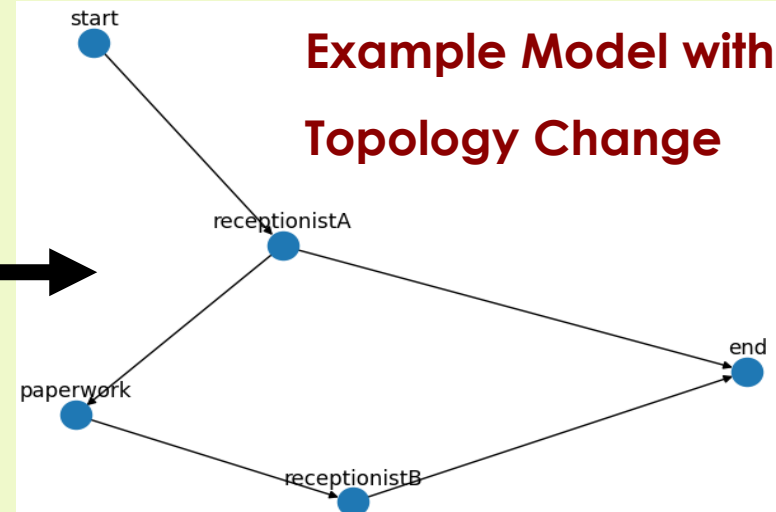
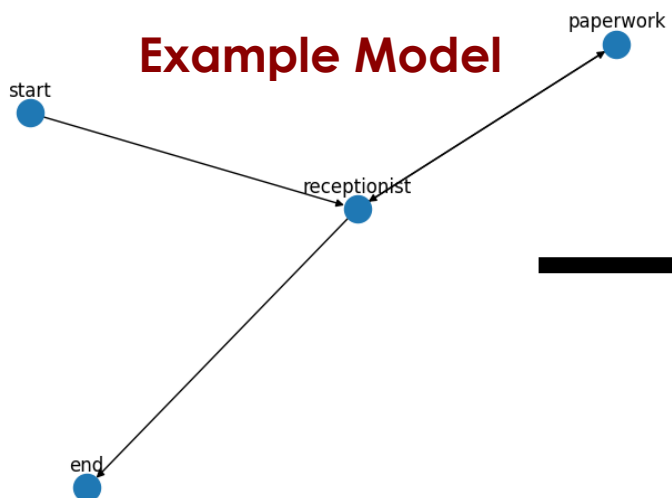
Nathan Preuss, Lin Guo, Janet K. Allen, Farrokh Mistree

Importance

- Patients are **unhappy** when they wait long times for treatment
- **Analyze patient flow** in a hospital to identify hidden bottlenecks and reduce patient wait times

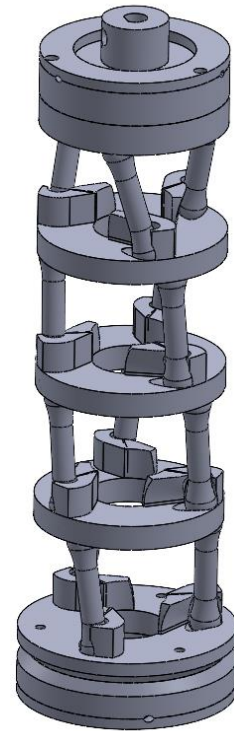
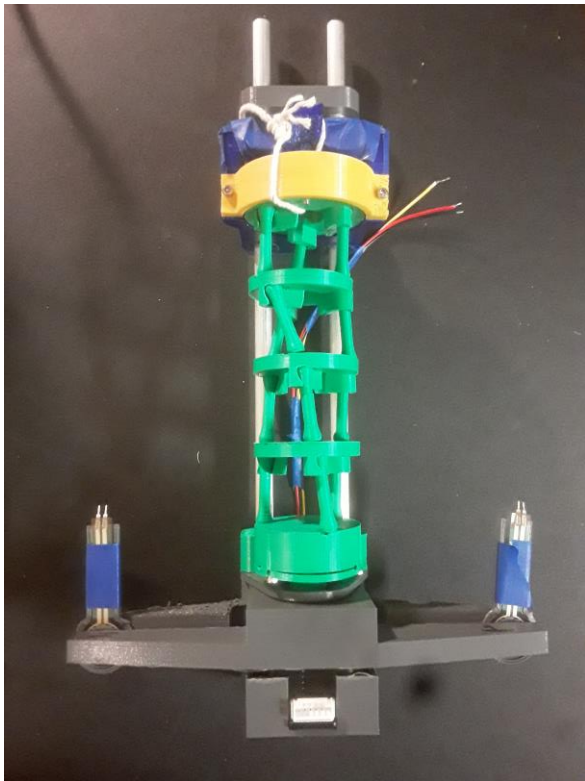
Expected Outcomes

- **Curate** synthetic data simulating patient arrivals
- Change the **network topology** and flow capacity to **remove bottlenecks**
- Removing bottlenecks **reduces patient wait time**
- Build a network model of a **primary care clinic**.

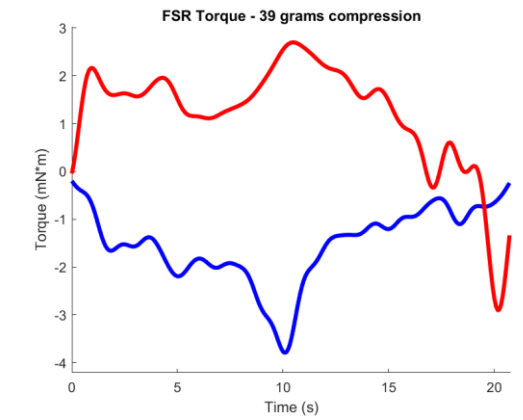
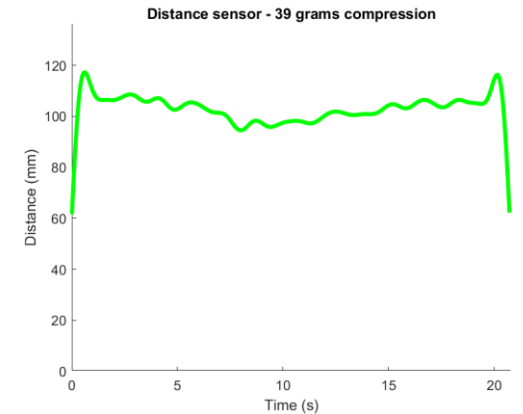


Linear Actuator with Large Relative Displacement

Joel Quarnstrom (OSU)



- Design utilizes coiling of helical wires to cause linear motion
- Seven 3D printed prototypes were constructed
- The system was tested, and the displacement and input torque were recorded

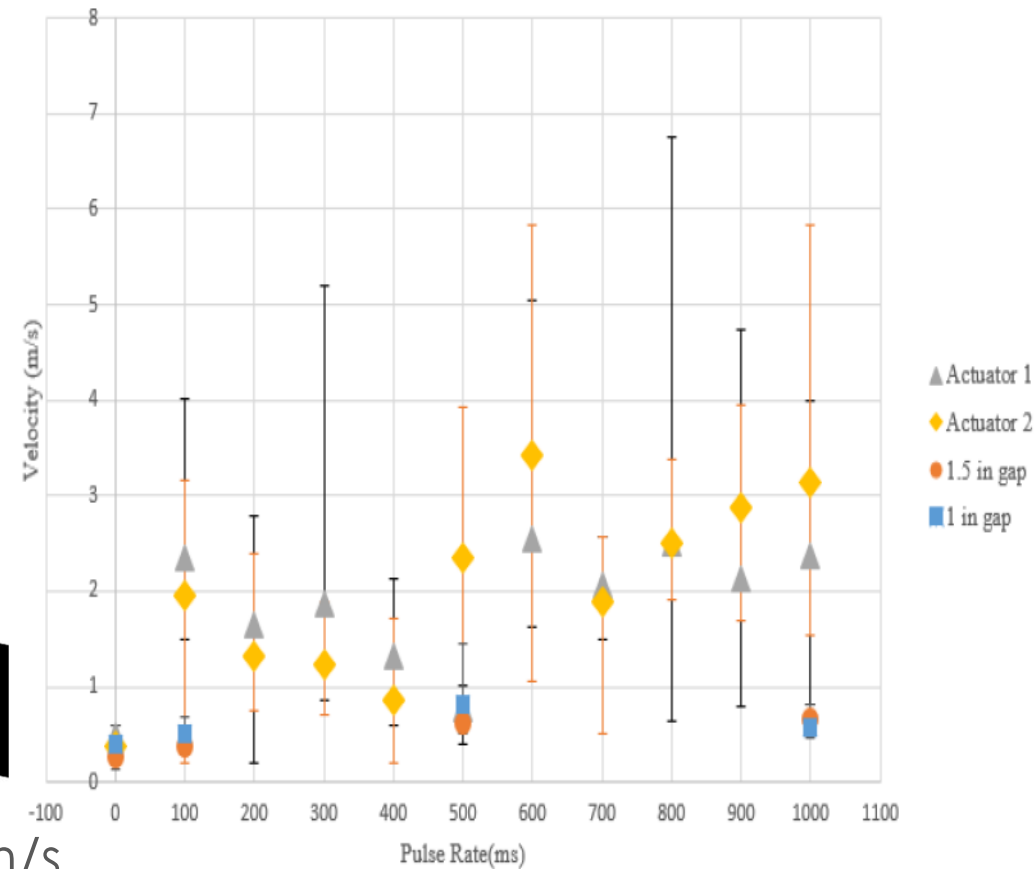
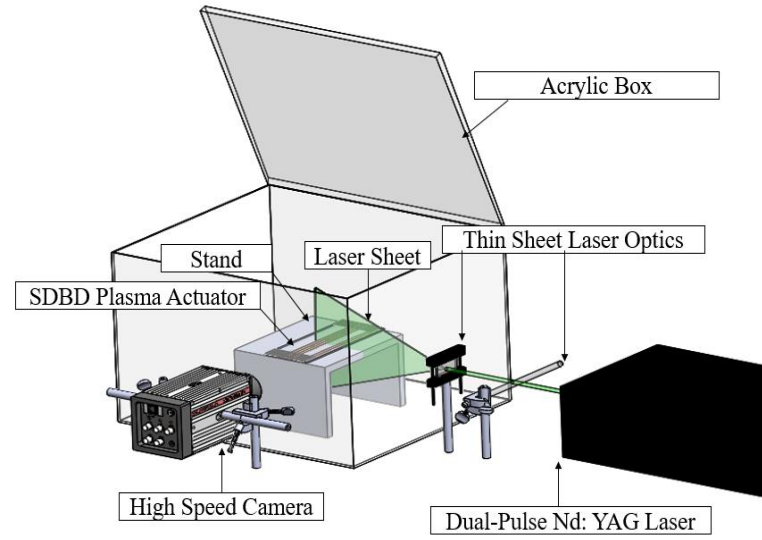
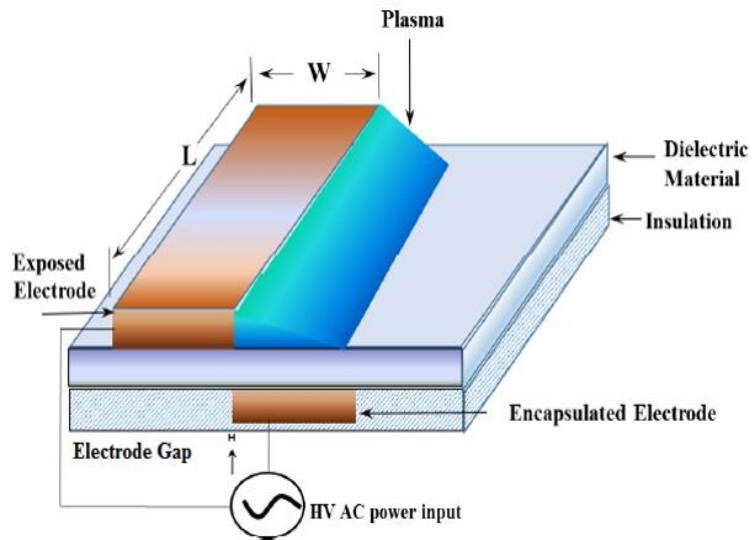


Parametric Analysis of Surface Dielectric Barrier Discharge Plasma Actuators

Andrew Quinton (OSU), Alvin Ngo, and Jamey Jacob

Exploration and optimization of solid state electrical propulsion

- Primary propulsion system for a low speed environmentally friendly UAV
- Integrating with or replacing specific flow control devices



A single actuator is able to average speeds around 3 m/s

The data gathered here sets a baseline of the actuators performance, but more testing of pulse rates and distances between actuators are needed.

Air-Assisted Atomization of Beveled Needle Point Injector

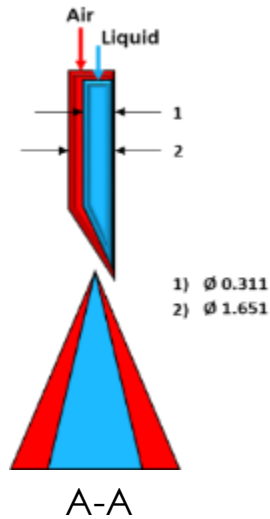
M.S. Raza, Alex Valiaev, R. Taylor, and Khaled Sallam

Motivation

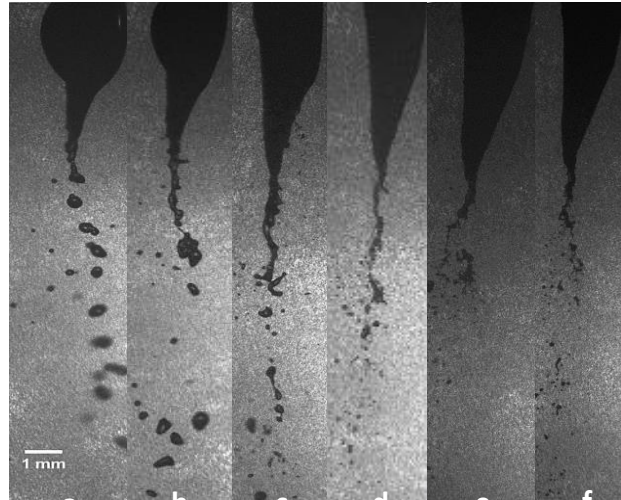
Can we construct a disposable and affordable air-assisted atomizer that can be used to provide the same results as industrial atomizers.

Objectives

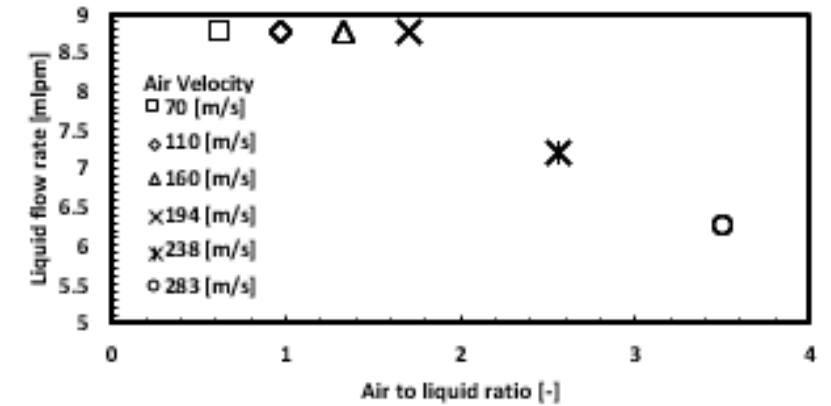
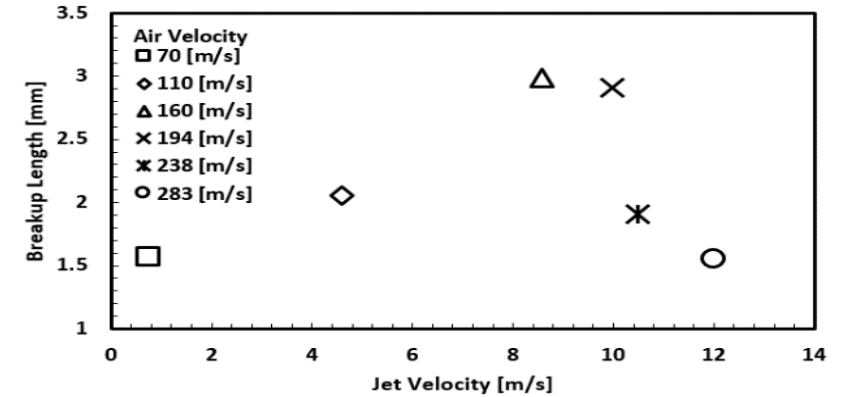
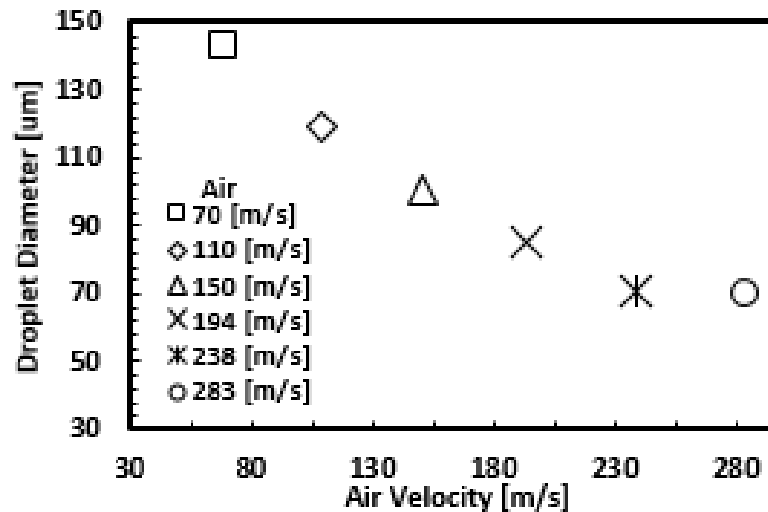
1. Investigate the atomization outcomes from a cheap air-assisted atomizer.
2. Investigate whether the droplet sizes can be controlled by the air speed.



Increasing air velocity from left to right.

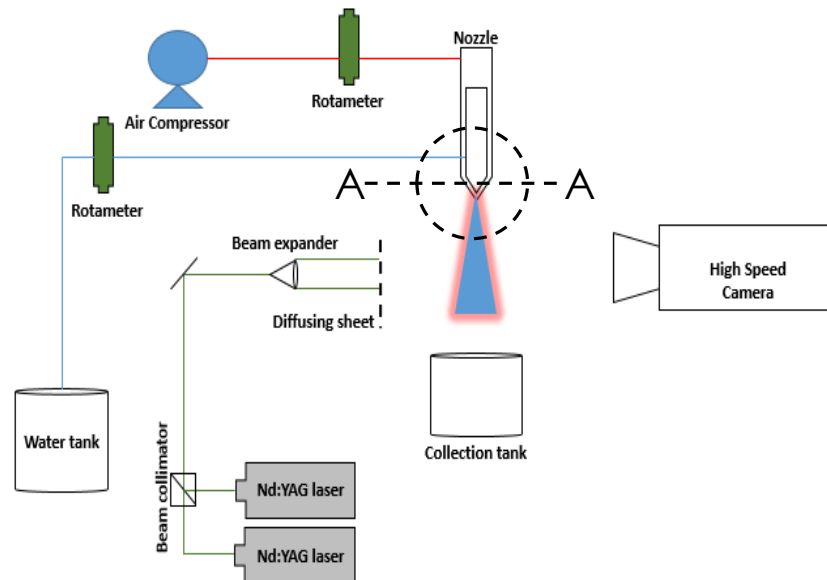


We 0.04 [-] 0.04 [-] 0.04 [-] 0.04 [-] 0.03 [-] 0.02 [-]



Conclusions

- The variation in air velocity impact the size of the droplets directly.
- The higher air velocities produced a water cloud which indicates much smaller droplets being formed.
- The current atomizer was effective in producing smaller droplets.



L. Rezaei ^{a*}, J. Perez ^a, G. Scalet ^b, M. Peigney ^c, A. Azoug ^a

^a MS²M lab, School of Mechanical and Aerospace Engineering, Oklahoma State University, USA.

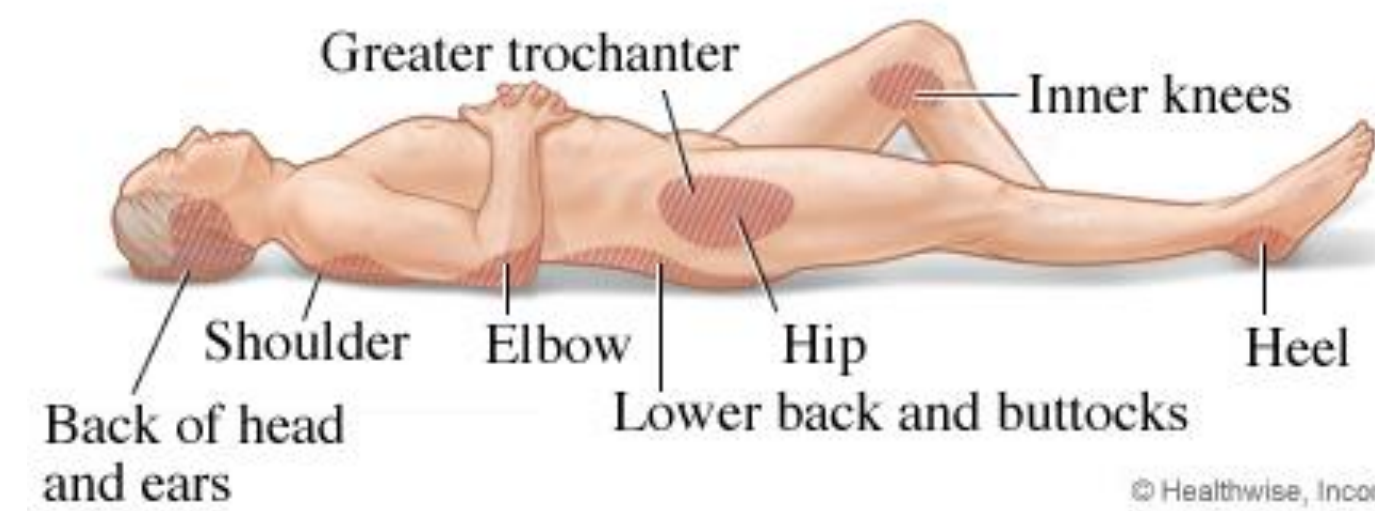
^b Department of Civil Engineering and Architecture, University of Pavia, Italy.

^c Université Paris-Est, Laboratoire Navier (UMR 8205), CNRS, Ecole des Ponts ParisTech, France.

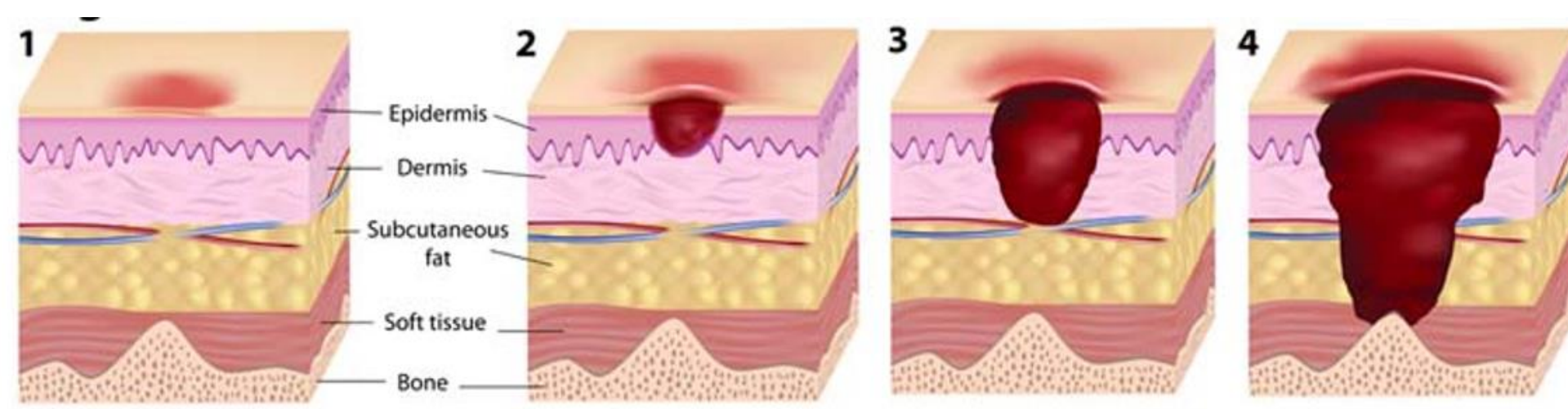
* leila.rezaei@okstate.edu

Introduction

Pressure ulcers = bed sores



- common health condition
- cost \$11B a year to treat [2]
- target patients unable to feel skin aching
- linked to sustained pressure under a bony prominence, such as the heel
- necrosis of the skin until bone is reached
- start after 4-6 hours of immobility [3]
- currently prevented by regularly moving the patient using special mattresses

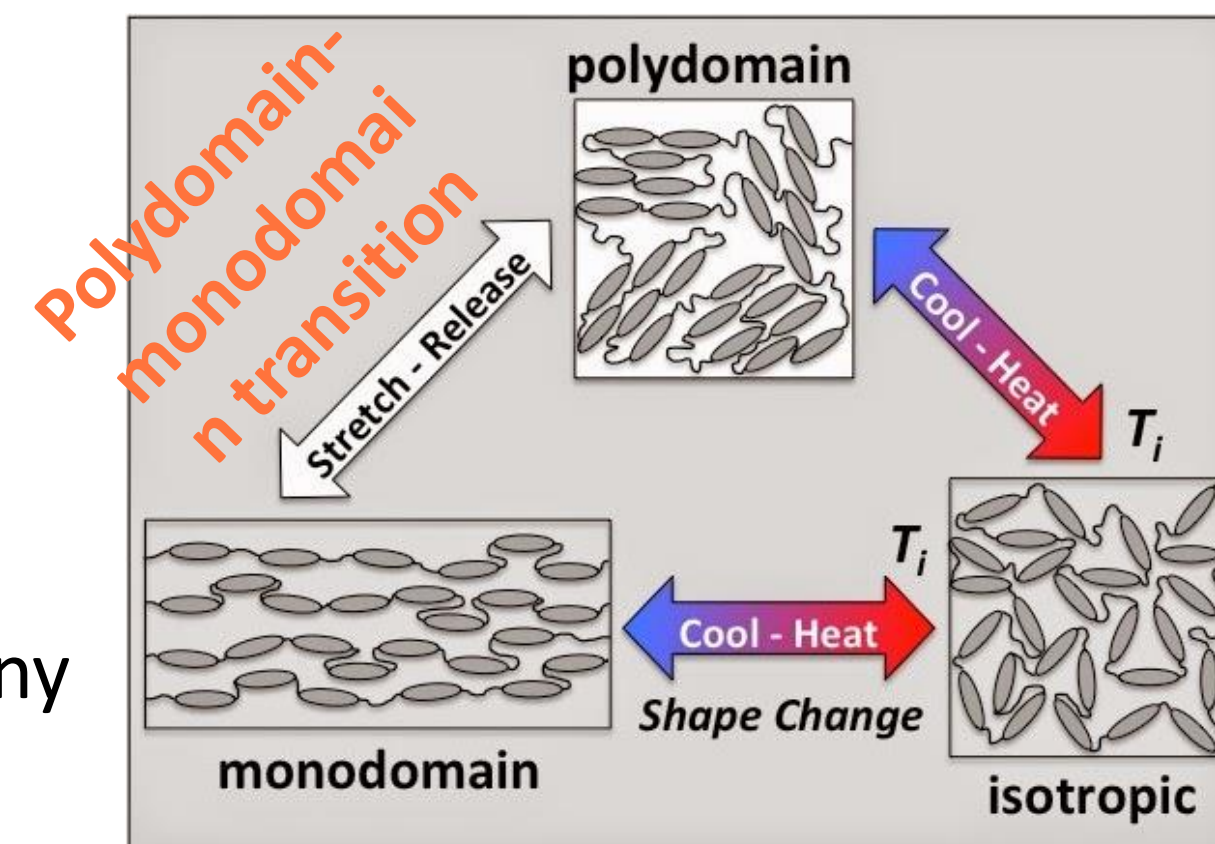


LCE smart skin

- redistributes pressure under bony prominence through soft elasticity
- dissipate energy, damps vibration through viscoelasticity
- adapts to patient changing position through recovery

Liquid crystal elastomers (LCEs)

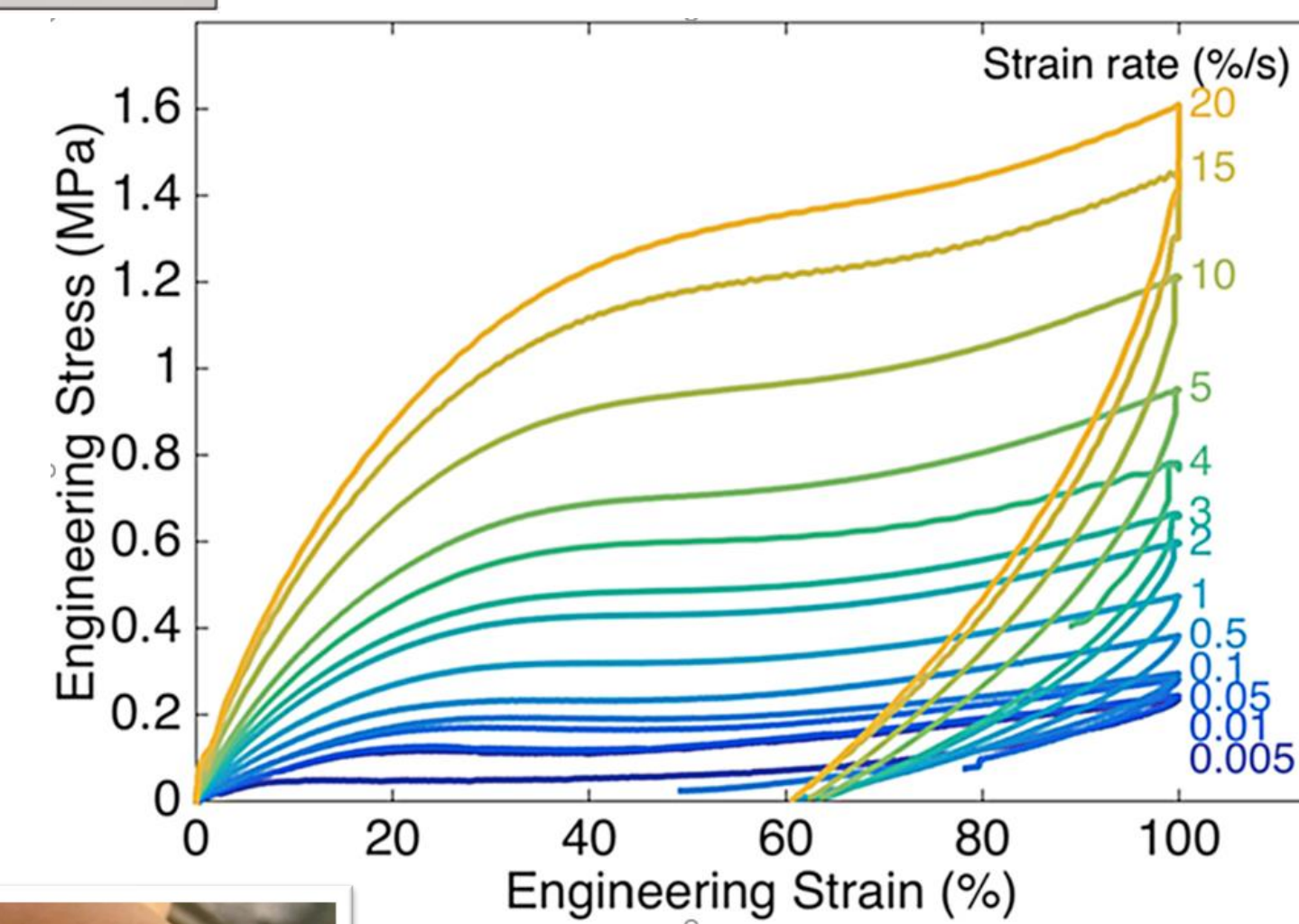
smart elastomers, combining rubber elasticity of the cross-linked elastomer with orientation of liquid crystals.



Remarkable properties

- Viscoelasticity
- Soft elasticity [6]
- Shape memory
- Biocompatibility

Phases of LCEs [5]



Objectives

Assess the ability of LCEs to mitigate pressure ulcers by distributing pressure under bony prominence.

- Model the viscoelastic mechanical behavior of LCEs in tension and compression
- Implement model in finite element software
- Identify model parameters with experimental data
- Simulate the smart skin under the heel

References

- [1] <https://myhealth.alberta.ca/Health/Pages/conditions.aspx?hwid=zm2441&lang=en-ca>
- [2] Chandan K. Sen PhD Gayle M. Gordillo MD Sashwati Roy PhD Robert Kirsner MD Lynn Lambert CHT Thomas K. Hunt MD Finn Gottrup MD Geoffrey C. Gurtner MD Michael T. Longaker MD, Human skin wounds: A major and snowballing threat to public health and the economy, Wound Repair and Regeneration, 2009, 17(6)
- [3] A. Gefen, How Much Time Does it Take to Get a Pressure Ulcer? Integrated Evidence from Human, Animal, and In Vitro Studies Ostomy Wound Management, 2008;54(10):26-35.
- [4] <https://www.aafp.org/afp/2015/1115/p888.html>
- [5] M.O. Saed, A.H. Torbati, D.P. Nair, C.M. Yakacki, Synthesis of Programmable Main-chain Liquid-crystalline Elastomers Using a Two-stage Thiol-acrylate Reaction, 2016, Journal of Visualized Experiments : JoVE, 107: 53546.
- [6] A. Azoug, V. Vasconcellos, J. Dooling, M. Saed, C. M. Yakacki and T. D. Nguyen, Viscoelasticity of the polydomain-monomain transition in main-chain liquid crystal elastomers, Polymer, 2016, 98, 165–171.
- [7] G. Scalet, M. Peigney (2017) A robust and efficient radial return algorithm based on incremental energy minimization for the 3D Souza-Auricchio model for shape memory alloys. Eur. J. Mech. A 61:364–382
- [8] F. Auricchio, L. Petrini, 2004. A three dimensional model describing stress-temperature induced solid phase transformations: solution algorithm and boundary value problems. International Journal for Numerical Methods in Engineering 61, 807-836.

Constitutive Model

- Inspired by the Souza-Auricchio model [7,8]
- Viscoelasticity introduced as linear Maxwell model

$$\sigma = \mathbb{C} : (\varepsilon - e^{tr}) + \sum_{m=1}^M \int_0^t E_m e^{-(t-s)/\tau_m} (\dot{\varepsilon}(s) - \dot{e}^{tr}(s)) ds$$

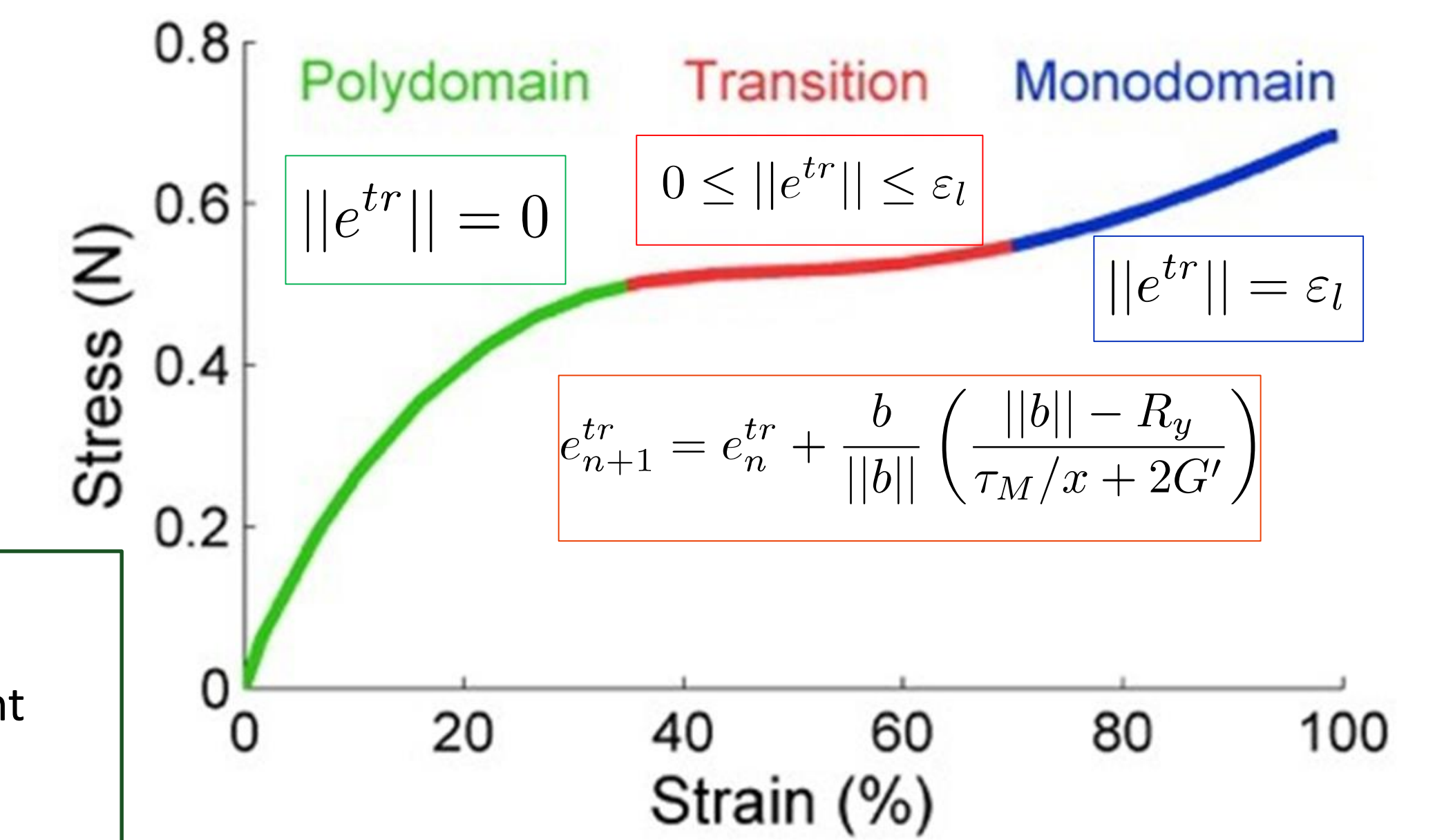
Elastic part

Viscoelastic part

$$E = \left(1 - \frac{\|e^{tr}\|}{\varepsilon_L}\right) E_P + \frac{\|e^{tr}\|}{\varepsilon_L} E_M$$

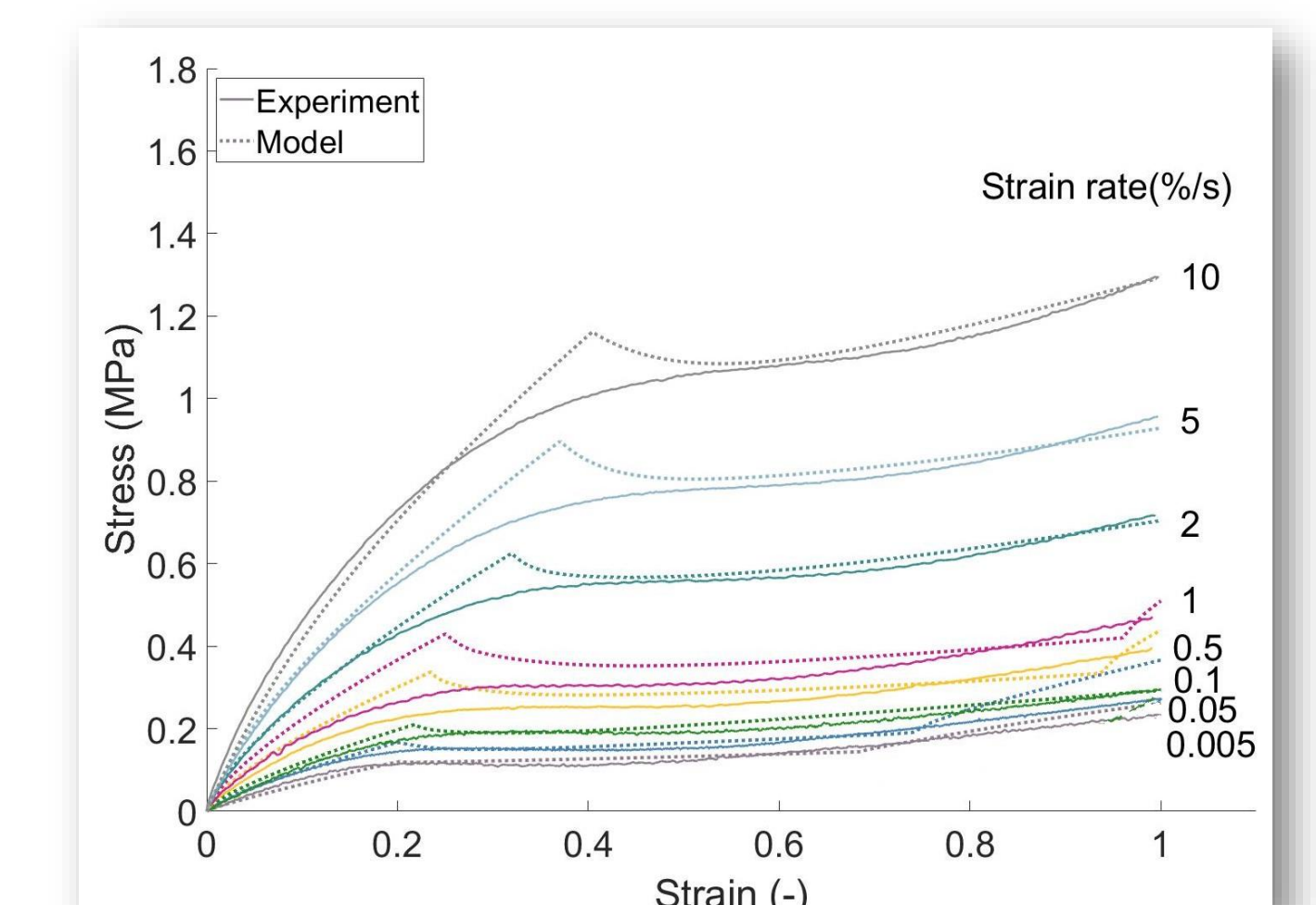
Model parameters

- ν : Poisson's ratio
- E_P : Polydomain modulus
- E_M : Monodomain modulus
- E_m : Viscoelastic moduli
- τ_m : Viscoelastic relaxation times
- ε_L : Residual strain
- β : Scalar transition start point
- R_Y : Hysteresis parameter
- h : Transition hardening



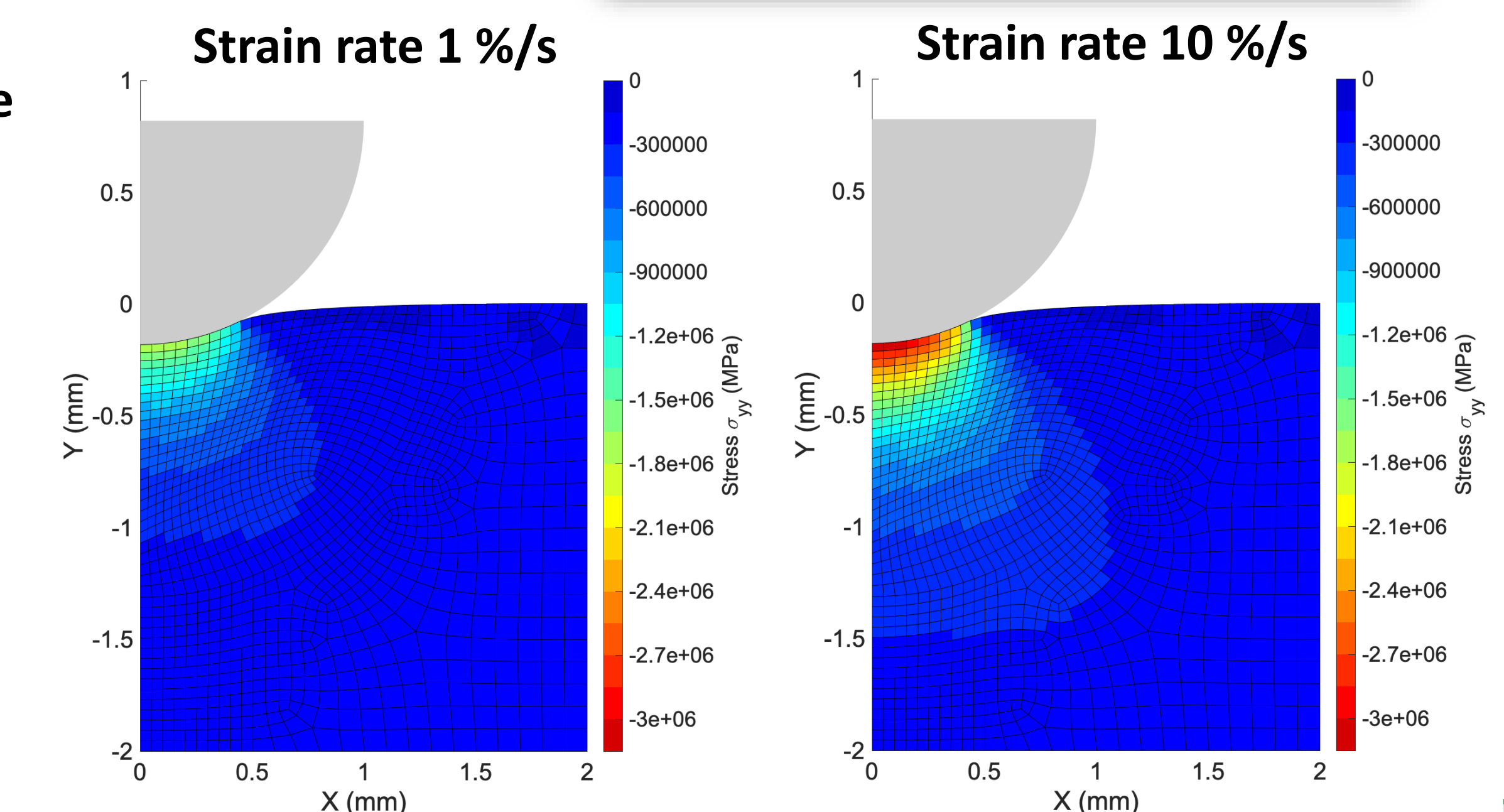
Results and Discussion

- The model predicts the slope in polydomain and soft elasticity regions at small and high strain rates.
- The model predicts when transition starts and ends.
- The model is less accurate in monodomain region, especially at high strain rates.
- Viscoelasticity has a strong influence on the initiation and end of the soft elasticity region

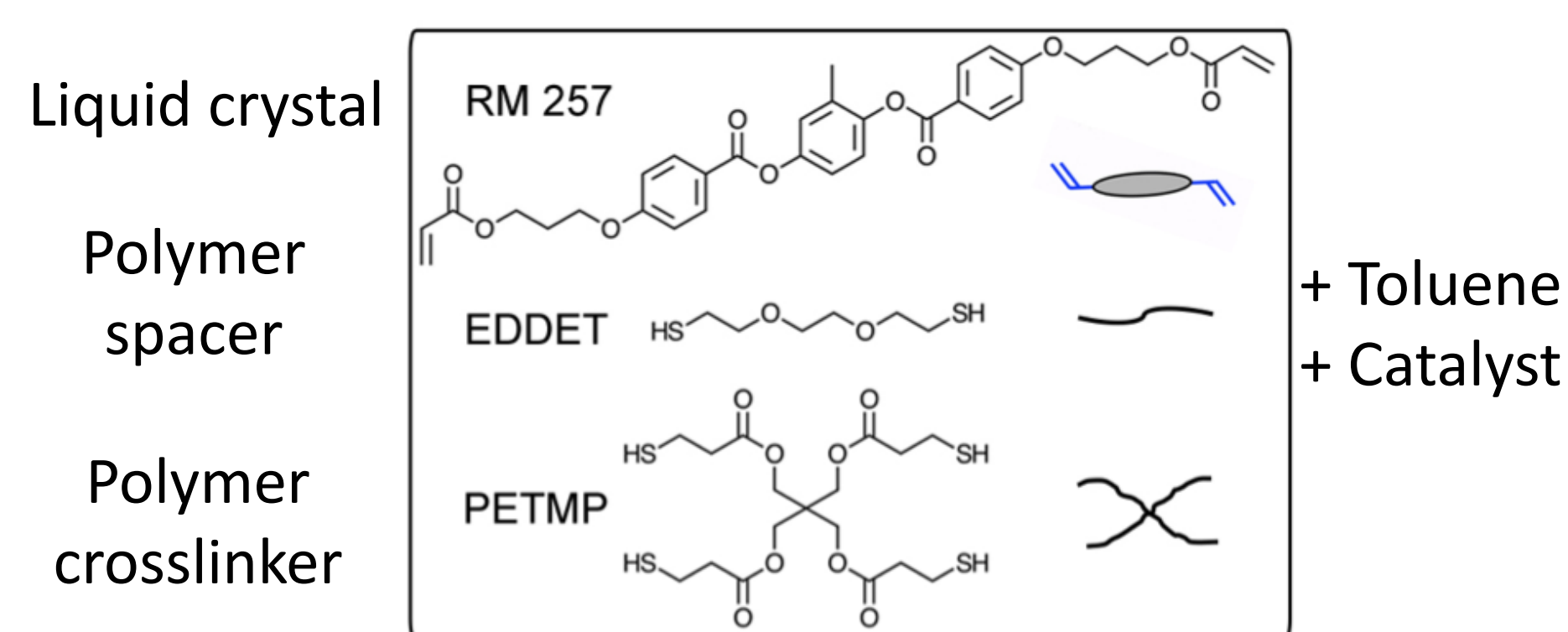


Simulation of compression under a bony prominence

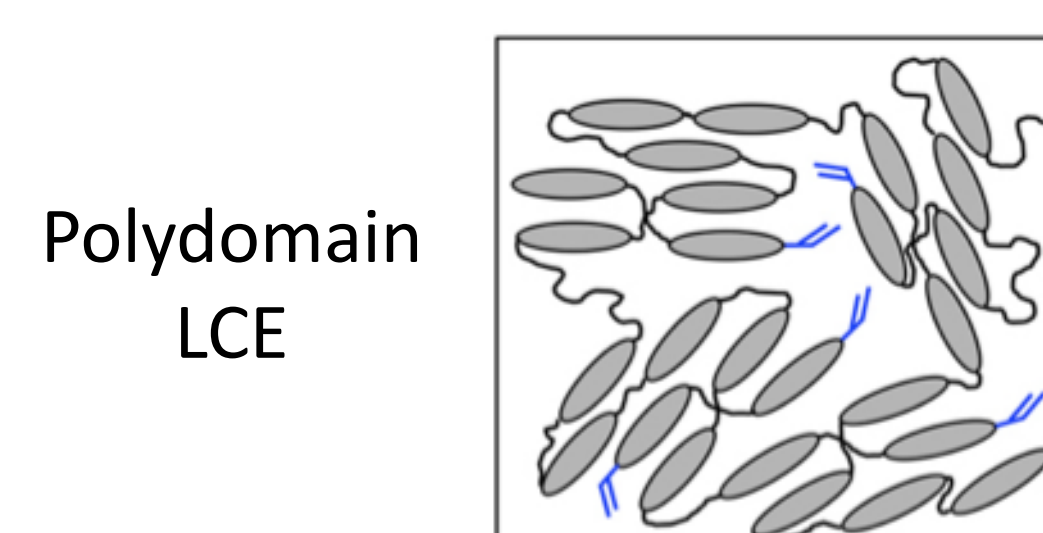
- During local compression, bony prominence applies pressure on the smart skin.
- Viscoelasticity: pressure depends on the speed at which the bony prominence compresses the support.
- Pressure at 10% compression strain is 3 times higher at 10%/s than at 1%/s strain rate.
- Viscoelasticity: at constant strain, pressure relaxes with time to reach an equilibrium value.



LCE Materials Synthesis



Michael addition



Conclusions

- Model represents the soft elasticity behavior of LCEs
- Model represents the viscoelasticity of LCEs
- Material parameters fitted to experiments
- Model implemented in FEAP software
- Simulations show the pressure under local compression
- Problems remain with combining contact problem with the softening behavior

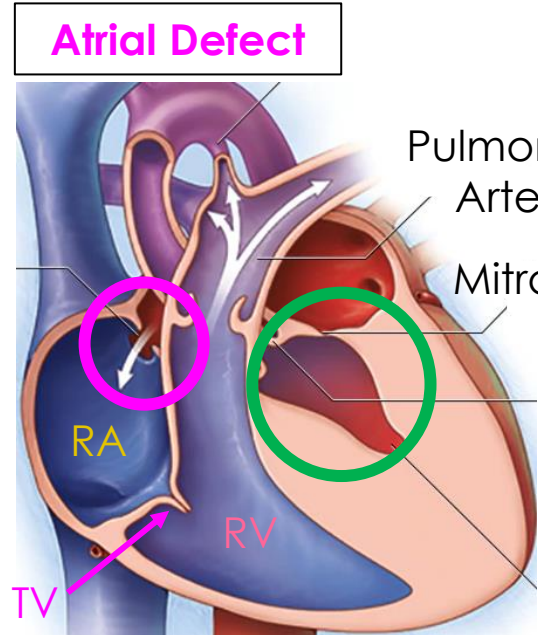
Future work

- Study and model the viscoelastic behavior of LCEs in compression
- Compare the LCE behavior and its parameters in compression and tension
- Simulate in detail the soft elasticity under compression
- Compare simulations to experiments of local compression on LCEs
- Test the smart skin under the heel of human subjects.

Evaluation of the Tricuspid Valve Annulus Mechanics in Newborns with Hypoplastic Left Heart Syndrome Using 4D Echocardiograms

Colton Ross (OU), Arshid Mir (OUHSC), Harold Burkhart (OUHSC), and Chung-Hao Lee (OU)

HLHS-afflicted heart



Atrial Defect

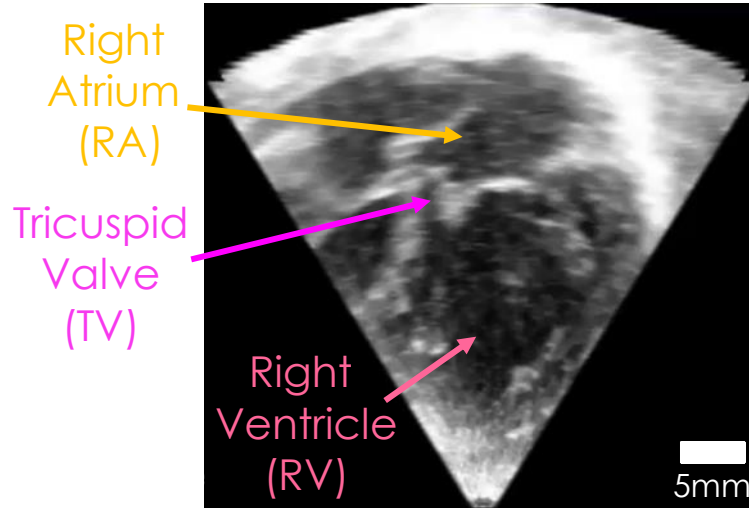
Pulmonary Artery
Mitral Valve

RA
RV

TV

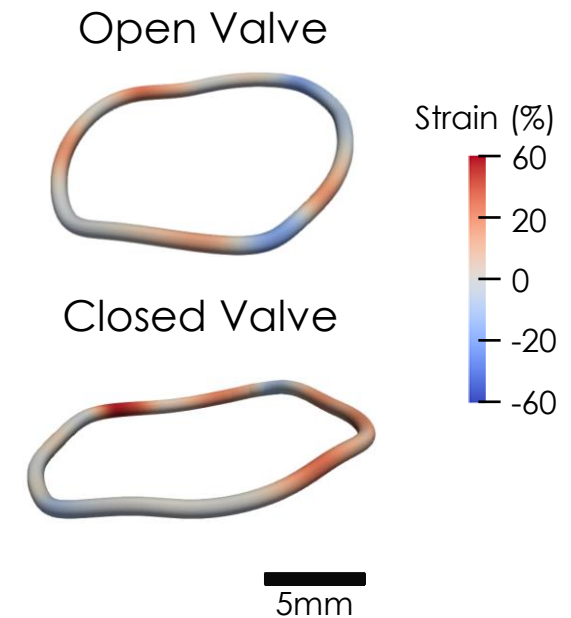
Underdeveloped Left Side of the Heart

4D Echocardiogram



Newborn heart after Stage 1 Surgical Palliation

Annulus Mechanics



Key Findings

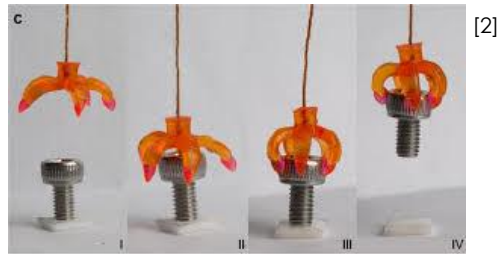
- Peak strains of $\sim 45\%$ and strain rates of $\sim 1500\%/s$ just after leaflet closing
- Highest strains in the *septal-posterior* and *antero-lateral* annulus regions

Structure-property Relationships in 4D-printed Liquid Crystal Elastomers

Zozef Siddiqui(OSU), James E. Smay and Aurelie Azoug

Introduction

4D printing: process of **additively manufacturing an object that changes shape** under the influence of an external stimulus such as temperature, light, or other environmental input [1].



Liquid Crystal Elastomers (LCEs): active materials that exhibit two-way shape changes via the transition between the ordered liquid crystal state and the disordered isotropic state [3].

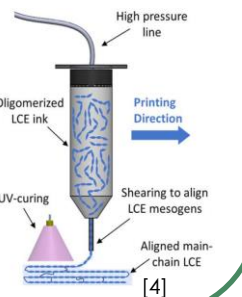
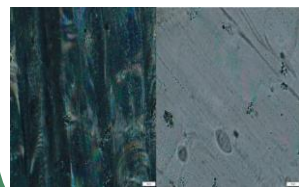
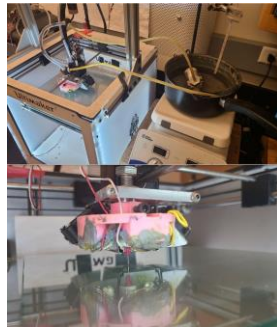
Materials and Methods

LCE ink synthesis

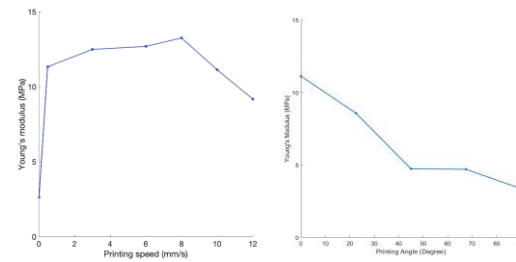
Mesogens RM82 + polymer spacers + photo-initiator (2%wt)

Mechanical properties

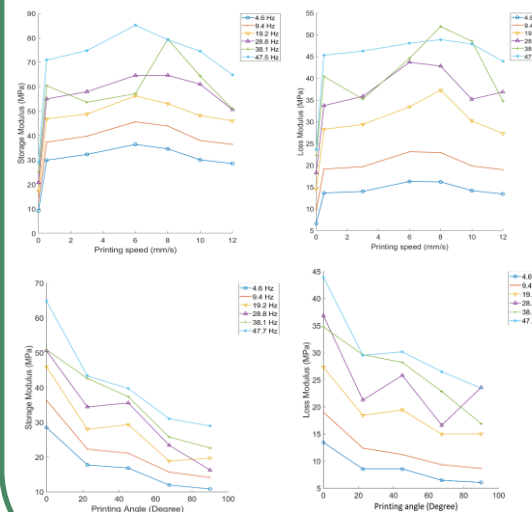
- Tensile tests 1%/s strain rate until failure, room temperature
- Dynamic Mechanical Analysis 0.1% strain amplitude, 5-10-20-30-40-50-60 Hz, room temperature



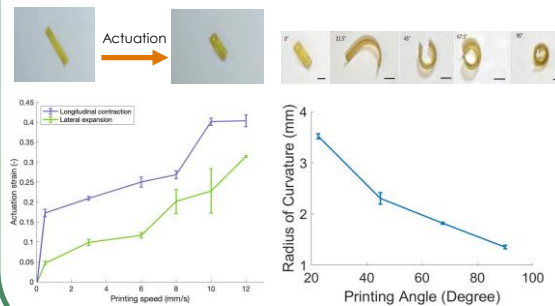
Influence of printing speed and angle on tensile properties



Influence of printing speed and angle on viscoelastic properties



Influence of printing speed and angle on Actuation

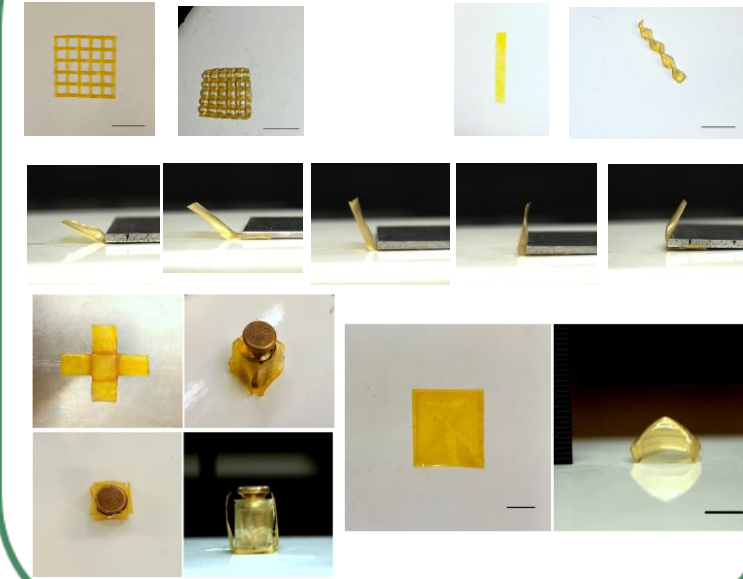


Objectives

What are the properties of 4D printed LCEs? How do they depend on printing parameters?

How to print complex structures with controlled actuation?

Application to soft robotics



Conclusion

What are the properties of 4D printed LCEs? How do they depend on printing parameters?

- Alignment and actuation (contraction) increase with printing speed.
- Printing angle creates bending.
- Young's modulus increase with printing speed up to a threshold.
- Young's modulus decrease with printing angle.
- Storage and loss modulus present the same trends as the Young's modulus.

How to print complex structures with controlled actuation?

- Trial and errors
- Controlled 2D to 3D actuations in multiple directions

References

- Tibbitts, S., 2014. 4D printing: multi-material shape change. *Architectural Design*, 84(1), pp.116-121.
- Warner, M., Bloadon, P., and Terentjev, E.M., 1994. "Soft elasticity"—deformation without resistance in liquid crystal elastomers. *Journal de Physique II*, 4(1), pp.93-102.
- Ge, Q., Sakhaei, A.H., Lee, H., Dunn, C.K., Fang, N.X. and Dunn, M.L., 2016. Multimaterial 4D printing with tailorable shape memory polymers. *Scientific reports*, 6, p.31110.
- Roach, D.J., Kuang, X., Yuan, C., Chen, K. and Qi, H.J., 2018. Novel ink for ambient condition printing of liquid crystal elastomers for 4D printing. *Smart Materials and Structures*, 27(12), p.125011.

Quantifying Social Drivers for Policy Recommendations

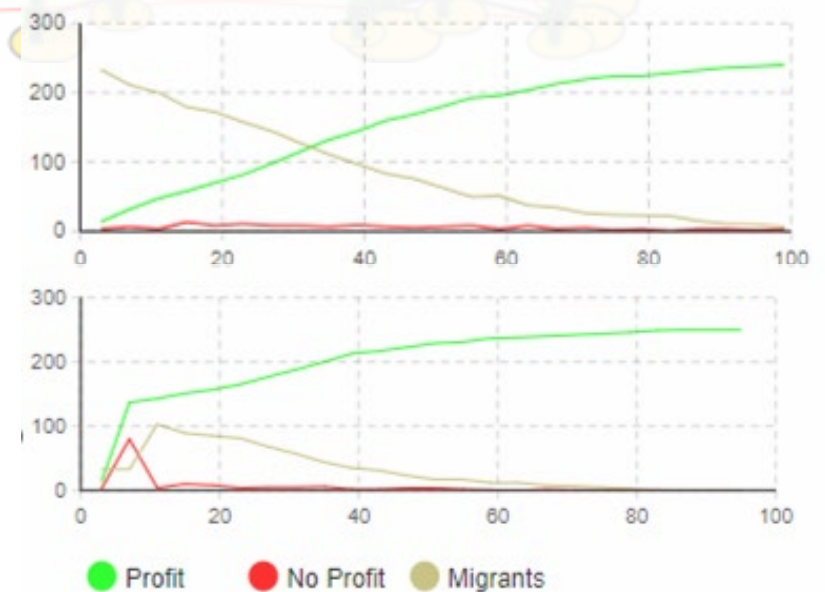
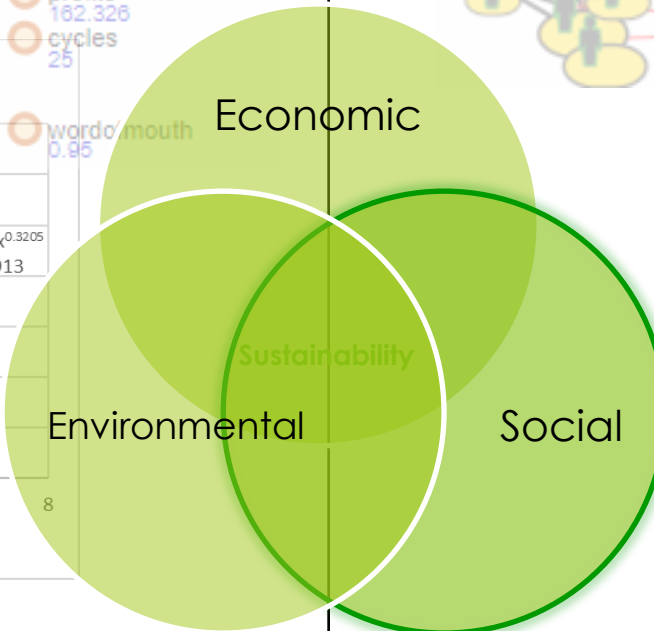
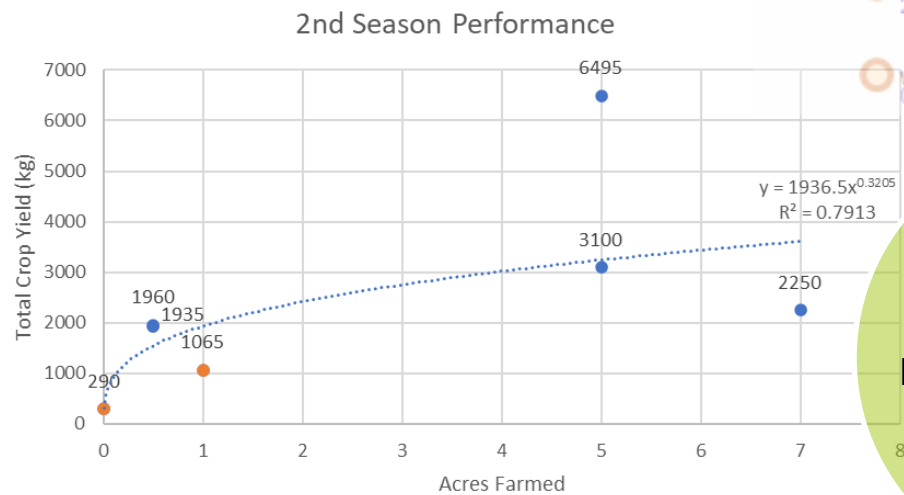
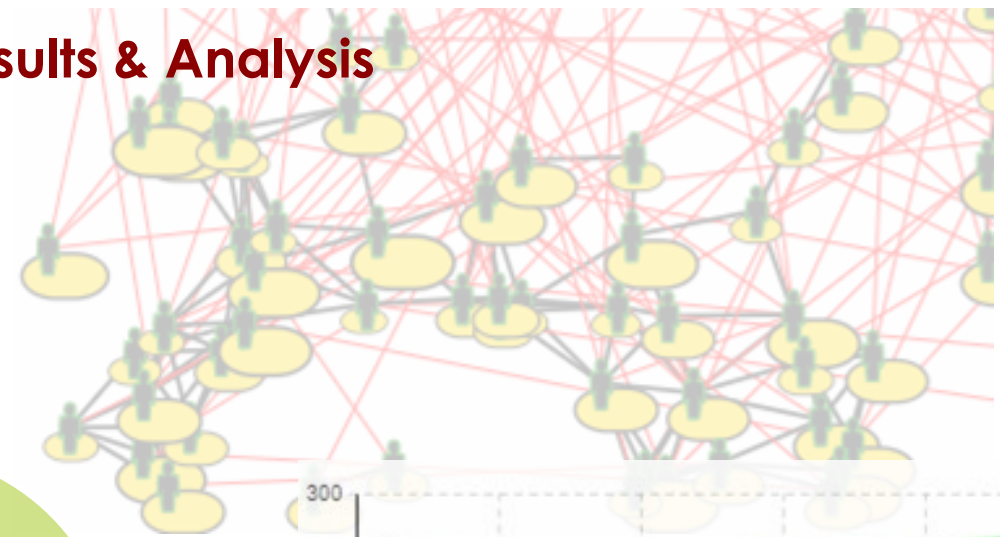
Jacob Starks, Lin Guo, and Janet K. Allen and Farrokh Mistree

Background and Formulation

- Human behavior is often governed by social factors that are “immeasurables”.
- Quantifying them can allow improve the implementation of developmental policies.



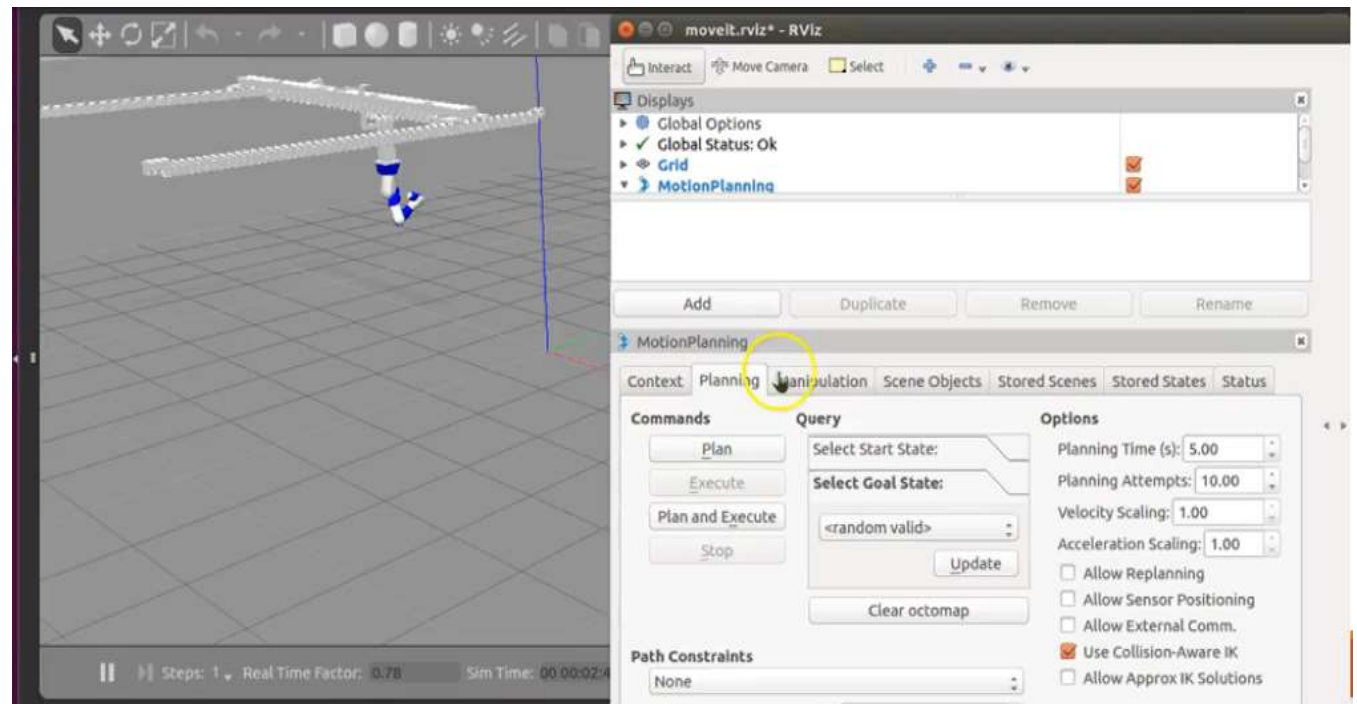
Results & Analysis



Development of a Robotic Arm-Gantry Simulation Using ROS and Gazebo

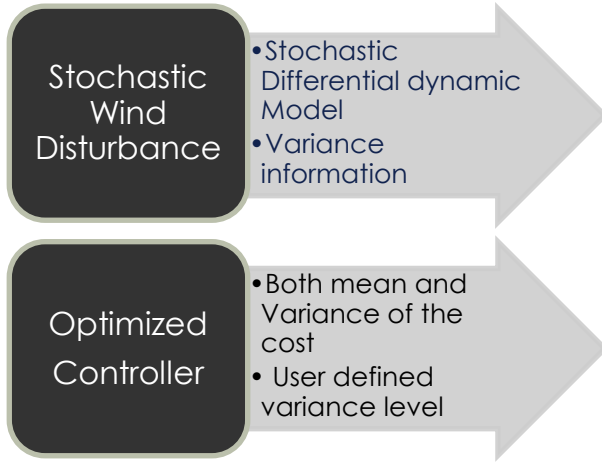
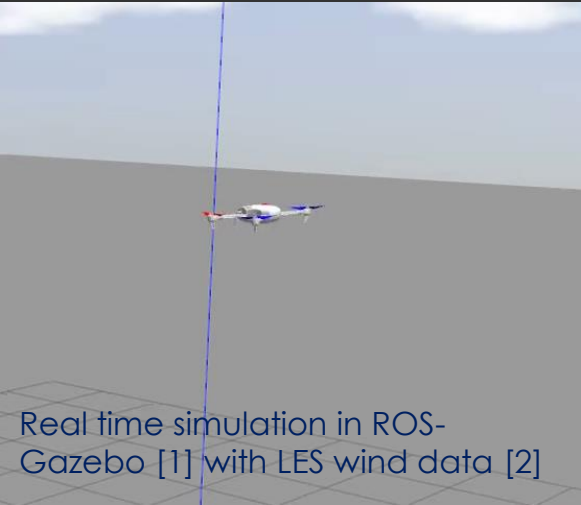
Shahbaz P Qadri Syed(OSU), Dr. He Bai

- In most of the Robotic applications, prototype testing is not always feasible.
- Simulation provides a means to perform initial testing and visualization before interfacing with actual hardware.
- In the present work, the ROS, Gazebo framework is integrated with moveit for motion planning and execution.



Minimum Cost Variance Controller for Quadrotor Under Stochastic Wind Turbulence

Asma Tabassum(OSU), and He Bai



$$dx = (Ax + Bu)dt + Gdw \quad \leftarrow \text{Stochastic process}$$

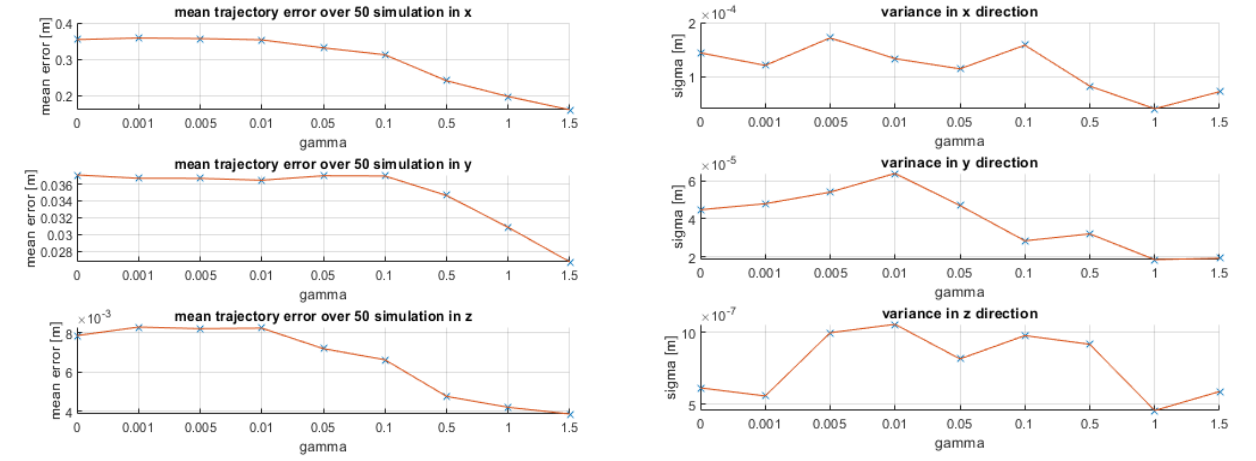
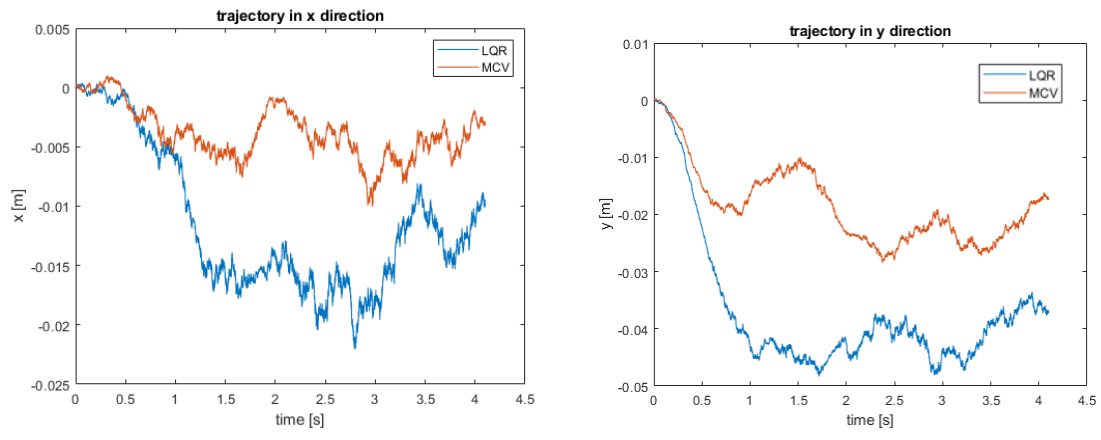
G is Calculated from LES

$$J(x, u, t_f) = \int_0^{t_f} (x^T Qx + u^T Ru) d\tau$$

$$j(x, u) = \lim_{t_f \rightarrow \infty} \frac{E(J(x, u, t_f))}{t_f} + \gamma \lim_{t_f \rightarrow \infty} \frac{\text{var}(J(x, u, t_f))}{t_f}$$

↓ Tuning parameter

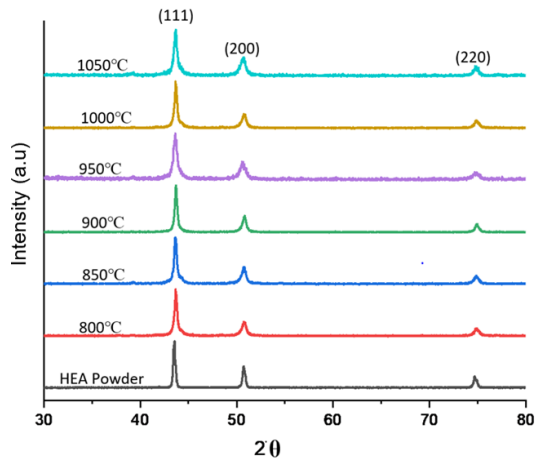
Trajectory Comparison



[1] Available at: https://github.com/CoRAL-OSU/RotorS_wind
 [2] Vuppla,Rohit and Kursat Kara, "Large-Eddy Simulation of Atmospheric Boundary-Layer Gusts for Small Unmanned Air Systems" ,73rd Annual Meeting of the APS Division of Fluid Dynamics 2020.

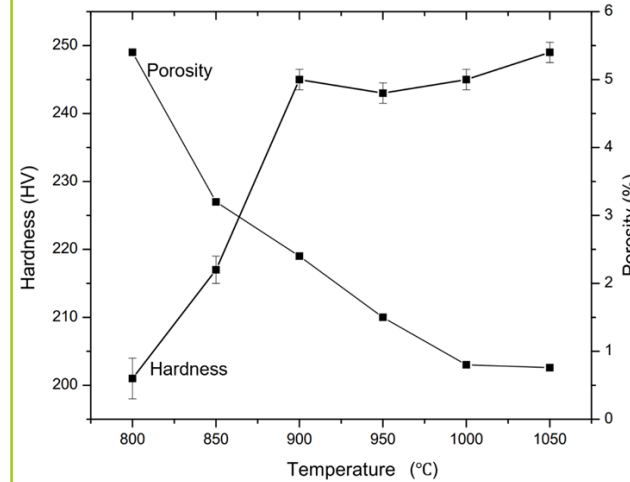
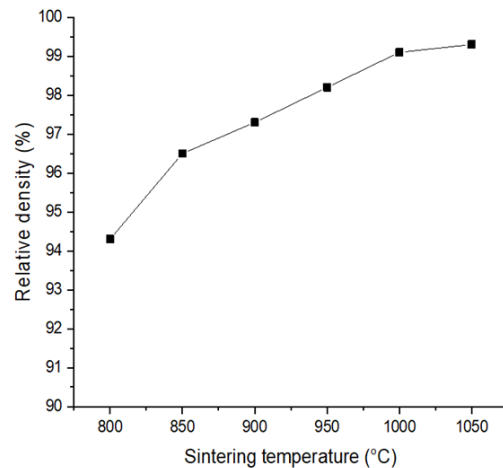
Densification and Wear behavior of Non-equiatomic $\text{Al}_{0.5}\text{CoCrFeNi}_2$ High Entropy Alloy

Abhishek Tikar, Shubhankar Padwal, and Sandip P Harimkar



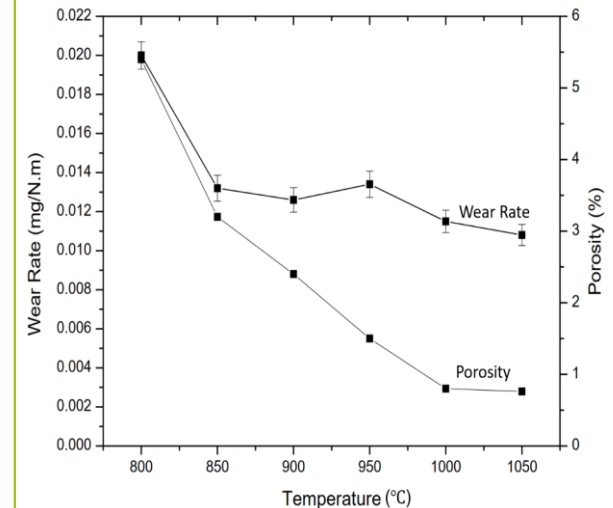
- Stable FCC Phase
- Low Concentration of Al and high concentration of Ni

- Complete densification at 1000°C
- Porosity pinning observed



- High porosity samples show lower hardness values
- Comparable aged Inconel 718

- Porosity increases wear rate
- Oxidation assisted wear behavior



A Machine Learning Approach to Predict Wind Field Data

Rohit K. S. S. Vuppala(OSU), Dr. Kursat Kara.

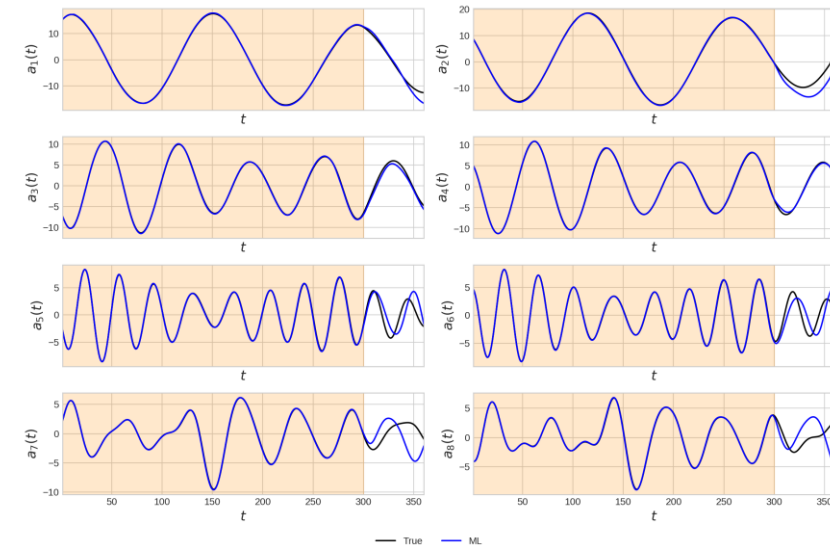
Motivation:

Spatio-temporal wind-field prediction is increasingly essential in many applications like: Unmanned Air Systems and Climate/weather forecasting.

Why use Machine Learning?:

- Neural Networks can learn characteristics from extensive data available from simulations.
- Machine Learning predictions are easier and quicker than Numerical Simulation like LES.

We choose a Stable Boundary Layer case and compare ML results with LES.



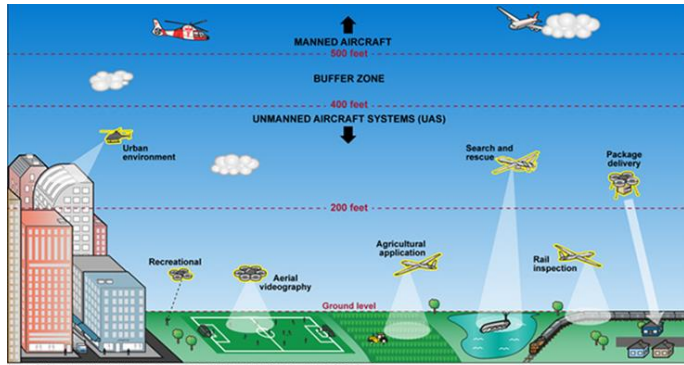
Modes, predictions vs actual

Conclusions:

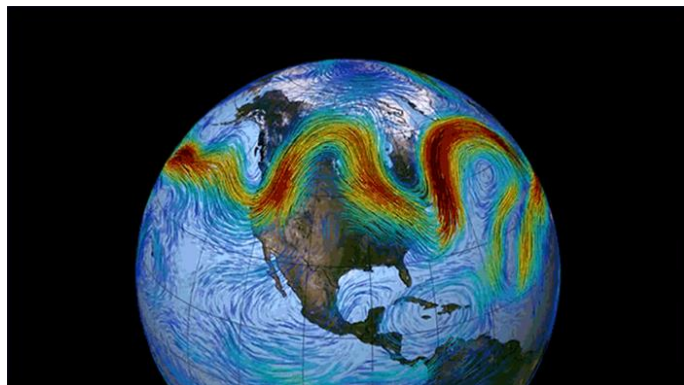
- Good agreement between predictions and actual values.

Future work:

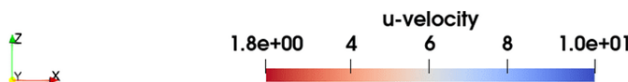
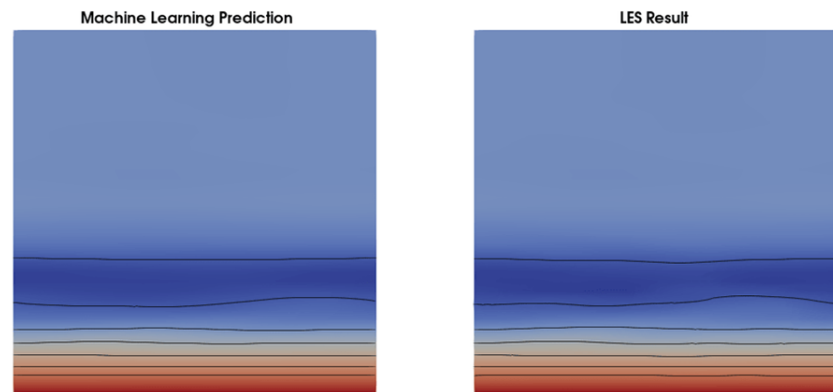
- Encoder-Decoder and CNN-LSTM type networks.



Unmanned Air Systems

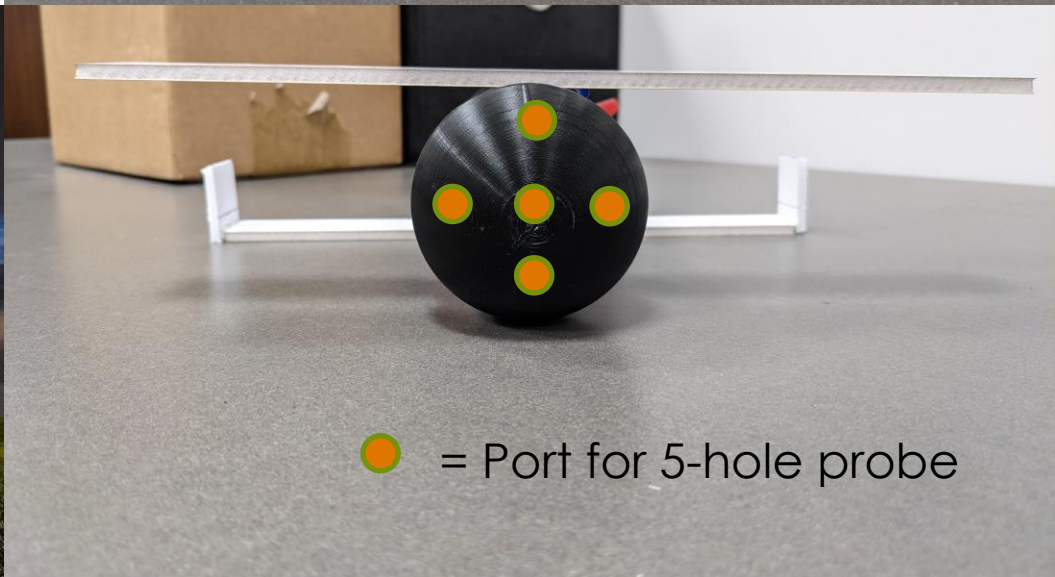
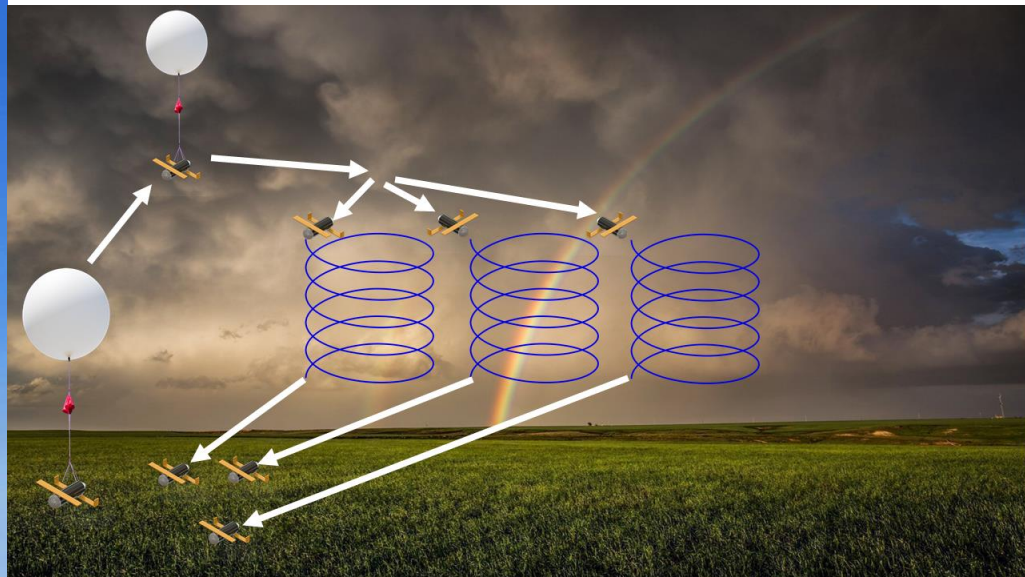
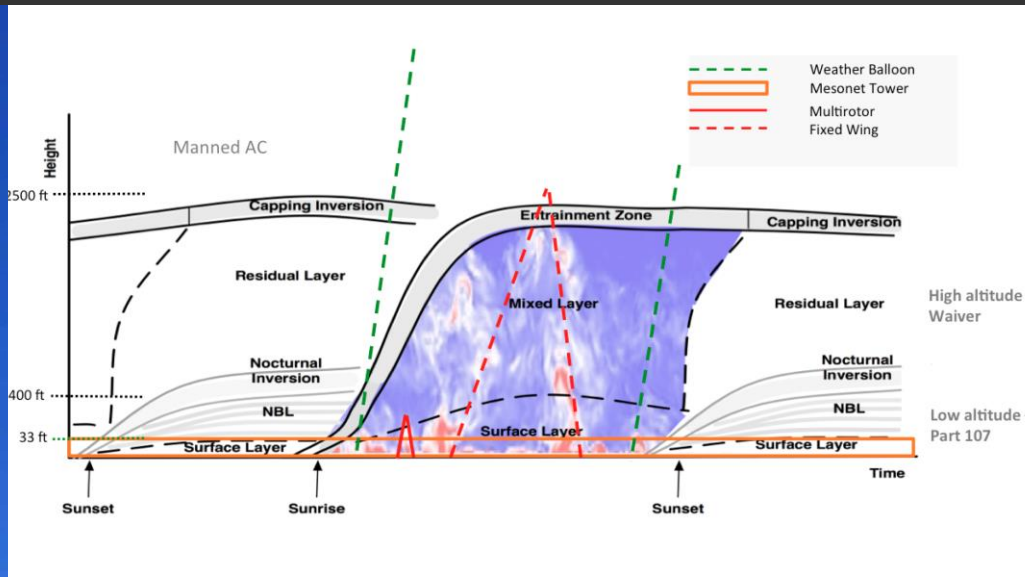


Climate/Weather Forecasting



Design, Development, and Flight Testing of a MAV for Meteorological Data Collection

Andrew Walsh (OSU) and Jamey Jacob



A Bellwether of Aircraft Design

Scott Weekley (OSU)



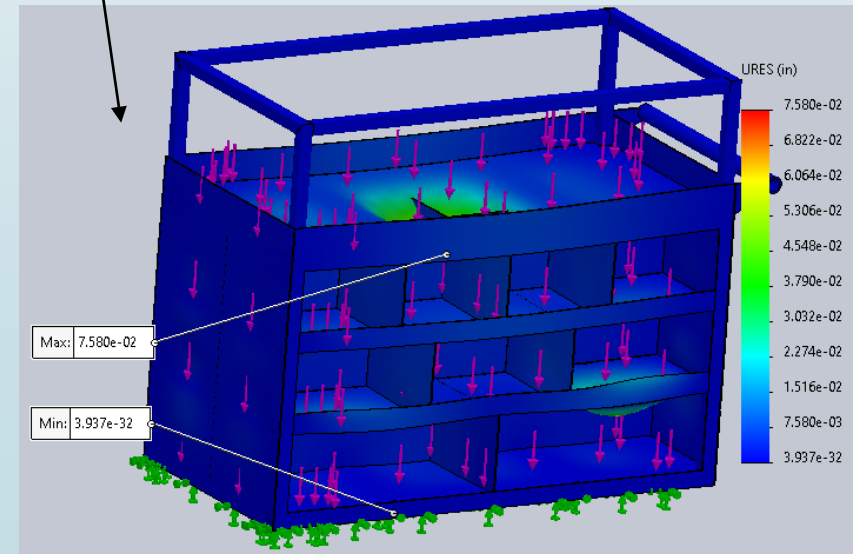
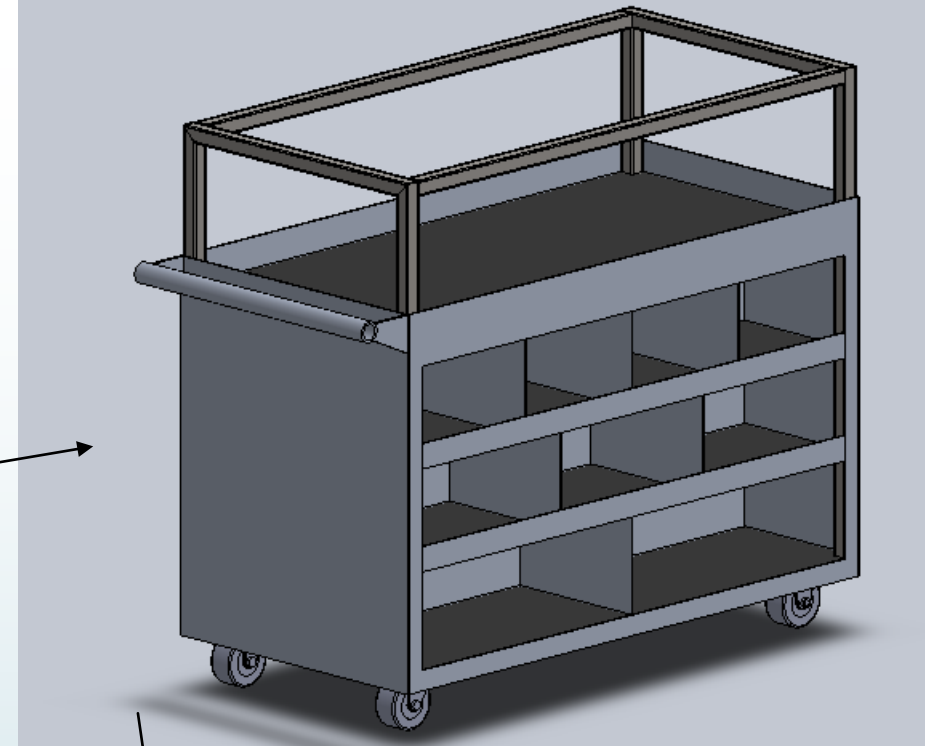
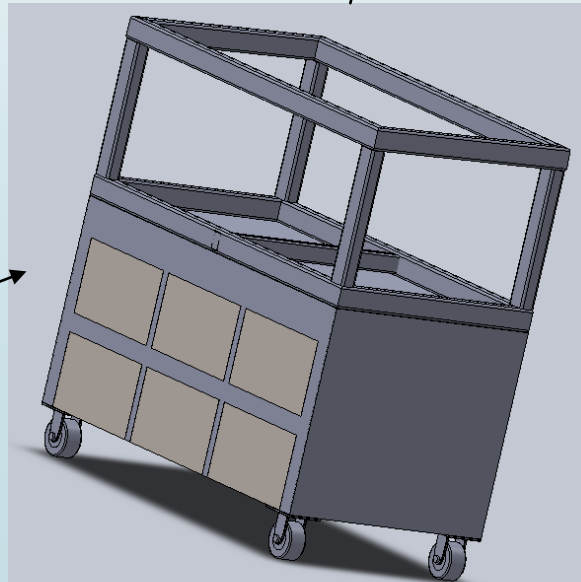
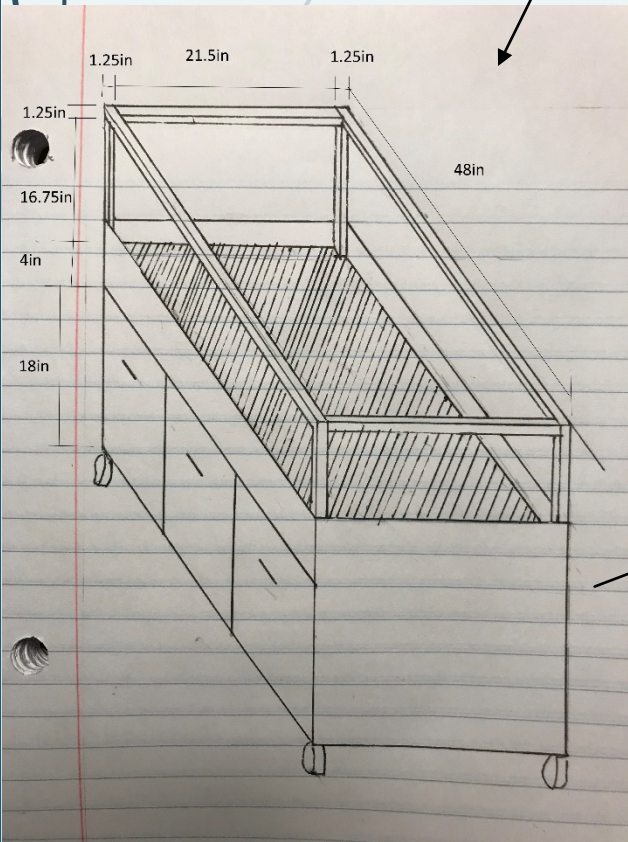
- A new aerodynamic theory is used in the design of the unmanned aircraft, **Bellwether**.
- Computational fluid dynamics (CFD) on this design shows greater aerodynamic performance than the industry-standard theory implemented for over 100 years.
- The implementation of this theory appears to explain the efficiency of avian flight formation and how birds can coordinate turns without the use of observable yaw control.

Southwest United Cart – ORU

Jaime Hernandez, Karl Nguema, Stacey Van Tassel, and Aaron Wendel

“We need a cart to protect our products from being damaged”

“We want shelves”



A Novel Compression and Expansion Fusion for Improving Vapor Compression Refrigeration Cycles

Andrew J. Williamson(OSU), Khaled Sallam

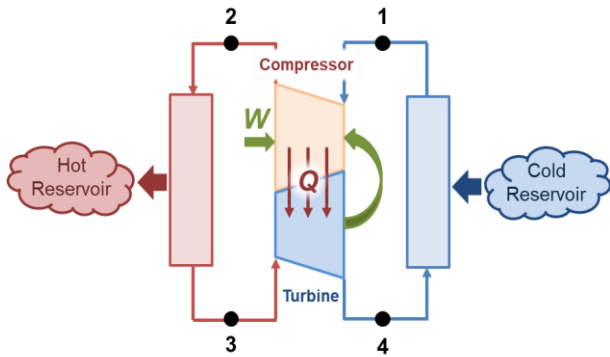
MOTIVATION

Refrigeration and air-conditioning accounts for 20% of the world's overall electricity consumption.

"The IIR estimates that global electricity demand for refrigeration – including air conditioning – could more than double by 2050" - 38th informatory Note on Refrigeration Technologies

WHAT IS CT-FUSION?

Compressor-Turbine (CT) Fusion device is a combination of the expansion and compression into a single unit such that the compressor transfers heat into the expander in a counter-flow configuration.



ANALYTICAL METHOD

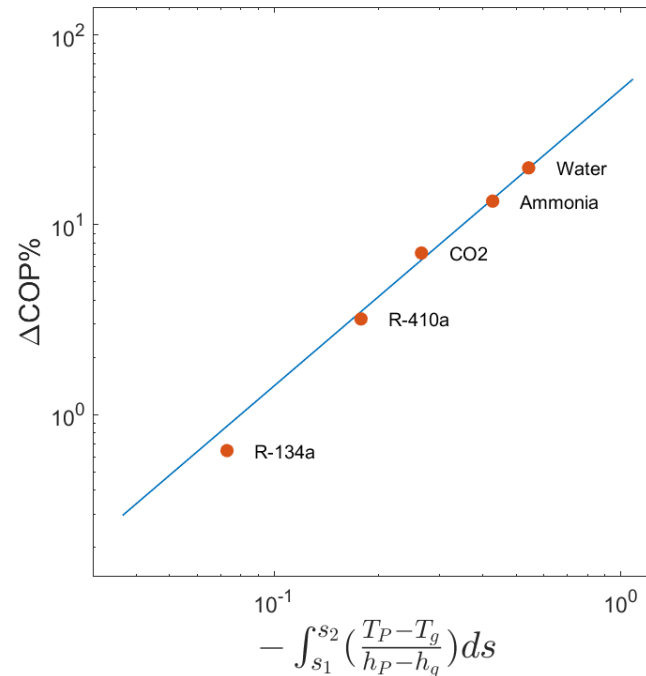
Thermodynamic analysis was performed using the following form of the 1st Law:

$$\delta Q = \delta W + dh$$

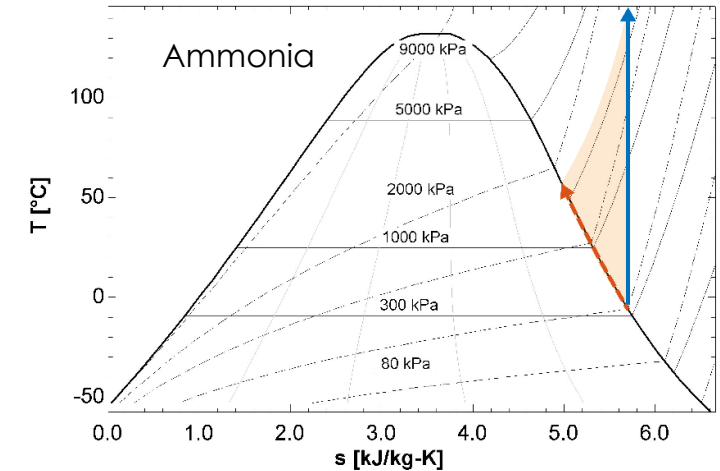
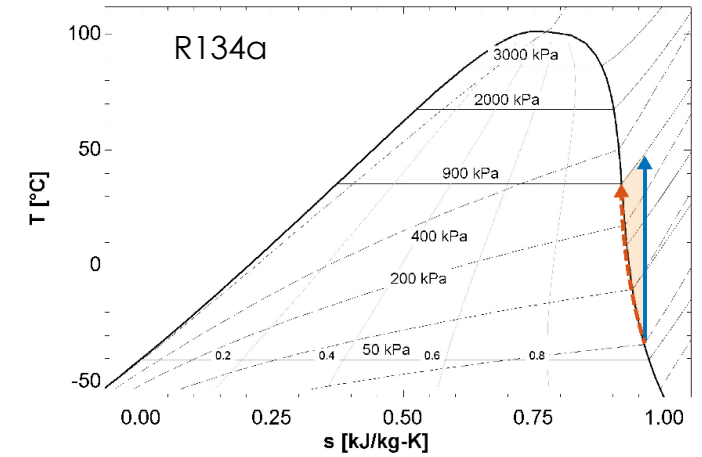
The CT-Fusion device was shown to improve the COP of the VC cycle past that of adding an expander alone.

RESULTS

The COP increase available was dependent on the working fluid and was shown to be a strong function of the compressor operating conditions.



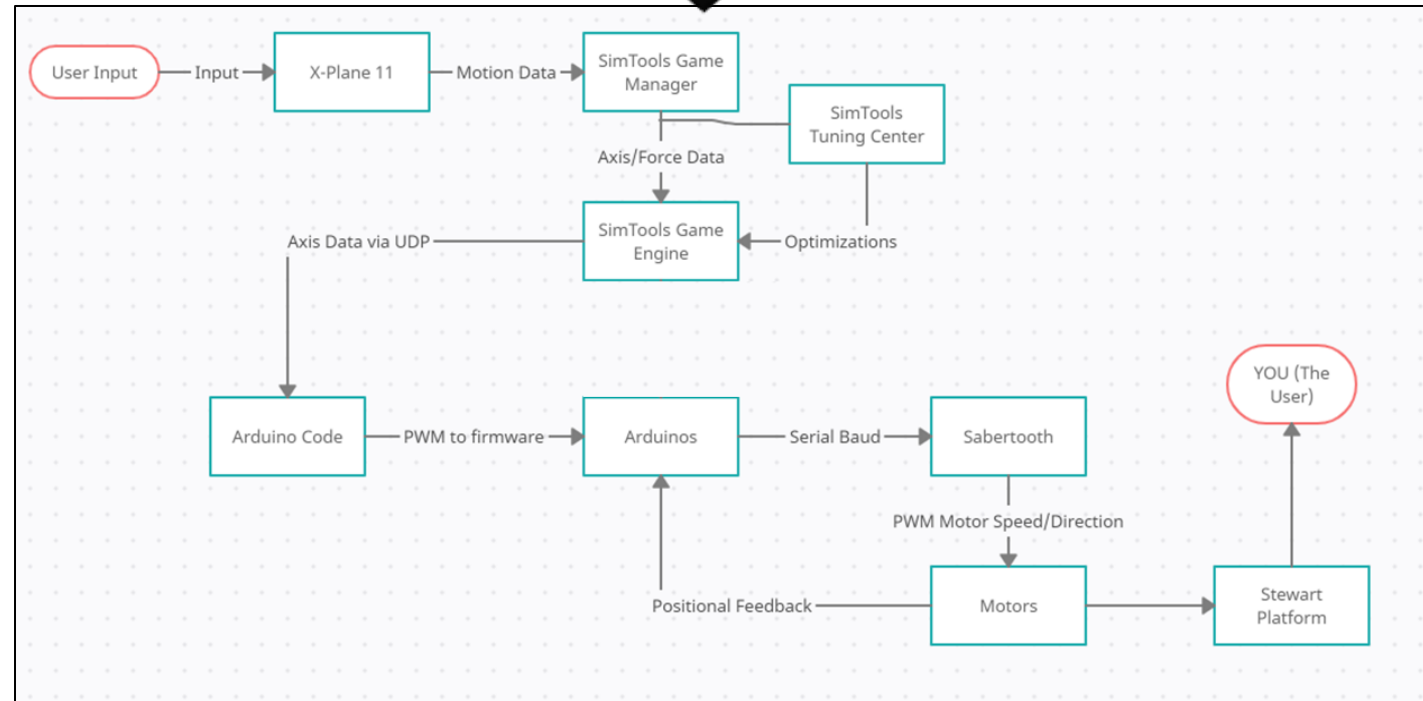
The available COP increase can be visualized as the area between isentropic and ideal CT compression on the respective T-s diagrams.



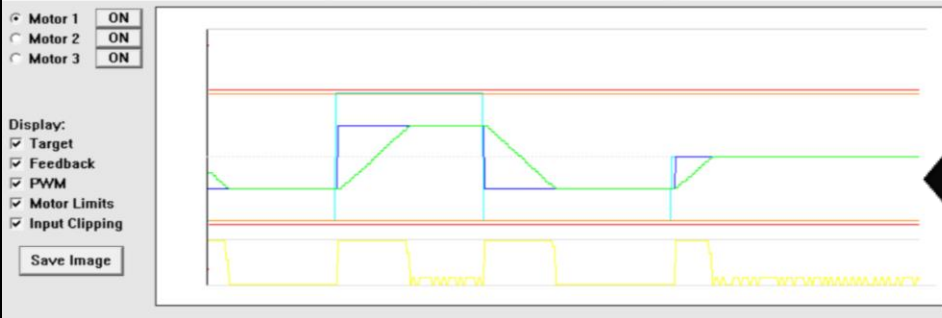
Computer Software Integration in a Virtual Reality Flight Simulator

Presented by: *Geoffrey Willis*, Michael VanDusen

Block Diagram for Communication within the Simulator



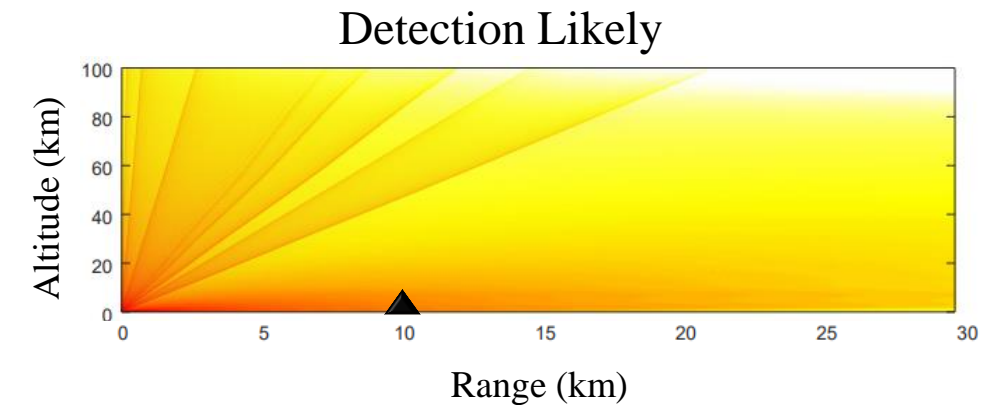
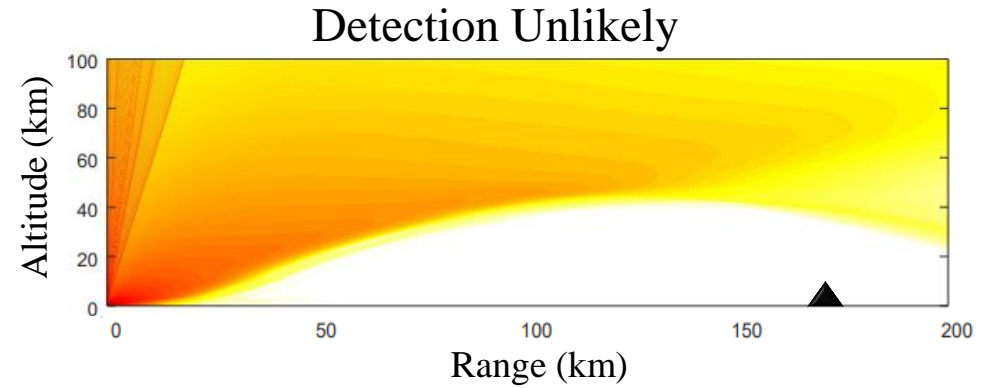
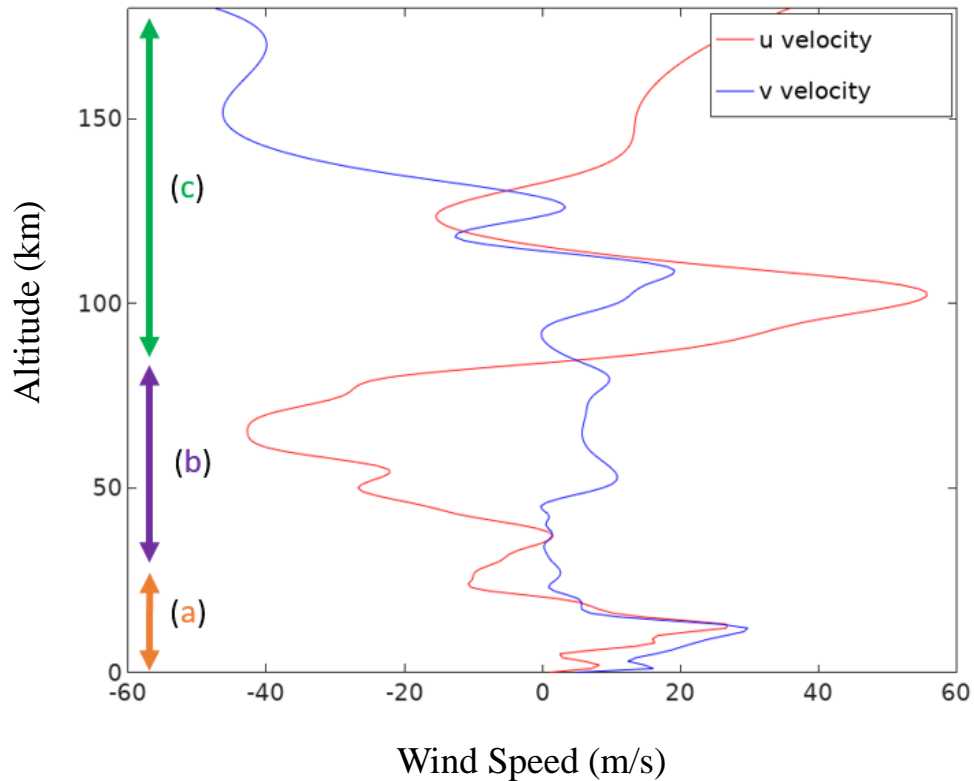
Completed Assembly of the Flight Simulator



Motor Response from Control Signal

Infrasound Propagation in the Atmospheric Conditions of Tornado Producing Storms

Trevor C. Wilson (OSU), Brian R. Elbing



*Triangle indicates receiver location

Effects of Shock and Vibration on Electronic Components

Ben Worwag (OSU), Chulho Yang, Ph.D., Young Chang, Ph.D., and Avimanyu Sahoo, Ph.D.

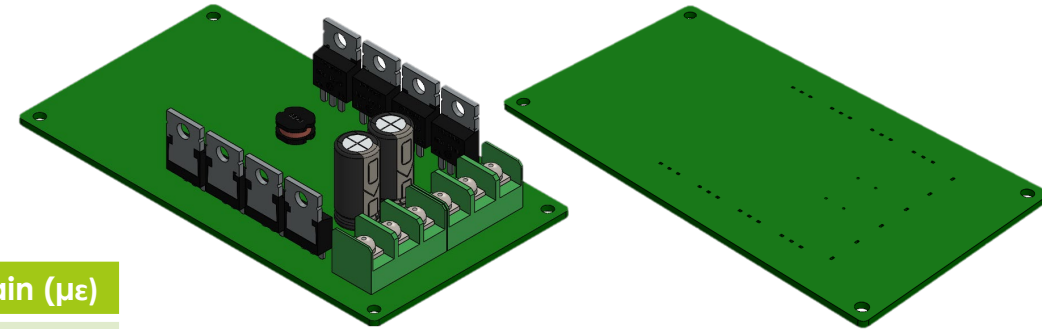
Project Goal:

Examine failure mechanisms and develop failure prediction methods.

Modal and Static Analysis Results:

Mode Shape	Frequency (Hz)
1	360.31
2	651.61
3	984.79
4	1392.4
5	1517.2

Load	Deformation (mm)	Eq. Stress (MPa)	Eq. Strain ($\mu\epsilon$)
Bending	1.769	31.02	547.6
Torsion	0.176	4.234	75.86



Experimentation Plan:

1. Design fixture to attach PCB to MB Dynamics PM50A mechanical shaker.
2. Set up accelerometer and strain gauges at selected points to collect data.
3. Run experiments to replicate the boundary conditions of the simulation.
4. Compare experimental results to calculations performed through simulation.

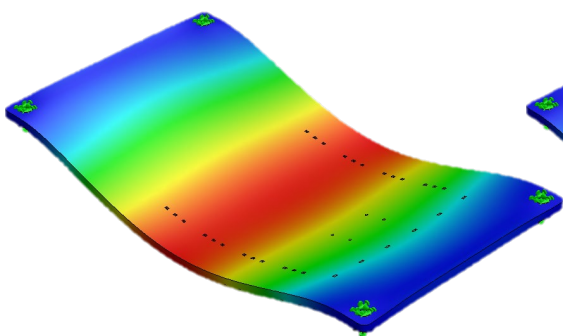


Figure 3: Mode Shape 1

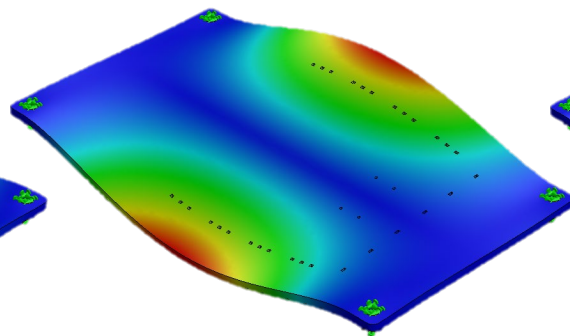


Figure 4: Mode Shape 2

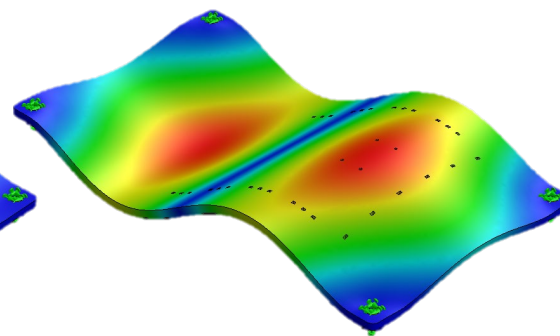


Figure 5: Mode Shape 3

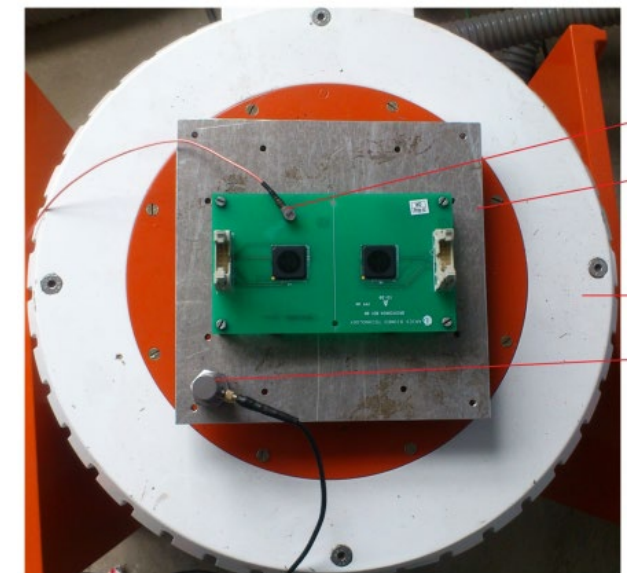


Figure 6: Testing Apparatus (from S. Jayesh and J. Elias: Int. J. Simul. Multidisci. Des. Optim. 10, A11 (2019))

Enhanced photodegradation in polystyrene/C₆₀ blends

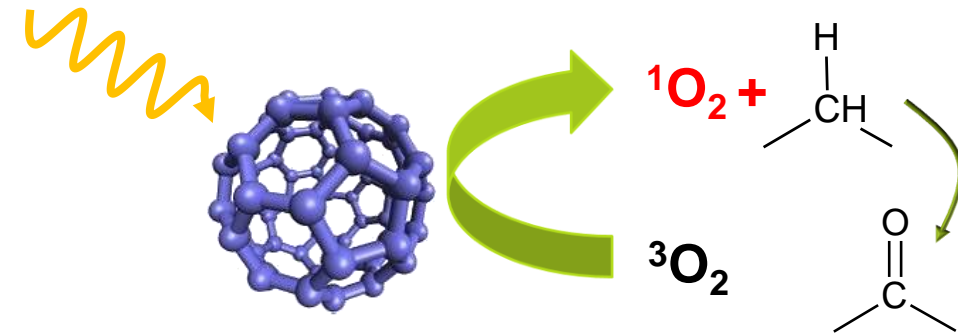
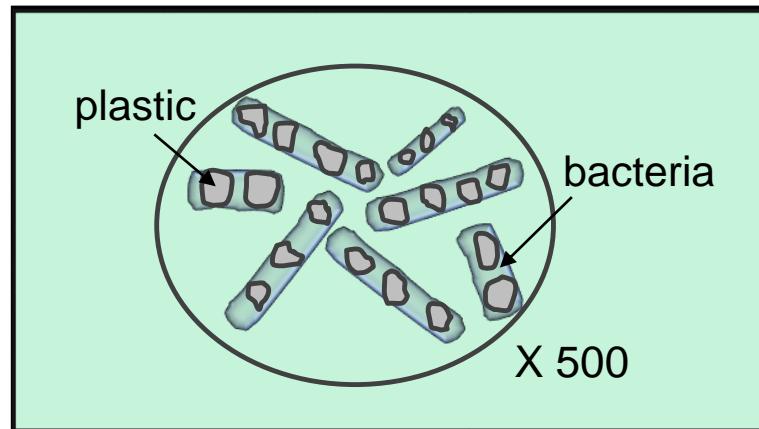
Linqi Zhang and A. Kaan Kalkan*



Degradation of plastics



<http://sustpkgg.blogspot.com/>



Plastic photodegradation

Before

After

